

論文 / 著書情報
Article / Book Information

題目(和文)	
Title(English)	Catalyst Preparation Using Microwave Induced Plasma
著者(和文)	チョンジェヨン
Author(English)	JaiYoung Chung
出典(和文)	学位:博士(工学), 学位授与機関:東京工業大学, 報告番号:甲第11478号, 授与年月日:2020年3月26日, 学位の種別:課程博士, 審査員:関口 秀俊,山口 猛央,多湖 輝興,吉川 史郎,森 伸介
Citation(English)	Degree:Doctor (Engineering), Conferring organization: Tokyo Institute of Technology, Report number:甲第11478号, Conferred date:2020/3/26, Degree Type:Course doctor, Examiner:,,,,,
学位種別(和文)	博士論文
Type(English)	Doctoral Thesis

Tokyo Institute of Technology

Doctoral Thesis Academic Year 2019



Catalyst Preparation Using Microwave Induced Plasma

Chung Jai Young

Supervisor

Professor Hidetoshi Sekiguchi

Department of Chemical Science and Engineering

School of Materials and Chemical Technology

CONTENTS

CONTENTS	3
Chapter 1 - Introduction	7
1.1 Plasma	9
1.1.1 Plasma generation techniques by electric discharge	10
1.1.2 Application of non-thermal plasma for catalyst preparation	13
1.1.3 Microwave induced plasma under atmospheric pressure	14
1.2 Spouted bed	15
1.3 Objective	18
1.4 Structure of the thesis	19
Chapter 2 - Treatment of aluminum hydroxide with microwave induced plasma jet	23
2.1 Introduction	25
2.1.1 Decomposition pathway of aluminum hydroxide	25
2.2 Experimental set-up	27
2.2.1 Design of the spouted bed	28
2.2.2 The microwave induced plasma spouted bed	30

2.2.3 The fixed bed with the plasma irradiation	33
2.2.4 The electric furnace	35
2.2.5 Particle characterization	36
2.3 Result and discussion	36
2.3.1 Temperature measurement of the microwave induced plasma	36
2.3.2 Surface morphology by SEM	40
2.3.3 Crystal structure analysis by XRD	44
2.4 Conclusion	54
Chapter 3 - Preparation of Ni/Al₂O₃ with microwave induced plasma jet	57
3.1 Introduction	59
3.2 Experimental set-up	61
3.2.1 Catalyst preparation & treatment conditions	61
3.2.2 Catalyst evaluation (Ethylene hydrogenation)	64
3.2.3 Catalyst characterization	66
3.3 Result and discussion	67
3.3.1 Surface morphology by SEM	67
3.3.2 Crystal structure analysis by XRD	72
3.3.3 TEM analysis	76
3.3.4 Catalytic activity: Ethylene conversion	79

3.3.5 Catalytic activity: Methane and ethane selectivity	83
3.4 Conclusion	88
Chapter 4 - Preparation of Pd/Al₂O₃ with microwave induced plasma jet	89
4.1 Preparation of Pd/Al ₂ O ₃ with the microwave induced plasma jet combined with the spouted bed	91
4.1.1 Introduction.....	91
4.1.2 Experimental set-up	91
4.1.2.1 Catalyst preparation & treatment conditions	92
4.1.2.2 Catalyst evaluation (Acetylene hydrogenation).....	93
4.1.2.3 Catalyst characterization	94
4.1.3 Result and discussion	95
4.1.3.1 Characterization of the Pd/Al ₂ O ₃ catalysts.....	95
4.1.3.2 Catalytic activity: Acetylene conversion.....	100
4.1.3.3 Catalytic activity: Ethylene selectivity	102
4.1.3.4 The effects of the plasma spouted bed.....	104
4.2 Preparation of Pd/Al ₂ O ₃ by the fixed bed with the microwave induced plasma irradiation	108
4.2.1 Introduction.....	108
4.2.2 Experimental set-up	108

4.2.2.1 Catalyst preparation & treatment conditions	108
4.2.2.2 Catalyst evaluation (Acetylene hydrogenation)	109
4.2.2.3 Catalyst characterization	109
4.2.3 Result and discussion	110
4.2.3.1 Surface morphology by SEM	110
4.2.3.2 Crystal structure analysis by XRD	112
4.2.3.3 TEM analysis	114
4.2.3.4 Catalytic activity: Acetylene conversion	116
4.2.3.5 Catalytic activity: Ethylene and ethane selectivity	119
4.2.3.6 Comparison of the fixed bed with the plasma irradiation and the plasma spouted bed	120
4.3 Conclusion	122
Chapter 5 - Conclusion	123
5.1 Concluding remarks	125
5.2 Prospects and further studies	128
REFERENCES	129
ACKNOWLEDGEMENTS	138

CHAPTER 1

Introduction

1.1 Plasma

We can often hear the term ‘plasma’ in our everyday life as display device, illumination, or air cleaner etc. In addition to our everyday life, plasma is widely applied in many industrial fields. However a scientific meaning of plasma is not commonly known. Plasma, considered as a fourth state of matter, is a partially ionized gas that contains excited species as radicals. The sun and an aurora are notable examples of natural plasma generation. It could naturally be generated but also can be artificially produced. Fluorescent lamps are the most generally used and artificially produced plasma application in our life.

Artificially induced plasma can be divided into two classes: thermal plasma and non-thermal plasma. Thermal plasma could be generated by raising ambient temperature at high pressure ($\geq 10^5$ Pa) [1]. The system of thermal plasma is an equilibrium state in thermodynamics i.e. electrons and heavy species (ions and neutrals) have almost the same temperature. On the other hand, non-thermal plasma is not in thermodynamically equilibrium, that is, electron temperature is much higher than that of ions and neutrals. This is why it is also called non-equilibrium plasma. Non-thermal plasma could conduct chemical reactions at a lower temperature range as compared with typical heat treatment using such as electric furnace. Non-thermal plasma could be used for materials which are vulnerable to high temperature circumstances. Moreover, plasma applied chemical reaction could show high reactivity due to active radicals in the plasma. For those reasons, non-thermal plasma has been widely used in practice since the 1990s in various industry field [2].

1.1.1 Plasma generation techniques by electric discharge

There are various ways to generate the plasma by supplying the necessary energy to targeted gases. The most widely used method for artificially generated plasma is to apply an electric field to gases [3]. There are various methods for utilizing electric field to generate discharge. The ways to apply the electric field can be mainly classified as direct current (DC) discharge, radio-frequency (RF) discharge and microwave discharge.

DC discharge

DC discharge can be categorized into townsend discharge, glow discharge and arc discharge depending on voltage upon current as shown in Fig. 1-1. The townsend discharge is formed at a low discharge current. As current increases, discharge transitions from the townsend discharge to glow discharge, and the discharge transfers into the arc discharge at further higher current (townsend→glow→arc).

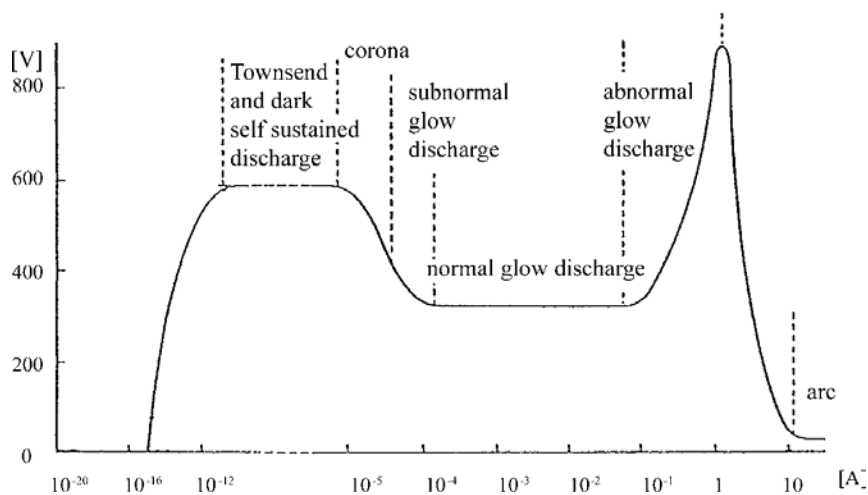


Fig. 1-1 The dependence of voltage upon current for dc discharges [3, 4].

RF discharge

There are two different methods for plasma generation by radio-frequency (RF) discharge: inductive discharge and capacitive discharge. Electromagnetic induction can be derived by a coil surrounding the reactor for inductive discharge, while, in capacitive discharge, electrodes arranged on the external surface of the reactor are used for the generation of the electromagnetic field [5]. Applications utilizing of RF discharge have been extensively reported in sterilizing, cleaning, sputtering as well as producing temperature-sensitive materials such as medical devices or polymers [6-8].

Microwave induced plasma

Microwave induced plasma has been widely applied in many industrial fields [9-12]. The most commonly used frequency is 2.45 GHz (wavelength of 12.2 cm) and many of them were operated under vacuum condition.

The discharge types of microwave can be classified into three types: discharges generated in closed structures, in open structures and on a plasma resonance [10-12]. In closed structures, the plasma chamber is surrounded by metallic walls to confine electromagnetic fields in microwave region. A typical example of open structures is microwave torch as shown in Fig. 1-2. Recently, many research of microwave induced plasma have been applied under atmospheric-pressure using various reactive gas in this structures [14, 15]. Detailed descriptions regarding to microwave induced plasma under atmospheric pressure are described in 1.2.

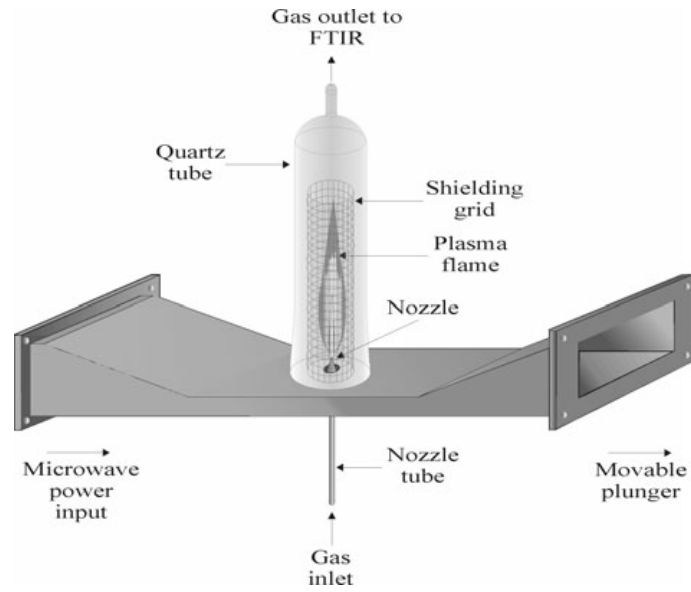


Fig. 1-2 Schematic of the moderate-power microwave torch plasma generator and plasma reactor for processing gas mixtures [10].

Electron cyclotron resonance (ECR) is a typical case of the plasma resonance discharge. It can be generated by introducing microwave into electrons when the electron cyclotron frequency (ω_{ce}) equals to frequency of incident radiation as shown in Fig. 1-3. The energy is strongly absorbed at the electron cyclotron resonance.

$$\omega_{ce} = \frac{eB}{m_e} \quad (1)$$

(Where e is charge on an electron, B is strength of a static magnetic field, and m_e is mass of an electron)

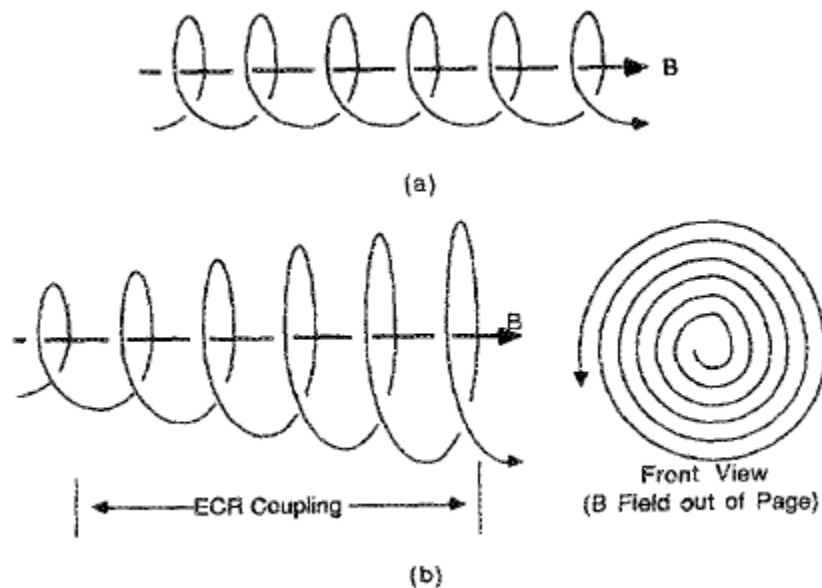


Fig. 1-3 Electron motion in a static magnetic field (a) when the electric field is zero and (b) ECR occur [11].

1.1.2 Application of non-thermal plasma for catalyst preparation

Non-thermal plasma has been applied for surface modification [16, 17], device manufacturing process of semiconductor [18, 19], and particles treatment for CNTs [20, 21] or catalyst, [22-30] etc. Especially for the catalyst preparation using the plasma, it has been widely reported for excellent performance of the catalyst.

The studies of the plasma for the catalyst preparation are described in detail below. Most of the researches were operated under vacuum condition. First of all, RF plasma was applied for the preparation of a NiMoN/C catalyst [22]. The catalyst was successfully prepared in a short preparation time at lower temperature and showed good performance in hydrogen evolution reaction. Dielectric barrier discharge (DBD) plasma of Ar/H₂ was applied to reduce the precursors of the Ni/ γ -Al₂O₃ and CeO₂-Ni/ γ -Al₂O₃ catalysts, which showed high reactivity in dry reforming and high durability in coke

resistance [23]. Plasma treatment resulted in the production of catalysts that possessed different crystal structures, which could derive the improvement in carbon resistance [24]. Generally, diverse crystal structures in metal show different behaviors in catalytic performance for specific catalytic reactions [25-29]. Microwave plasma was applied for the Ag/Al₂O₃ catalyst preparation under vacuum conditions. The plasma treatment for catalysts could enhance metal and support interactions [23, 24]. Microwave-induced plasma could create an environment of high temperature as compared with other non-thermal plasma, and it could provide active species such as radicals to substances with relatively high temperature. With this intervention, higher NO_x reduction efficiency in the selective catalytic reduction with ethanol was observed when compared to that of calcined catalysts [30].

1.1.3 Microwave induced plasma under atmospheric pressure

In the plasma industry, most of them are produced under reduced pressure due to stability of the plasma. Under reduced or vacuum condition, the plasma can be generated easily because the electrons can have sufficient energy to accelerate without energy loss from collision. Thus, the reaction rate is limited due to low density of the plasma resulting in collision frequency between particles. Meanwhile in atmospheric pressure plasma system, the density of active particle species in the plasma is high. Also a vacuum pump and exhaust equipment are unnecessary, causing experimental apparatus simplified and reaction rate enhanced due to high collision frequency of active particle species.

There are two types of methods for obtaining the plasma at atmospheric pressure: electrode discharge and electrodeless discharge. In the case of electrode discharge, the

electrodes are installed into the plasma. As a typical electrode discharge, as mentioned above, DC plasma such as glow discharge and arc discharge, and electrodeless plasma are well-known [31-33]. Since the electrodes directly contact the discharge, leading to the contamination of electrode. Meanwhile, microwave induced plasma is a typical example of electrodeless discharge. Using microwave discharge for the plasma generation has an advantage of no contamination of electrodes because there are no reactions between the electrode and gas, which make it possible to use reactive gases such as oxygen and carbon dioxide. Under atmospheric pressure, the microwave induced plasma could have higher temperature than that generated in vacuum condition. Thus, the plasma generated by microwave discharge under atmospheric pressure seems to have a potential for the heat source as well as to provide active species such as radicals. However, preserving stability of microwave induced plasma under atmospheric pressure is an exacting piece of work. Especially for particle treatment by the microwave induced plasma in solid interaction system, when a disturbance happens such as particles inclusion to the plasma, the plasma would be extinguished easily. Thus, it is required to control the conditions such as the output power of the microwave generator, tuning, particle movement and flow rates of gases.

1.2 Spouted bed

A spouted bed is a bed reactor where the particles are spouted by upward movement of fluid. The spouted bed has been widely used for the treatment of solid particles such as drying, heating and pyrolysis with a wide size distribution by making use of its advantages such as uniform particles mixing or good heat transfer between gas and particles [34-36]. A large amount of particle treatment can be operated in the spouted

bed. There are various state of particles spouting as shown in Fig. 1-4. The fixed bed is changed into stable spouting with increasing the air velocity. Further increase of the air velocity derives unstable spouting and brings out bubbling state followed by slugging flow.

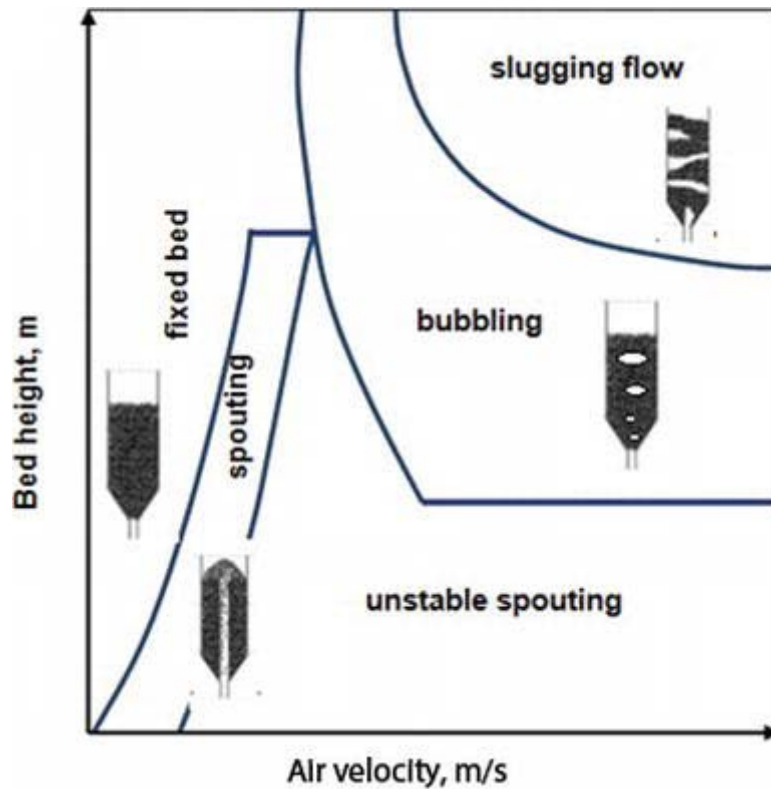


Fig. 1-4 Ranges of the bed structures [37-38].

The principle of pressure drop is an important concept for the spouted bed. The pressure drop is related with various parameters such as gas flow rates, shape of the reactor, and mass of the particles in the spouted bed. The dependence between the bed pressure drop and air velocity is presented in Fig. 1-5.

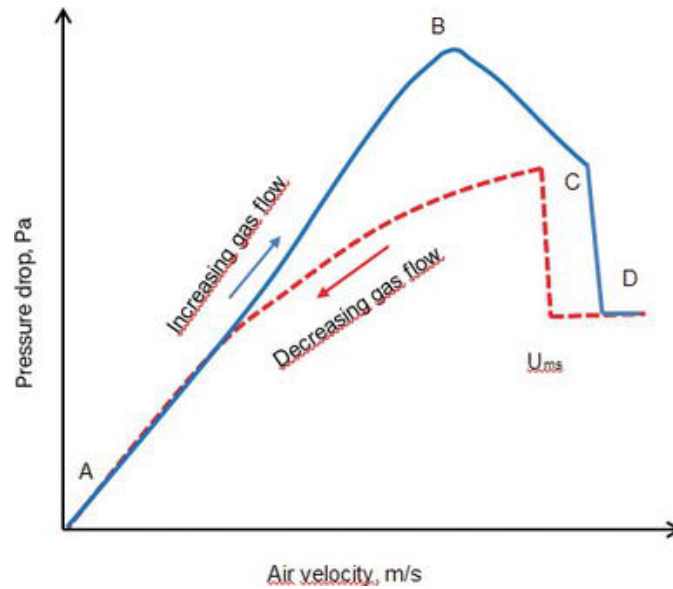


Fig. 1-5 Pressure drop as affected by gas velocity during spouted bed process

[37-38].

The increasing gas flow and the decreasing gas flow show different behavior of pressure drop. Firstly for the increasing gas flow, from initial point of A, the pressure drop rises directly to point B with increasing air velocities. From the flow rate between the point at A and at B, the particles still do not move. When the particles start to move, the pressure drop starts decreasing which corresponds to the point B. Further increase in air velocity, inclination of pressure drop changes from the point C. From the point D, the whole particle in the bed start to move. Further increase of flow rate induces slugging flow of the particle bed. On the other hand, for the decreasing gas flow from the point D, the energy for breaking between particle to particle contacts is unnecessary. The least point of the air velocity indicates the minimum spouting flow rate (U_{ms}). From this point, further decrease in air velocity derives a sharp rise in the pressure drop and the state of

the bed changes into a fixed bed [37]. Considering the complicated conditions of the spouted bed mentioned above, it has been considered to be difficult to combine the spouted bed with the microwave induced plasma under atmospheric pressure.

1.3 Objective

In the case of the heat treatment or the pyrolysis of substances using the spouted bed, the installation of a heat source is required. Plasma generated by various electric discharge seems to have a potential for the heat source as well as to provide active species such as radicals to the bed. By combining the microwave induced plasma with the spouted bed, it has a great potential for the processing of the particles. Moreover, the particle treatment using microwave induced plasma can be operated very fast compared with the conventional heating process using an electric furnace because the microwave induced plasma has high temperature. Most of the previous works using microwave as the plasma source of the spouted bed were under reduced pressure condition which was more costly and complicates the apparatus for the treatments. Few experimental studies on the plasma spouted bed under atmospheric pressure condition have been carried out. Here, we attempted to combine the microwave induced plasma with the spouted bed.

The objective of this research is to investigate effects of the microwave induced plasma combined with the spouted bed on the particle treatment. In this thesis, it is proposed to applying the microwave induced plasma to catalyst preparation using two types of reactors including a fixed bed and a spouted bed. The plasma jet generated by microwave discharge was directly irradiated to the particle bed in the former reactor, while the latter used the plasma jet for spouting particles. Three kinds of catalysts and catalyst support were chosen as model preparations: alumina (Chapter 2), Ni/alumina

(Chapter 3), and Pd/alumina (Chapter 4). For comparison, typical heat treatment using an electric furnace was also applied. A novel process as an advantageous substitute for the typical thermal treatment for particles can be developed and optimized, leading to provide the insight into the plasma applied industry.

1.4 Structure of the thesis

This research work aimed to investigate the effect of the microwave induced plasmas irradiation on the catalysts. To achieve this goal, the following tasks need to be completed:

- ✓ Confirm the effectiveness of the plasma spouted bed on the targeted materials.
- ✓ Compare with the other treatment Methods (without the spouted bed and the typical treatment)
- ✓ Investigate the properties of the targeted materials
- ✓ Explain the mechanism of the effects

According to these tasks, the thesis is structured in the five chapters as follows:

Chapter 1: Introduction, describes a background of the thesis, the principles of the plasma, plasma generation techniques by the electric discharge, application of the non-thermal plasma for catalyst preparation, the microwave induced plasma under atmospheric pressure, the spouted bed, the objectives, and the structure of the thesis is introduced. The microwave induced plasma was presented as an advantageous substitute for typical thermal heating. A review of the plasma spouted bed for the enhancement of the process was conducted and objectives for research were set.

Chapter 2: Treatment of aluminum hydroxide with microwave induced plasma jet, describes the experimental study of the plasma spouted bed for the particles treatment. Aluminum hydroxide was chosen as a model particle. Alumina is the most popular catalyst support due to its high specific surface area especially for γ -alumina. Aluminum hydroxide has various decomposition pathway depending on several factors such as types of particle, heating rate and pressure etc. The performance of the microwave induced plasma combined with the spouted bed was investigated for treatment of aluminum hydroxide. For comparison, the fixed bed with the plasma irradiation and the conventional thermal treatment using the electric furnace was applied for the treatment of aluminum hydroxide.

Chapter 3: Preparation of Ni/Al₂O₃ catalyst with microwave induced plasma jet, describes the experimental study of the microwave induced plasma irradiation applied for the catalyst preparation. As the most widely used catalyst, Ni-based catalyst was prepared by the microwave induced plasma treatment. For comparison, the fixed bed with the plasma irradiation and the conventional thermal treatment using the electric furnace was also applied. Catalyst characterizations were carried out by SEM, XRD, TEM, and H₂ chemisorption. Ethylene hydrogenation was chosen as a model catalyst reaction for the catalyst evaluation. The catalyst reaction and mechanism was discussed.

Chapter 4: Preparation of Pd/Al₂O₃ with microwave induced plasma jet, describes the experimental study for the microwave induced plasma irradiation on applied for the Pd/Al₂O₃ catalyst preparation. Pd metal has an excellent ability to take in hydrogen and it can store much more hydrogen than its own volume. Thus, it is widely used for hydrogenation reaction as a catalyst. In this chapter, Pd metal was impregnated on the alumina support and treated by the plasma spouted bed. The effects of the microwave plasma and the spouted bed on the catalyst preparation was experimentally investigated. The fixed bed with the plasma irradiation and the conventional thermal treatment using the electric furnace were also operated for a comparative analysis. SEM, XRD, TEM, and H₂ chemisorption analyses were carried out for catalyst characterizations. For the evaluation of the Pd/Al₂O₃ catalyst, hydrogenation of acetylene to ethylene was chosen for their catalytic activity.

Chapter 5: Conclusion, summarizes the findings of this study.

A schematic diagram in Fig. 1-6 demonstrates the structure of the thesis.

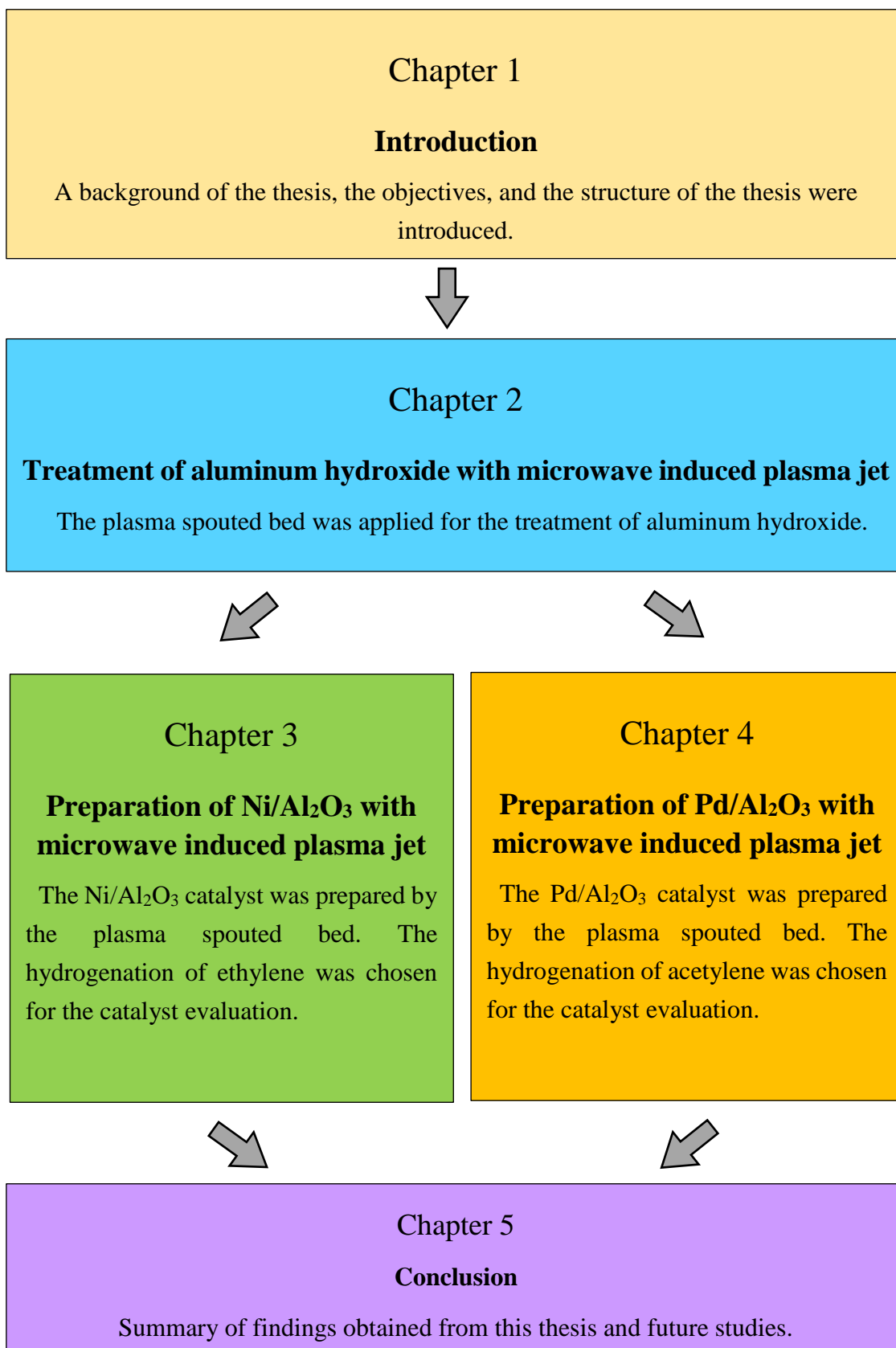


Fig. 1-6 Schematic of the thesis structure.

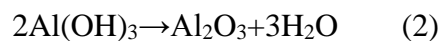
CHAPTER 2

**Treatment of aluminum hydroxide
with microwave induced plasma jet**

2.1 Introduction

2.1.1 Decomposition pathway of aluminum hydroxide

When the aluminum hydroxide is heated, the water is removed and the aluminum hydroxide is transformed to alumina with the following chemical reaction:



Alumina has numerous phase such as γ , θ , or α -alumina. Above all, α -alumina is considered as the most stable phase. Phase transition has no more occurred on α -alumina. There are various decomposition pathways of aluminum hydroxide when it transfers into α -alumina as shown in Fig. 2-1. These depend on several parameters, e.g. temperature, heating rate, and particle size.

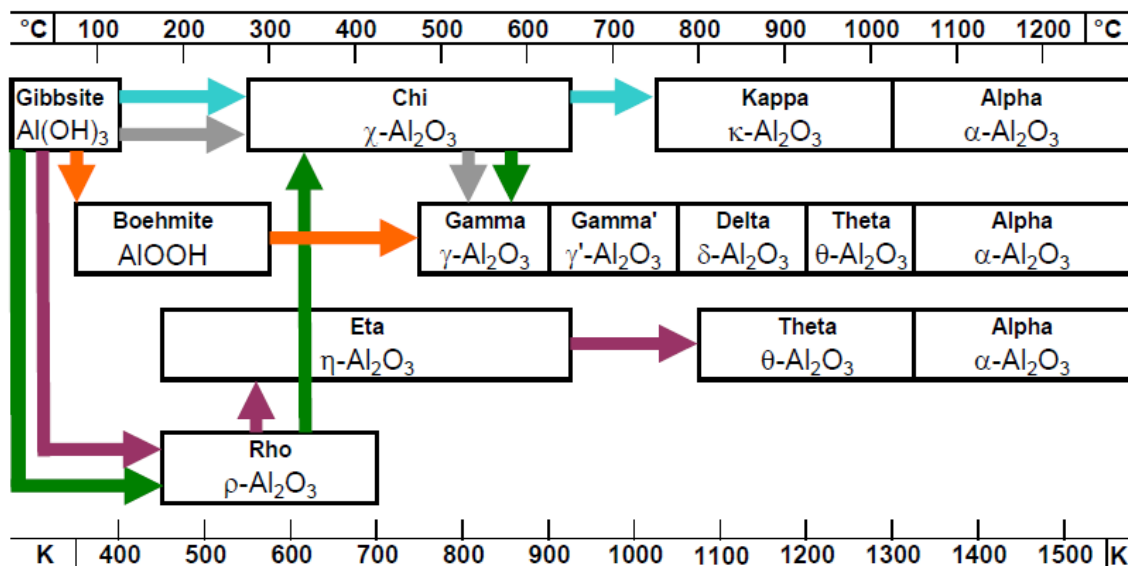
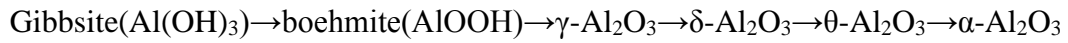


Fig. 2-1 Thermal decomposition pathways of $\text{Al}(\text{OH})_3$ adapted from the literature [39-44].

Among those various decomposition pathways, the following pathway is the most common for aluminum hydroxide decomposition:



Boehmite is formed from gibbsite at the temperature of between 100°C and 300°C. The decomposition of boehmite is followed at a higher temperature by a series of transformation from the γ phase to α phase. For all the decomposition pathways, α -alumina forms as it is the most thermodynamically stable phase at a temperature above 1050°C. The phase transformation sequence was investigated at various temperatures in other research [44]. The XRD pattern corresponding to the samples heated at various temperature is shown in Fig. 2-2.

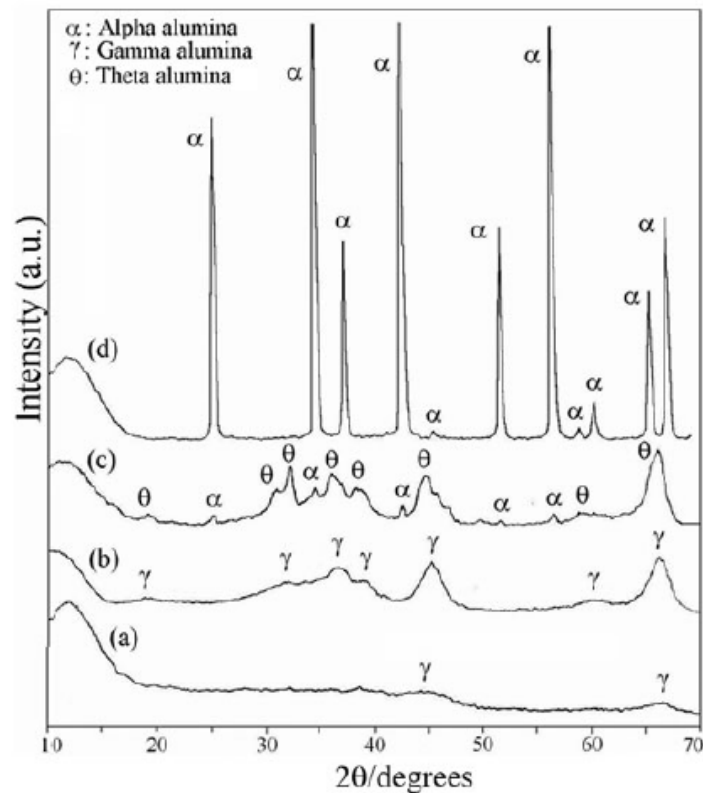


Fig. 2-2 XRD patterns of aluminum hydroxide heated at various temperatures for 30 min: (a) 400°C, (b) 800°C, (c) 1000°C, and (d) 1150°C, adapted from Contreras et al [44].

In Fig. 2-2, aluminum hydroxide was heated at (a) 400°C, (b) 800°C, (c) 1000°C and (d) 1150°C, for 30 min. The sample (b) heated at 800°C shows only γ -alumina. The crystalline phase of γ -alumina is detected mainly at three values, specifically 37.6°, 47.4° and 67.2° (JCPDS card, file No. 10-0425). The intermediate state of θ -alumina phase was detected at (c)1000°C which coexisted with α -alumina. The diffraction peaks at 31.2°, 32.8°, 34.9°, 36.7°, 40.0°, 44.8°, 47.6°, 59.9°, 36.9°, and 67.4° correspond to the θ -alumina (JCPDS file no.00-23-1009), and the diffraction peaks (2θ) at 25.6°, 35.1°, 37.8°, 43.4°, and 52.6° correspond to the α -alumina peak (JCPDS card, file No. 46-1212). At higher heating temperature at (d)1150°C, the peaks of θ -alumina disappeared, and only α phase peaks remained. For the typical phase transition of gibbsite, in the presence of θ -alumina is the essential intermediate phase, when γ -alumina converts into α -alumina.

2.2 Experimental set-up

The spouted bed combined with the microwave induced plasma irradiation was applied for the treatment of aluminum hydroxide in this study. For comparison, the plasma irradiation with the fixed bed and the typical thermal treatment using an electric furnace were also applied for the treatment of aluminum hydroxide. For brevity, the appellation of samples treated by the plasma spouted bed, the fixed bed with the plasma irradiation, and the conventional thermal treatment using the electric furnace are abbreviated to PS, PF, and CM below.

2.2.1 Design of the spouted bed

In the spouted bed, there are lower and upper limits of the gas flow rate that can sustain a stable jet state. In the study on the spouted bed, the minimum velocity at which particles spout was defined as the minimum jet velocity, and the behavior of the particles was analyzed and summarized in Equation (3) [45]. Using the equation, it is possible to predict the minimum jet velocity using the particle physical properties (particle size, density), the nozzle size at the inlet of the reactor, the inner diameter of the reactor, etc. as variables, and the size of the spouted bed is determined.

$$U_{ms} = 0.25 \left(\frac{D_p}{D_c}\right)^{0.65} \left(\frac{D_n}{D_c}\right)^{0.312} \left(\frac{H}{D_c}\right)^{0.254} \left[\sqrt{\frac{2gH(\rho_p - \rho_f)}{\rho_f}} \right] \quad (3)$$

D_p = Particle diameter [m]

D_c = Column diameter [m]

D_n = Inlet nozzle diameter [m]

H = Bed height [m]

ρ_p = Density of fluid [kg/m³]

ρ_f = Density of particle [kg/m³]

g =Gravity acceleration [m/s]

U_{ms} = Minimum spouting velocity [m/s]

In this study, the spouted bed reactor was prepared considering the maximum jet height and the minimum spouting velocity to operate the particle treatment. From the physical properties of the reactor and particles summarized in Table 2-1 and Equation (3), the minimum jet velocity was 0.064 m/s or 2.2 L/min. It was experimentally confirmed that the particles were spouted at a flow rate of 2.5 L/min or more. Even under conditions where the gas flowed stably before plasma generation, the flow state in the spouted bed became intense, exceeding the jet height and being unable to process when the plasma was generated. Furthermore, it was observed that particles were spouted even when the flow rate was lower than the minimum spouting velocity when the plasma was generated. This is supposed to be due to the increase in the velocity as the gas temperature rise by the plasma generation. From this, the experiment was conducted by the procedure of starting the jet at a flow rate higher than the minimum jet velocity and adjusting the gas flow rate after plasma generation.

Table 2-1 Properties of microwave spouted bed reactor and particle.

Property	Value
Dp (m)	0.00011
Dc (m)	0.027
D_n (m)	0.009
g (m/s ²)	9.8
H (m)	0.01
ρ_p (kg/m ³)	2420
ρ_f (kg/m ³)	1.7

2.2.2 The microwave induced plasma spouted bed

The schematic diagram of the spouted bed reactor with microwave plasma is shown in Fig. 2-3. Microwave generated by a 2.45 GHz microwave generator (IDX Corp. ING-25) was supplied to a quartz glass tube through a resonance cavity. Plasma was generated under atmospheric pressure. The properties of the reactor were summarized in Table 2-1. The plasma spouted bed consisted of quartz glass having an internal diameter of 27 mm, a nozzle diameter of 9mm, and a length of 370mm. The inlet was inclined upwardly at an angle of 60°. A mixture of Ar and H₂ was used as a plasma gas for aluminum hydroxide treatment and was injected from the bottom of the spouted bed to spout the particles. Enlarged view of the spouted bed from Fig. 2-3 is shown in Fig. 2-4 (a) and a photograph are shown in Fig. 2-4 (b).

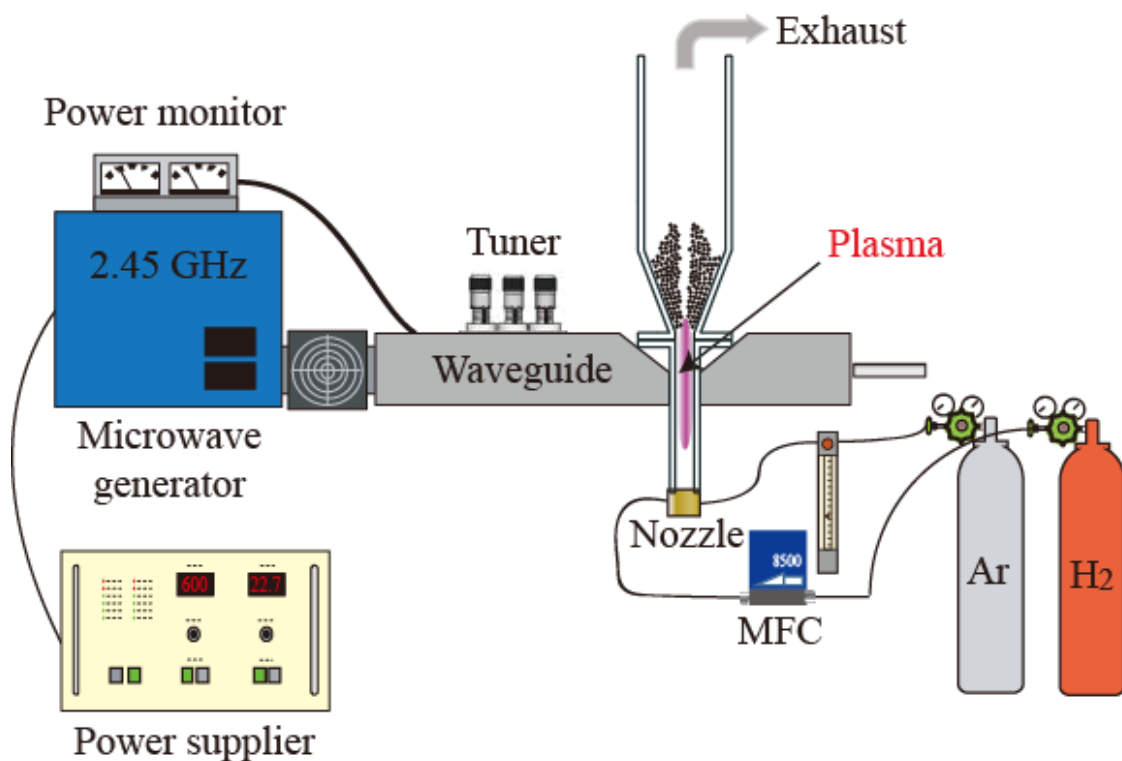


Fig. 2-3 Schematic diagram of the plasma spouted bed.

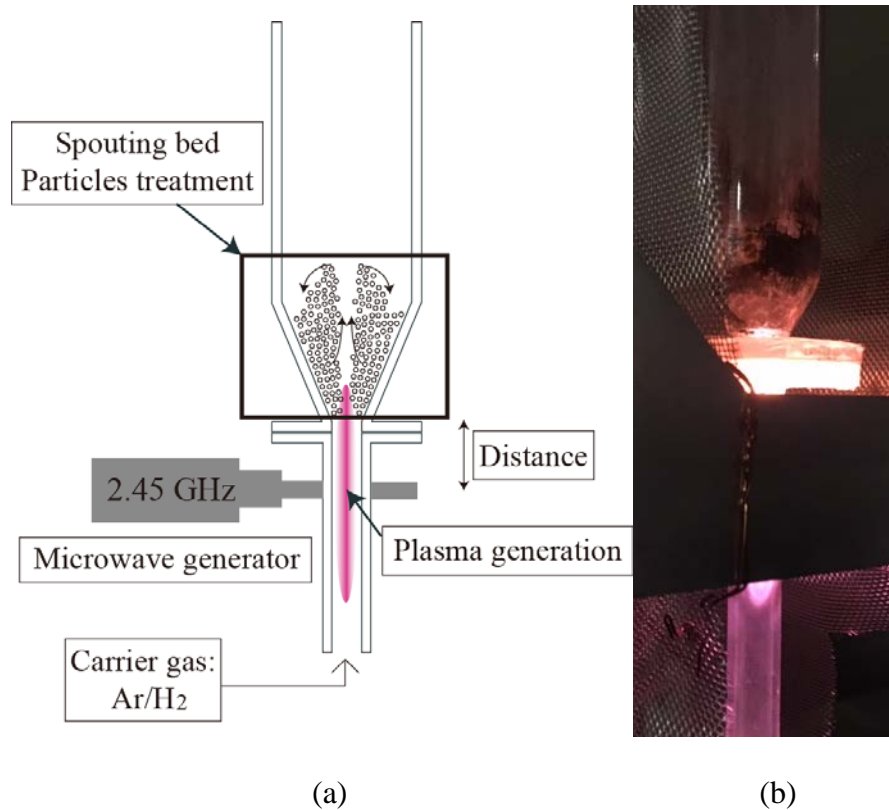


Fig. 2-4 (a) Enlarged view of the spouted bed and (b) a photograph of plasma in the spouted bed.

Depending on the types of carrier gas used, the plasma emitted different colors of light. The violet-colored plasma could be generated with Ar/H₂ carrier gas. The particles circulated by the carrier gas and the particles below the spouted bed were treated with plasma.

Fig. 2-5 shows a nozzle structure from a front side and an upper side of the plasma spouted bed. Each gas nozzle was connected tangentially to the quartz tube. Since the tangential gas flow induced an annular swirl gas flow, the minimum pressure could be localized to the center of the tube due to centrifugal forces, resulting in stable plasma generation. The quartz tube was fixed with silicone rubber for preventing gas leak.

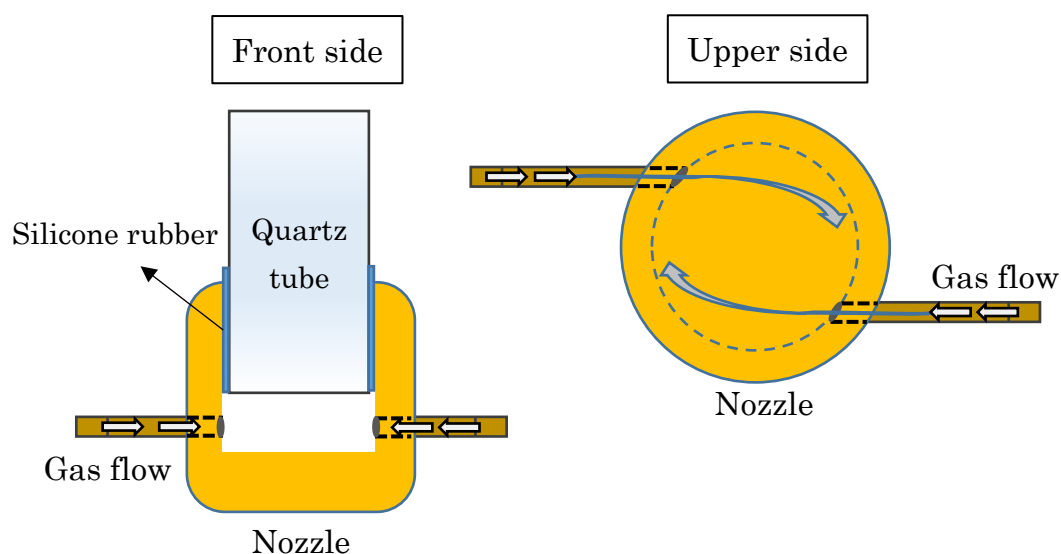


Fig. 2-5 The nozzle structure from a front side and an upper side of the plasma spouted bed.

The procedure of plasma generation combined with the spouted bed is as follows:

- <Step 1> The target particles were introduced from the upper side of the spouted bed. (Since the treatment was operated under atmospheric pressure, the upper side was opened)
- <Step 2> Ar gas was injected tangentially to the quartz tube and the target particles were spouted.
- <Step 3> The microwave generator was turned on and the power was supplied.
- <Step 4> A high frequency generator (BD-10A, Electro-technic products, Inc.) was operated for causing static electricity and Ar plasma was generated.
- <Step 5> H₂ gas was injected slowly to the quartz tube and the treatment was started.

Details of the treatment conditions for the plasma spouted bed are shown in Table 2-2. The treatment time and the output of the microwave generator were changed for the plasma spouted bed.

Table 2-2 Treatment conditions of the plasma spouted bed for aluminum hydroxide treatment.

Sample	Power (W)	Distance ¹ (cm)	Ar Flow Rate (L/min)	H ₂ Flow Rate (mL/min)	Treatment Time (min)	Mass (g)
PS-5	270	1.0	2.5	60	5	1.0
PS-10	270	1.0	2.5	60	10	1.0
PS-15	270	1.0	2.5	60	15	1.0
PS-25	270	1.0	2.5	60	25	1.0
PS-15W	385	1.0	2.5	60	15	1.0

¹ The distance from the waveguide and the particle bed shown in Fig. 2-4.

2.2.3 The fixed bed with the plasma irradiation

The schematic diagram of the fixed bed reactor with the plasma irradiation is shown in Fig. 2-6. The same apparatus (2.45 GHz microwave generator) was used for the plasma spouted bed. The quartz tube with an internal diameter of 9mm and a length of 20cm was used. Since the particle bed is fixed at the bottom with a quartz glass wool, the direction of gas insertion is reversed to bring plasma into direct contact with the particles which differ from the plasma spouted bed.

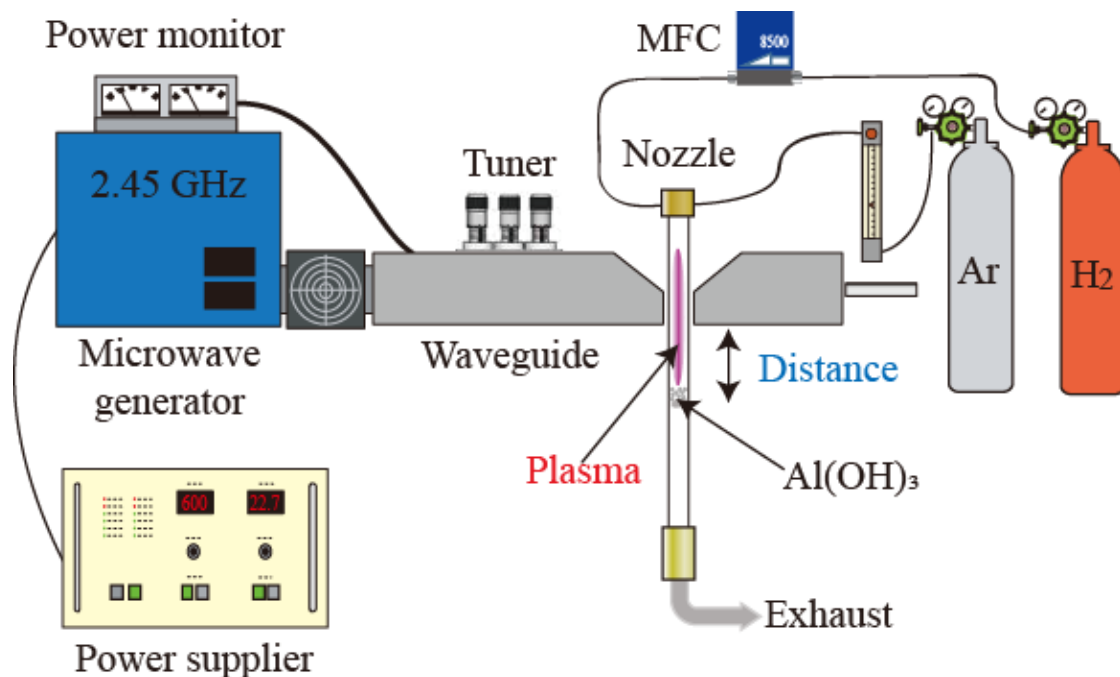


Fig. 2-6 Schematic diagram of the fixed bed with the plasma irradiation.

Details of the treatment conditions for the fixed bed with the plasma irradiation are shown in Table 2-3. The distance between the microwave waveguide and the particle bed was changed for the fixed bed with the plasma irradiation.

Table 2-3 Treatment conditions of the fixed bed with the plasma irradiation for aluminum hydroxide treatment.

Sample	Power (W)	Distance ¹ (cm)	Ar Flow Rate (L/min)	H ₂ Flow Rate (mL/min)	Treatment Time (min)	Mass (g)
PF-3	270	3.0	2.5	60	7	1.0
PF-5	270	5.0	2.5	60	15	1.0

¹ The distance from the waveguide and the particle bed shown in Fig. 2-6.

2.2.4 The electric furnace

As the typical thermal heat process, an electric furnace (ARFLC-30KC, Asahi Rika Seisakusho, Chiba, Japan) was used for treating aluminum hydroxide. The treatment temperature was changed for the treatment with the furnace. Details of the treatment conditions for the electric furnace treatment are shown in Table 2-4. For CM-number samples, the number indicates a heated temperature for aluminum hydroxide. For CM-1100', treatment time increases to 60min. The particles were suddenly injected to the furnace set to the 1100°C for CM-1100''. Moreover, the sample treated by the plasma spouted bed for 15min (PS-15) was followed by heating in the furnace at 1100°C for 60min, which correspond to PS-15-CM-1100'.

Table 2-4 Treatment conditions for the electric furnace.

Sample	Sample state	Temperature (°C)	Treatment Time (min)	Heat up rate (K/min)	Mass (g)
CM-500	Al(OH) ₃	500	15	20	1.0
CM-700	Al(OH) ₃	700	15	20	1.0
CM-900	Al(OH) ₃	900	15	20	1.0
CM-1100	Al(OH) ₃	1100	15	20	1.0
CM-1100'	Al(OH) ₃	1100	60	20	1.0
CM-1100''	Al(OH) ₃	1100	60	∞	1.0
PS-15-CM-1100'	PS-15(γ-Al ₂ O ₃)	1100	60	20	1.0

2.2.5 Particle characterization

The surface morphology of the catalyst was analyzed using scanning electron microscopy (SEM, Keyence VE-9800, Osaka, Japan). To investigate the crystallite phase of the catalyst, X-ray power diffraction (XRD) was performed using Cu K α radiation (40 kV, 15 mA, Rigaku Mini Flex 600, Tokyo, Japan). The diffraction patterns were recorded for 2θ values between 20° and 80° in 0.010° steps.

2.3 Result and discussion

2.3.1 Temperature measurement of the microwave induced plasma

An infrared thermometer (Chino IR-AH) has been used for the measurement of plasma temperature [46]. Due to its characteristics, it is difficult to accurately measure plasma temperature with a thermometer, however it can be used as an indicator for determining the effect of the plasma. The temperature of the plasma at two position (Upper region and Lower region) was measured as shown in Fig. 2-7. The upper region is the inlet of the spouted bed, while the lower region is the point where plasma is generated (the lower part of the plasma column). The actual temperature was expected to be higher than as measured because infrared radiation was transmitted through quartz glass. Photographs of the plasma and the values of the infrared thermometer at the lower and upper regions are shown in Fig. 2-8 and 2-9, respectively. Details of the treatment conditions and measured temperature are shown in Table 2-5 and 2-6, for the lower and upper regions, respectively. In the lower region, the temperature of the Ar/H $_2$ plasma was lower than that in the argon plasma, but the opposite result was obtained in the upper region. In the lower region, the energy supplied from the microwave generator was used

for the H_2 dissociation in plasma, which made the temperature lower than Ar plasma. On the other hand, in the upper region, the temperature change would be caused by an exothermic reaction due to the recombination of excited hydrogen atoms which plays an important role in the extinction process of plasma.

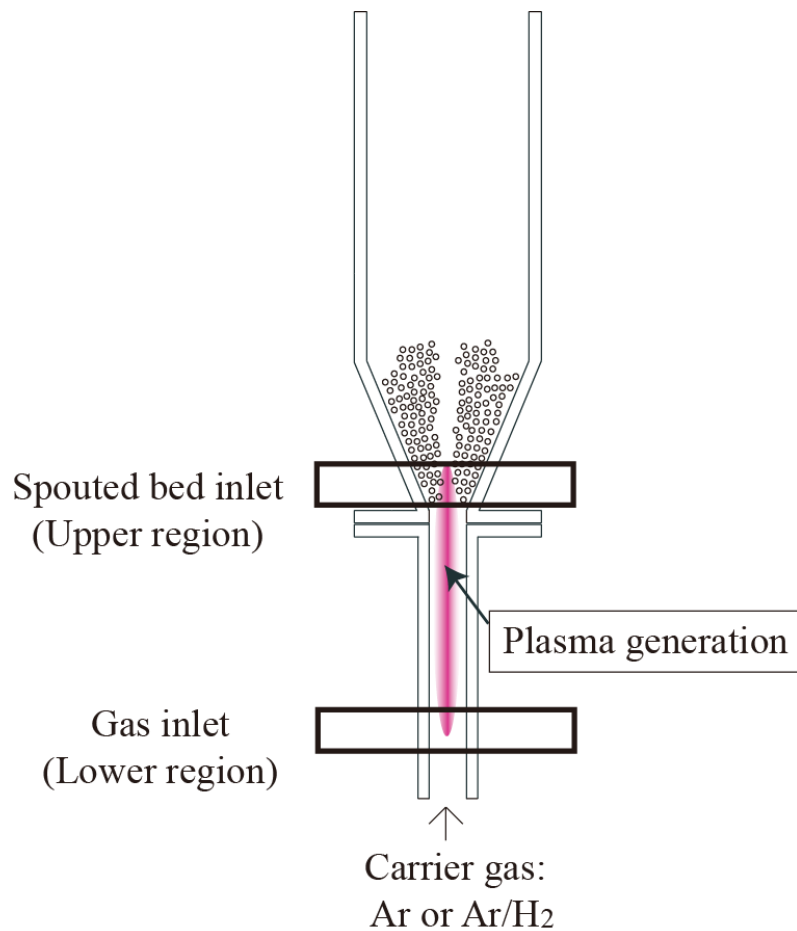


Fig. 2-7 Temperature measurement location of the plasma spouted bed for Ar and Ar/H₂ plasma by the infrared thermometer.

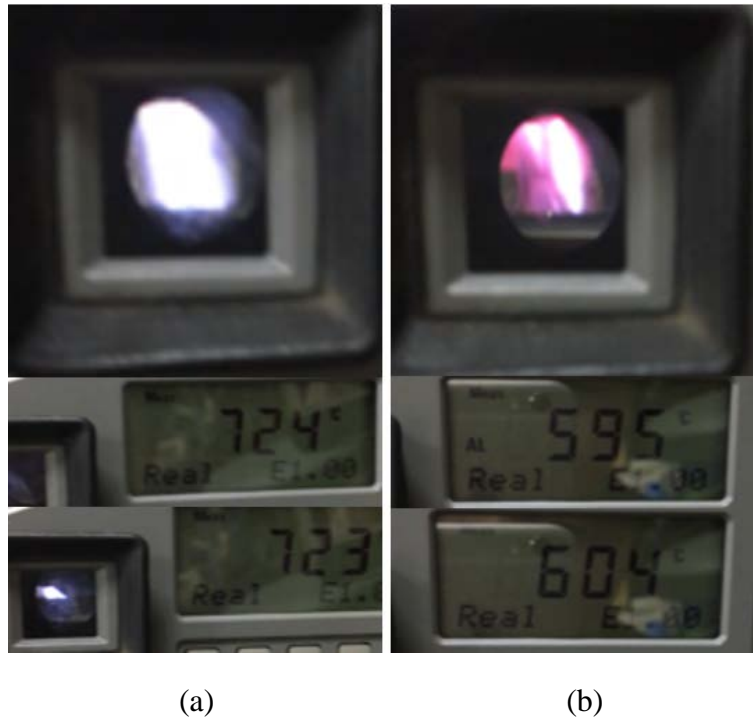


Fig. 2-8 Temperature measurement at the location of the lower region for (a) Ar plasma and (b) Ar/H₂ plasma by the infrared thermometer.

Table 2-5 Conditions for temperature measurement at the lower region for Ar plasma and Ar/H₂ plasma.

Gas	Power (W)	Distance ¹ (cm)	Ar Flow Rate (L/min)	H ₂ Flow Rate (mL/min)	Temperature (°C)
Ar	270	1.0	2.5	0	720±10
Ar&H ₂	270	1.0	2.5	60	600±10

¹ The distance from the waveguide and the particle bed in Fig. 2-4.



Fig. 2-9 Temperature measurement at the location of the upper region for (a) Ar plasma and (b) Ar/H₂ plasma by the infrared thermometer.

Table 2-6 Conditions for temperature measurement at the upper region for Ar plasma and Ar/H₂ plasma.

Gas	Power (W)	Distance¹ (cm)	Ar Flow Rate (L/min)	H₂ Flow Rate (mL/min)	Temperature (°C)
Ar	270	1.0	2.5	0	950±20
Ar&H ₂	270	1.0	2.5	60	1070±10

¹ The distance from the waveguide and the particle bed in Fig. 2-4.

2.3.2 Surface morphology by SEM

Fig. 2-10 (a) and (b) shows the surface morphology of original aluminum hydroxide. From the image, the surface is smooth and no crack was observed. From the grain boundary, crystallite with the size range from several tens of micros to several microns can be observed. Aluminum hydroxide derived fragments can be observed in some places.

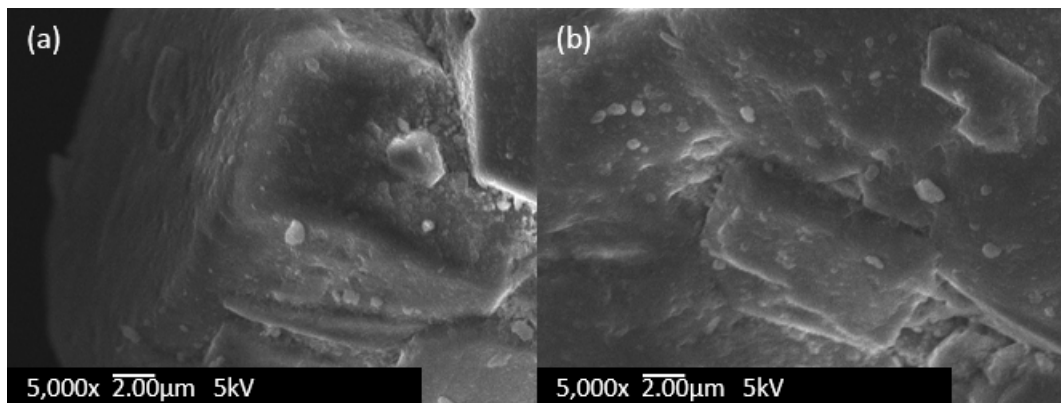


Fig. 2-10 SEM images of original aluminum hydroxide.

Fig. 2-11 shows SEM images of PS-5, PS-10, PS-15, and PS-25. The samples treated by the plasma spouted bed had numerous cracks on the surface. The damages on the surface increased with the treatment time i.g.5min<10min<15min<25min. These cracks might be derived from a large amount of water escaped from the materials during dehydration to form alumina as mentioned above. Exposure to high temperature circumstance lead to crystal structure change and also dehydration of free or chemically bonded water. When the external temperature increases, those free or chemically bonded water molecules included inside of alumina rapidly migrate towards the surface of alumina and escape. This phenomenon would cause cracking of the structure. It could

derive internal damage in the overall structure of alumina.

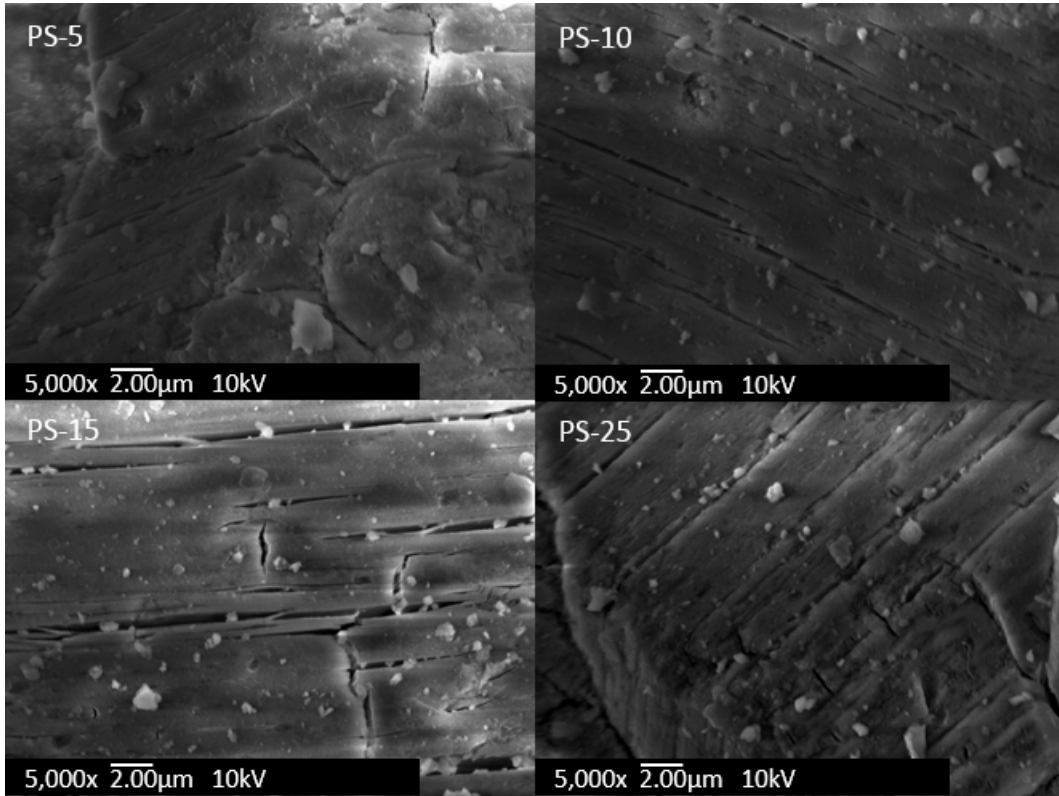


Fig. 2-11 SEM images of PS-5, PS-10, PS-15, and PS-25.

Fig. 2-12 shows SEM images of PS-15W. The surface morphology for PS-15W was entirely scratched even more than those of PS-25 (Fig. 2-12 PS-25). This indicates that the cracks on the surface could be affected more by the output of the microwave generator than treatment time in the plasma spouted bed.

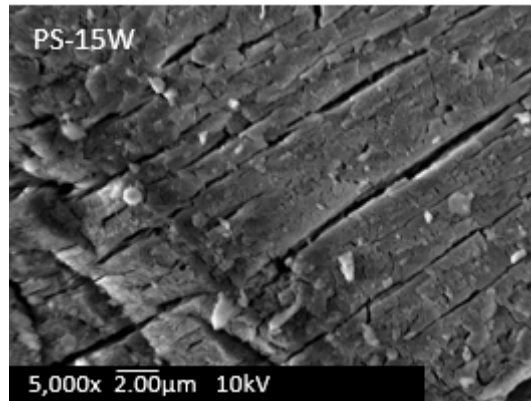


Fig. 2-12 SEM image of PS-15W.

Fig. 2-13 shows SEM images of PF-3 and PF-5. Cracks were also found on the surface of the sample treated in the fixed bed with the plasma irradiation. Although it was a short time, the effect of cracking was greater at shorter distances than that of at longer distances.

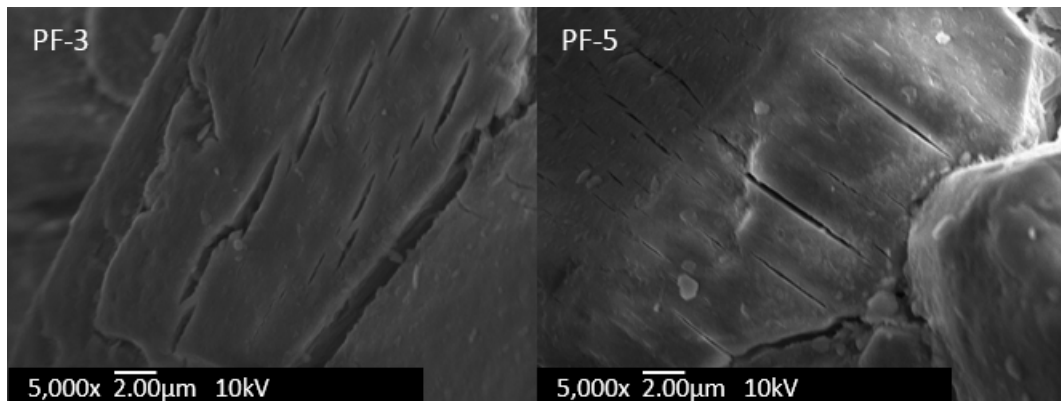


Fig. 2-13 SEM images of PF-3 and PF-5.

Fig. 2-14 shows SEM images of CM-500, CM-700, CM-900, and CM-1100. After temperature treatment at 500°C, slight amount of cracks and several microns of the fragments on the surface have been observed (Fig. 2-14 CM-500). The grain boundary of

alumina crystallite can be clearly distinguished. Temperature increase at 700°C, the number of cracks on the surface increased shown in Fig. 2-14 CM-700. The horizontal width has an expansion of cracks, and their number also increased with further increased temperature at 900°C and 1100°C, Fig. 2-14 CM-900 and CM-1100 respectively. From the investigation of the surface morphology heated by the electric furnace, it was observed that the higher the temperature, the more cracked on the surface.

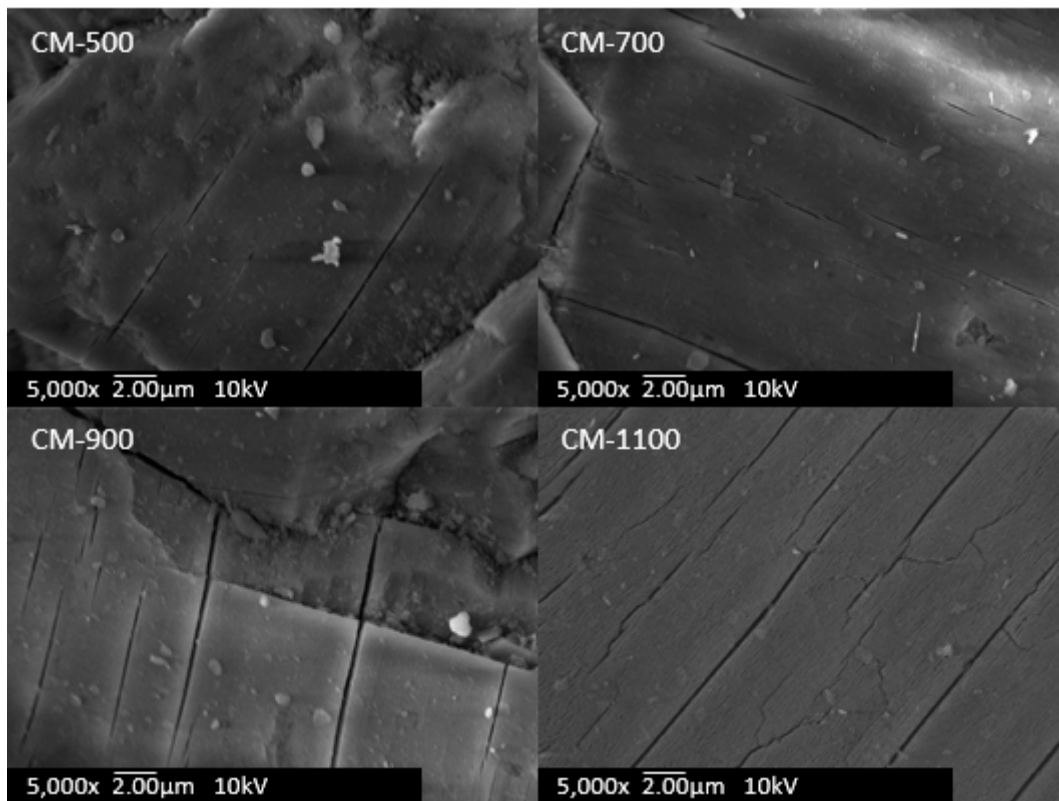


Fig. 2-14 SEM images of CM-500, CM-700, CM-900, and CM-1100.

To investigate the effect of heating time on cracking of the surface, treatment time increase to 60min at 1100°C, which shown in Fig. 2-15. The surface morphology for CM-1100' had a similar surface morphology as CM-1100. From this results, it can be concluded that the increase in heating time did not make much difference in surface

morphology.

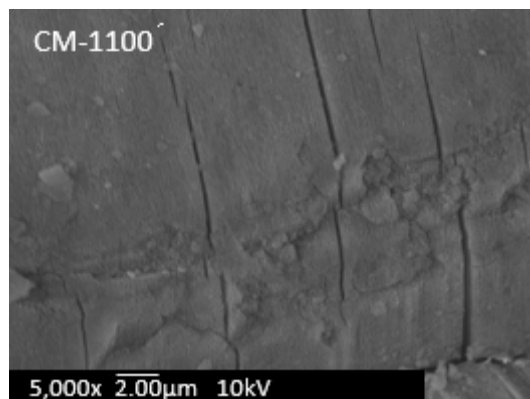


Fig. 2-15 SEM image of CM-1100'

Compared to plasma treated surface morphology (PS, PF), a little damaged surface and the narrow space width of cracks were observed with those of the furnace heated samples (CM). This indicates that water escape was more intense in PS and PF than in CM due to high temperature condition of the plasma.

2.3.3 Crystal structure analysis by XRD

Fig. 2-16 shows XRD pattern of PS-5, PS-10, PS-15, and PS-25. For PS-5, boehmite and γ -alumina were detected for a 5min treated sample. Boehmite (AlOOH) peaks can be detected at 28.0° , 38.6° , 48.7° , and 49.3° from JCPDS card, file No. 21-1307. The diffraction peaks for PS-10 and PS-15 showed no boehmite peaks and only the peaks corresponding to γ -alumina were detected. For PS-25, in addition to the peaks of γ -alumina, the peaks corresponding to α -alumina were also detected. It could be found that alumina decomposition proceeds with treatment time, and from 25min, the most stable phase of α -alumina was formed. Significantly, θ -alumina is an essential

intermediate in the transition pathway from γ -alumina to α -alumina, as described in Fig. 2-1 and Fig. 2-2. However, for PS-25, the diffraction peaks of γ -alumina and α -alumina co-existed without the detection of the peaks corresponding to θ -alumina.

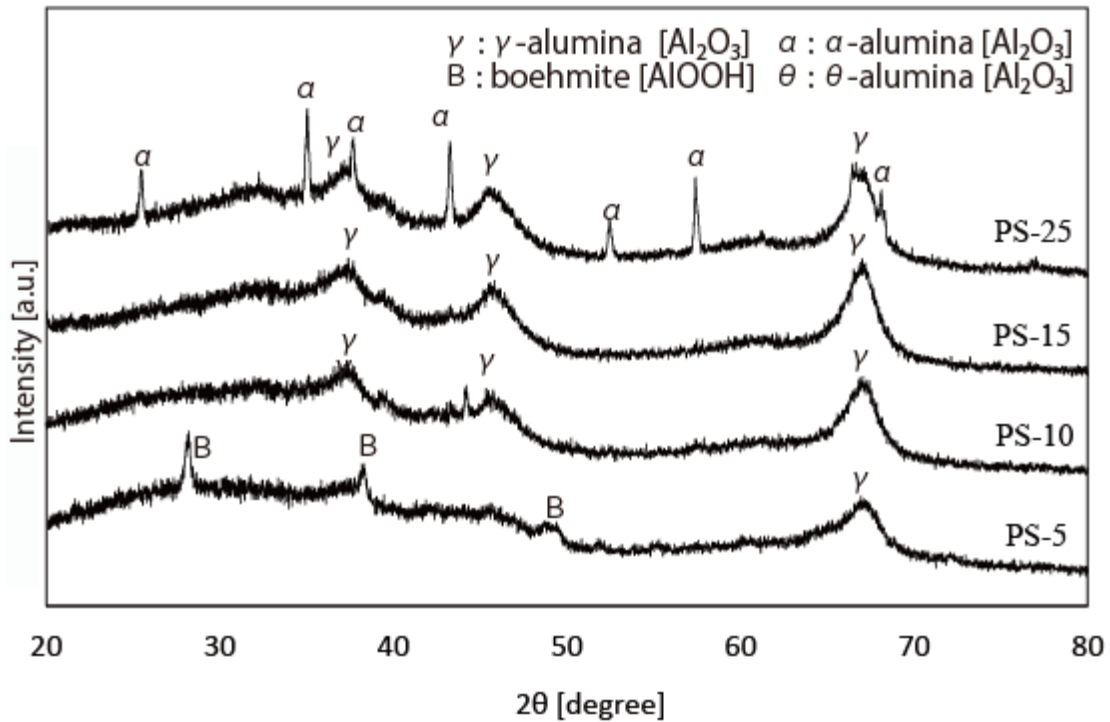


Fig. 2-16 XRD pattern of PS-5, PS-10, PS-15, and PS-25.

Fig. 2-17 shows XRD pattern of PS-15W. The peaks with sharp intensity of α -alumina were observed, and the peaks derived from γ -alumina were vaguely detected. Enhanced power could synthesize α -alumina in 15 min, even in a short period of treatment time and the peaks of θ -alumina were still not detected. The crystal structure of alumina treated by the plasma spouted bed would highly depend on the power of the microwave generator.

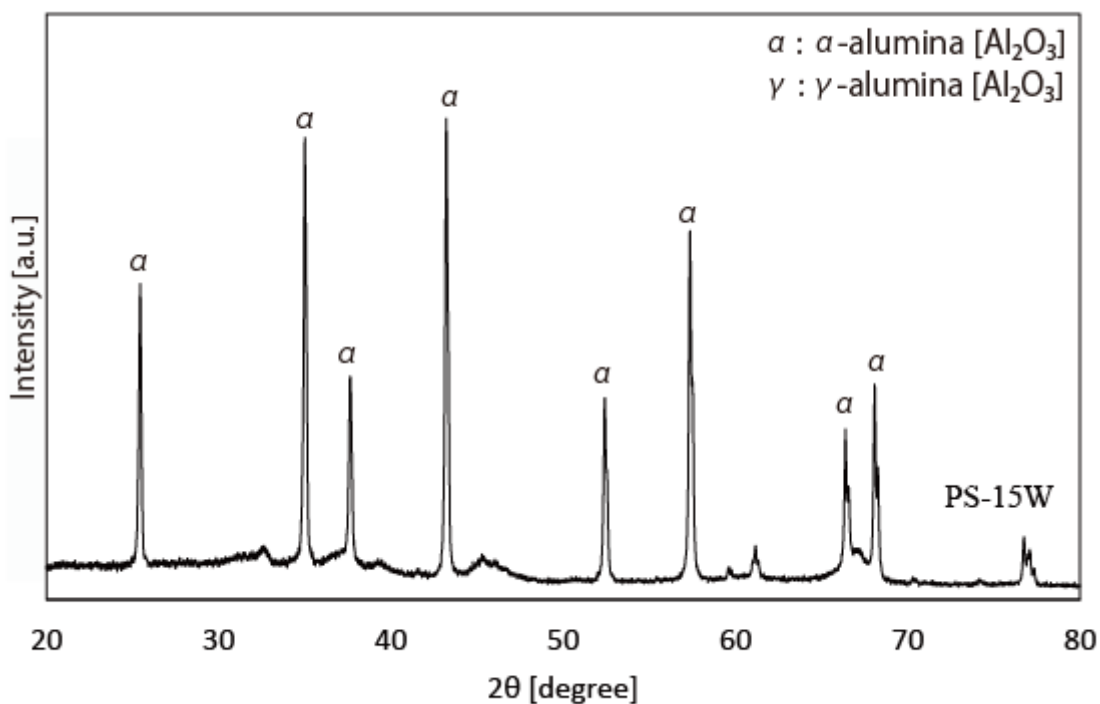


Fig. 2-17 XRD pattern of PS-15W.

Fig. 2-18 shows XRD pattern of PF-3 and PF-5. For PF-3, the similar diffraction patterns were obtained as those of PS-15W. The peaks of γ -alumina co-existed with those of α -alumina in the PF-1 sample. However, the peaks corresponding to θ -alumina were not detected. For PF-5, all aluminum hydroxide was transformed into γ -phase. The similar results were observed for PS-10 and PS-15. Thus, it was suggested that the spouted bed condition had not affected the transition behavior of aluminum hydroxide.

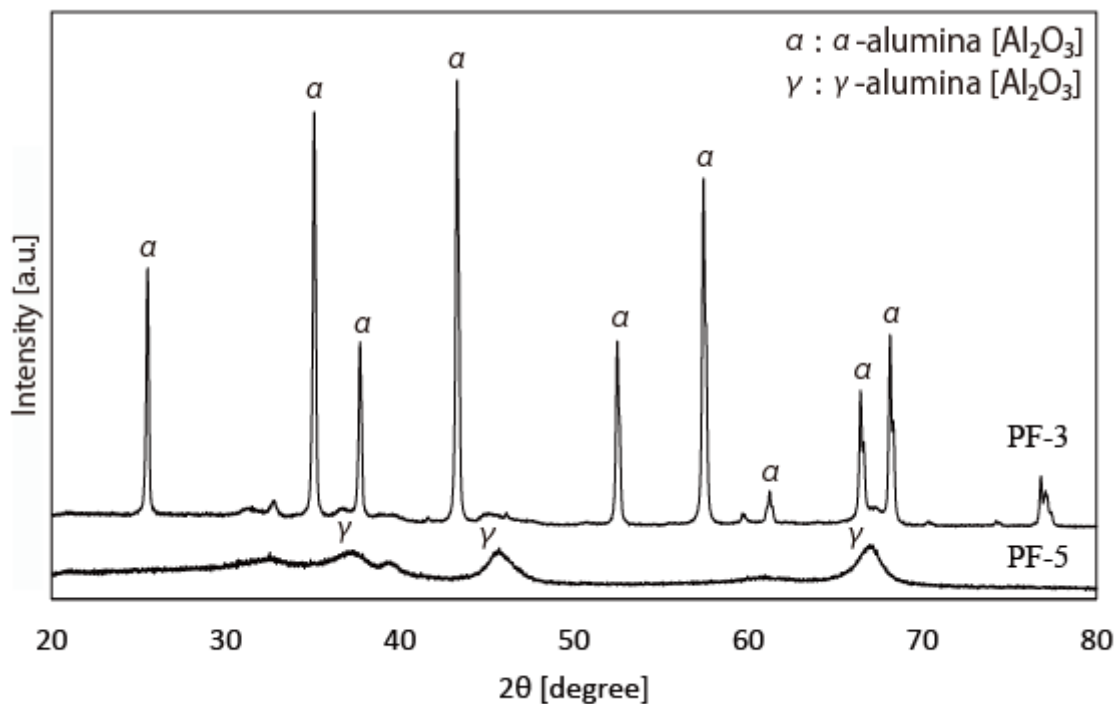


Fig. 2-18 XRD pattern of PF-3 and PF-5.

Fig. 2-19 shows XRD pattern of CM-500, CM-700, CM-900, CM-1100, and CM-1100'. For CM-500, aluminum hydroxide was not completely transformed into γ -alumina, and boehmite corresponding peaks were also observed. According to the reference shown in Fig. 2-1, boehmite (AlOOH) is produced between 200°C and 300°C , and γ -alumina is produced at approximately 300°C and above. This indicates that heating in an electric furnace for 15 minutes, was not enough for the transformation of all aluminum hydroxide to γ -alumina. For CM-700, all boehmite were decomposed into γ -alumina, and no other phase was observed. The same as CM-700, for CM-900, only the peaks corresponding to γ -alumina were observed. In contrast, for CM-1100, the peaks of θ -alumina were observed without α -alumina. This would be also because of the insufficient heating time. The peaks corresponding to α -alumina were detected by

increasing the heating time to 60min in CM-1100'. For CM-1100', intermediate state of θ -alumina was also detected as the same results as in Fig. 2-1. The typical thermal treatment could not derive the direct phase transformation from γ -alumina to α -alumina without θ -alumina. In conclusion, the decomposition pathway heated by the electric furnace gave the results in contrast to that of the plasma treatment (PS-25, PS-15W, and PF-1) despite the same aluminum hydroxide as the starting material.

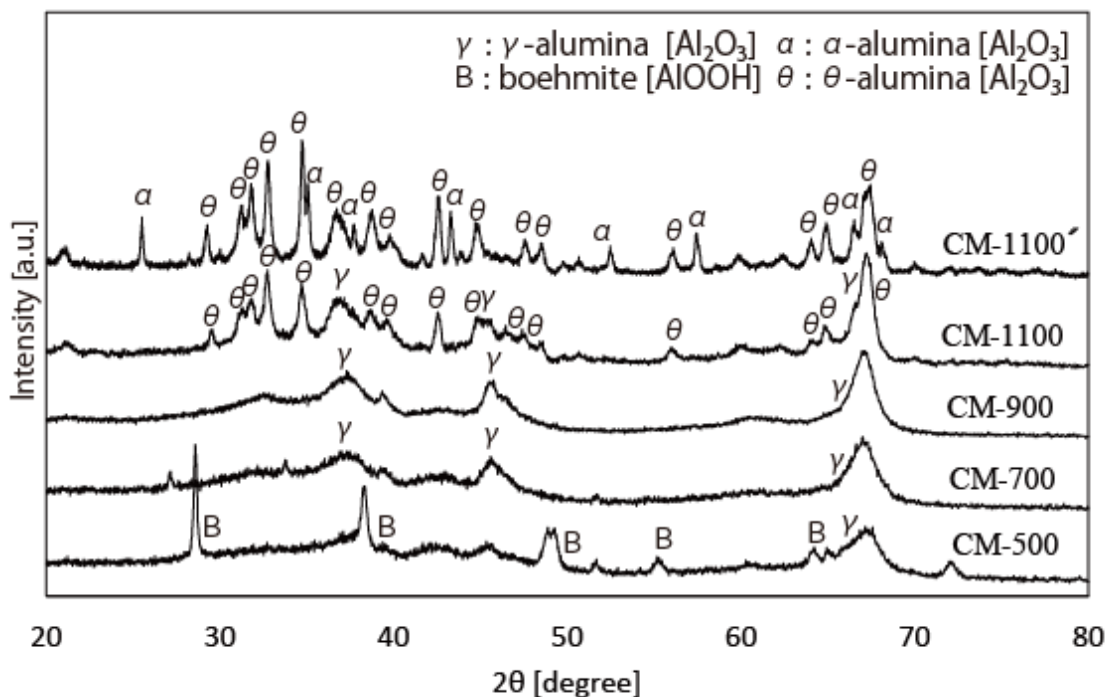


Fig. 2-19 XRD pattern of CM-500, CM-700, CM-900, CM-1100, and CM-1100'.

The main difference between the plasma treatment and the typical thermal treatment using the electric furnace is the presence of radicals and temperature condition. The high temperature condition of plasma as compared with that of the furnace could derive an exceedingly high heating rate. Thus, a rapid heat change of aluminum hydroxide

from the plasma treatment can be considered as one possibility for its transition behavior. For elucidating this effect, a similar temperature heating rate condition as that of PF and PS was made by introducing the particles into 1100°C of the furnace for 60 min which shown in Fig. 2-20. From the result, there was no difference from sample with the low heat up rate. The different pyrolysis processes between microwave induced plasma and typical thermal treatment using the electric furnace was suggested.

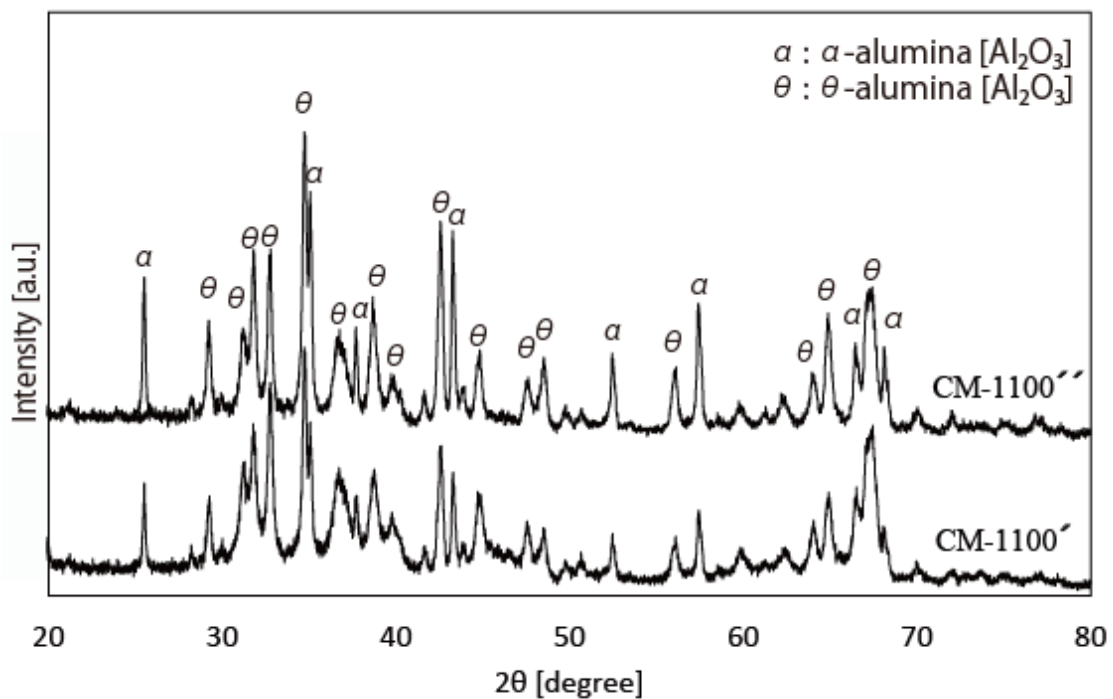


Fig. 2-20 XRD pattern of CM-1100' and CM-1100''.

Ball milling

Meanwhile, these decomposition behaviors ($\gamma \rightarrow \alpha$) could be obtained by the use of a planetary ball mill [47-50]. Fig. 2-21 shows the schematic diagram of a ball and powder motion in the single ball mill (a) and a pot motion in the planetary ball mill (b).

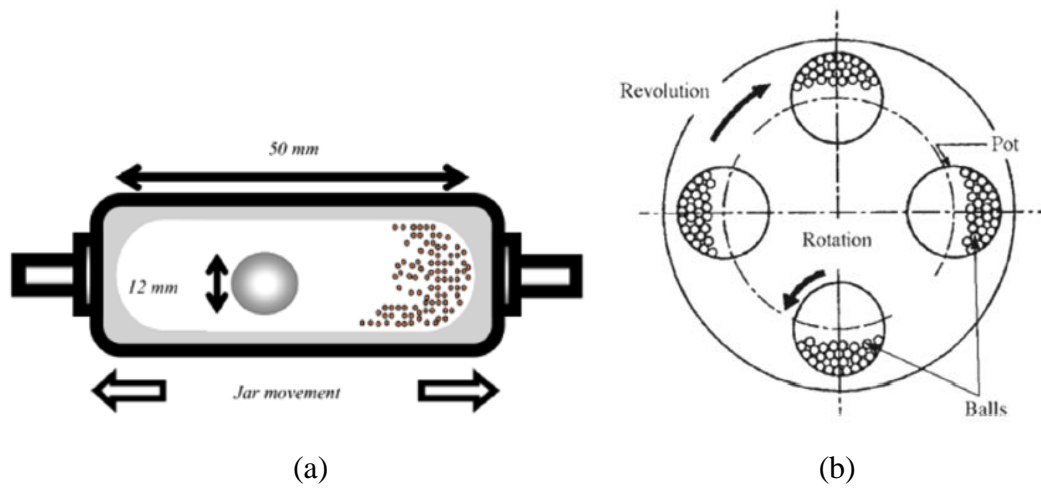


Fig. 2-21 Schematic diagram of (a) ball and powder motion in the single ball mill [51] and (b) pot motion in the planetary ball mill [47].

As a model powder, γ -alumina was used for the ball milling. They were attempting to derive direct transformation from γ -alumina to α -alumina only use for mechanochemical processes without thermal treatment. Fig. 2-22 shows the XRD pattern of sing ball mill (SBM) and planetary ball mill (PBM).

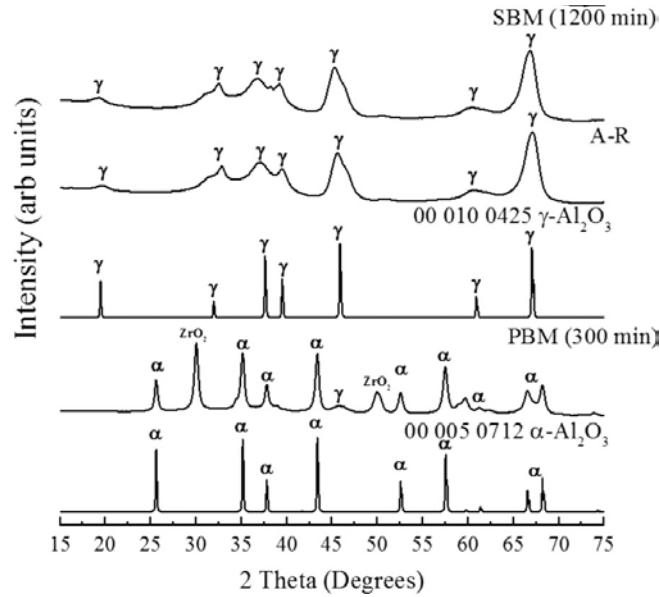


Fig. 2-22 as-received γ - Al_2O_3 and γ - Al_2O_3 after milling in SBM(1200min) and PBM(300min).

SBM for 1200 min didn't affect the crystal structure of γ -alumina. In contrast, pattern of PBM co-existed with γ -alumina and α -alumina phase. This indicates that the powder treated by PBM resulted in a change in the crystal structure inducing a phase transformation from the γ -alumina to the α -alumina. Typically, thermal heat treatment above 1100°C could change to α -alumina which is considered as the most thermodynamically stable state. Fig. 2-23 shows the crystal morphology of γ -alumina and α -alumina. An adequate amount of stress on the particles derives the crystal structure change from the cubic close packed structure to a hexagonally close packed structure [52]. Mechanochemical processes during milling also resulted in a transformation from γ -alumina to α -alumina without any observation of the essential intermediate state of θ -alumina as the same results when using the microwave induced plasma for the aluminum hydroxide treatment.

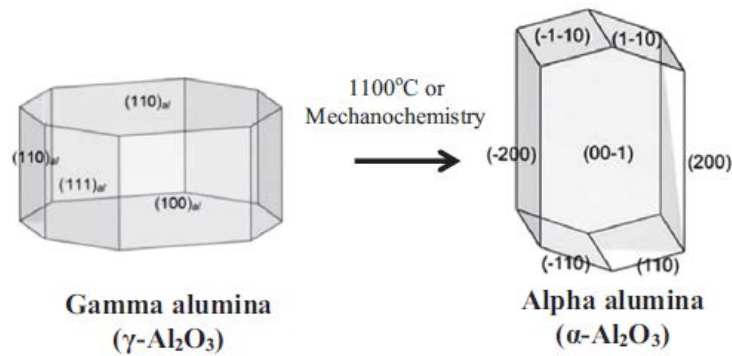


Fig. 2-23 Crystal morphologies for $\gamma\text{-Al}_2\text{O}_3$ and $\alpha\text{-Al}_2\text{O}_3$ [52].

It has been reported that α -alumina is produced by adding α -alumina seeds under conditions that cannot be produced by using a ball milling [53]. In their research, α -alumina seeds act as a nucleation for the occurrence of phase change of γ -alumina to α -alumina. Considering the possibility of nucleation when the plasma treatment occurred, the sample treated by plasma followed by typical heating with the electric furnace was investigated. Using the sample treated for 15 minutes in the plasma spouted bed, it was heated in the electric furnace at 1100°C for 60min and shown in Fig. 2-24. When compared with the typical treatment at 1100°C , the peaks corresponding to 29.2° , 31.8° , 35.2° , 42.7° , 48.6° , 56.2° , and 65.0° disappear in the sample of the plasma treatment followed by the furnace heating. From the results obtained here, although it could not be completely induced α -alumina, it was suggested that the plasma treatment could bring out the structural changes in some degree for γ -phase.

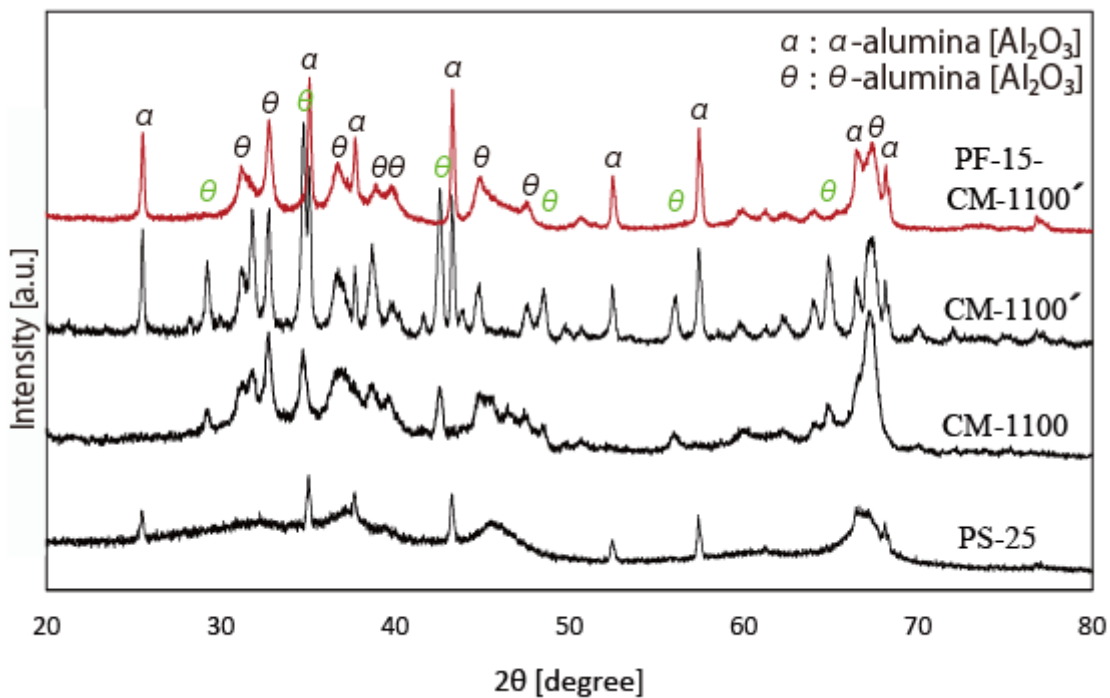


Fig. 2-24 XRD pattern of PF-15-CM-1100' (peaks with red color).

Unusual crystal structure transformation of alumina still might not be explained well for plasma treated samples. Although, the rationale for the transition behavior of alumina remains to be proven, the microwave induced plasma treatment showed the potential for the transition of a specific phase. In order to see how the plasma reactor affects the material, the catalytic reaction test was confirmed by impregnating nickel metal and palladium metal on aluminum hydroxide in chapter 3 and chapter 4, respectively.

2.4 Conclusion

In this chapter, the spouted bed combined with the microwave induced plasma irradiation was applied for the treatment of aluminum hydroxide in this work. For comparison, the plasma irradiation with the fixed bed and the typical thermal treatment using an electric furnace were also applied for the treatment of aluminum hydroxide. From the surface morphology of SEM, the plasma spouted bed and the fixed bed with the plasma irradiation differed in the degree of surface cracking. However there was no significant difference in the crystal structure change from XRD between the samples treated by the plasma spouted bed and the fixed bed with the plasma irradiation. In the electric furnace (CM) and the plasma irradiation (PS, PF), different decomposition pathway was observed in the transition of aluminum hydroxide. For the typical phase transition of aluminum hydroxide, θ -alumina is the essential intermediate phase, when converting γ -alumina into α -alumina. However, as shown in Fig. 2-25, the plasma treatment could derive the direct phase transformation from γ -alumina to α -alumina without θ -alumina, while typical thermal heat could not. A different kind of phase transition behavior has been suggested in the plasma irradiation and the typical thermal heating with the electric furnace during aluminum hydroxide treatment. The nature of the phase transitions information on alumina obtained from the experiments described here provides insights into the effects of the plasma spouted bed.

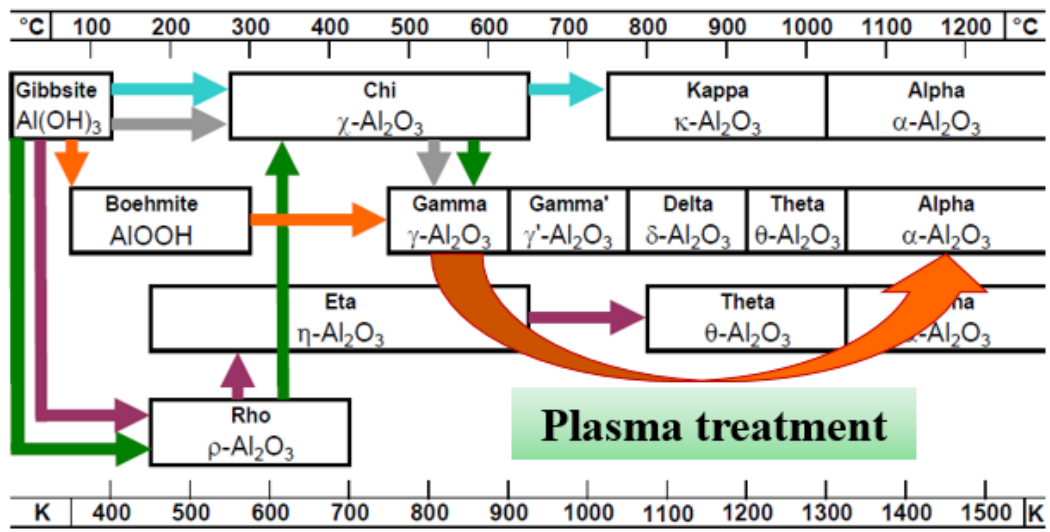


Fig. 2-25 Decomposition pathway of aluminum hydroxide treated by the plasma.

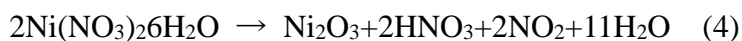
CHAPTER 3

**Preparation of Ni/Al₂O₃ with
microwave induced plasma jet**

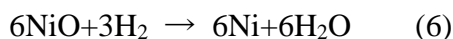
3.1 Introduction

A Ni-based catalyst has been widely used in industrial processes due to excellent catalytic performance, especially for hydrogenation reaction and low cost [54-57]. Ni metal has been generally supported onto alumina because of its ability to withstand reaction conditions and high specific surface [55]. Incipient wetness impregnation is the most widely used method for the preparation of the heterogeneous catalyst. The impregnation method involves three steps as follows: (1) impregnating metal solution on the support (2) drying the materials to remove the imbibed liquid and (3) activating the catalyst by calcination, reduction or other appropriate treatments [58].

In the calcination process by heating in an electric furnace, nickel nitrate undergoes moisture desorption and nitric acid decomposition by heating to form nickel oxide (III). By further raising the temperature, nickel oxide (III) becomes nickel oxide (II). Equations (4) and (5) show the respective reactions.



When the calcination is completed, the reaction of Equation (6) proceeds and nickel oxide is converted to metallic nickel by hydrogen reduction at a high temperature.



In the case of the plasma treatment, calcination and reduction were performed at the same time. It can be expected that the removal of nitric acid and impurities attached

to nickel and the reduction of nickel oxide would occur in one process. Fig. 3-1 shows the reaction mechanism when preparing nickel-supported alumina with plasma.

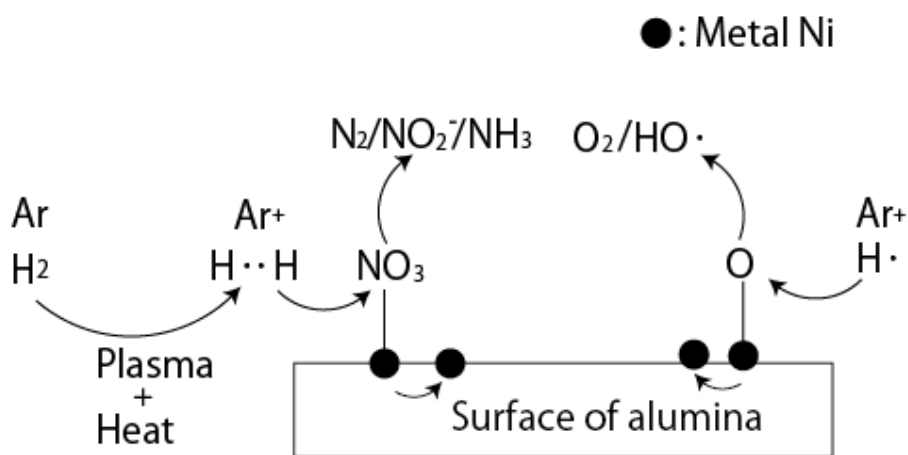


Fig. 3-1 Reduction mechanism of Ni/Al₂O₃ with hydrogen radical induced by microwave plasma.

The electrons accelerated by the microwave collide with hydrogen to generate hydrogen radicals. Heat and radicals contained in plasma can decompose nickel nitrate and remove impurities on the surface. Moreover, since it has excellent reducibility than hydrogen gas, the reduction of oxidized nickel can be promoted. In the electric furnace heating treatment, the decomposition and reduction of nickel nitrate can be promoted only by the heat; however, in the case of the plasma, in addition to the heat, the effect of highly reducible hydrogen radicals can be expected. Generally, the typical preparation of the catalyst takes several hours to several tens of hours. In contrast, when plasma is used, the treatment time could be shortened and improvement of catalytic performance also could be expected.

3.2 Experimental set-up

3.2.1 Catalyst preparation & treatment conditions

Three preparation methods were applied for the Ni/Al₂O₃ catalyst: a fixed particle bed with plasma irradiation (PF), a plasma spouted bed reactor (PS), and the conventional method (CM). The precursor of the Ni/Al₂O₃ catalyst containing 15 wt% of Ni was prepared according to the following procedure:

- <Step 1> Al(OH)₃ powder was added into nickel nitrate aqueous.
- <Step 2> The solution was dried at 80°C until slurry-like
- <Step 3> The slurry was dried at 110°C for 12 hours and was crushed with the size of 250-595 μm

The crushed particles were then treated by three preparation methods, specifically PF, the PS, and the CM as follows:

- <Step 4 (PF)> The crushed particles were treated in the plasma using the fixed bed under the following plasma conditions: power = 270 W, Ar flow rate = 2.5 L/min, H₂ flow rate = 60 mL/min, and treatment time = 15 min.
- <Step 4 (PS)> The crushed particles were treated using the plasma spouted bed reactor with the same plasma conditions as those used in PF.
- <Step 4 (CM)> In the same way as in PF, the crushed particles were heated to 500°C, 700°C or 900°C using the electric furnace with a 16.7% H₂/Ar mixture for 2 h.

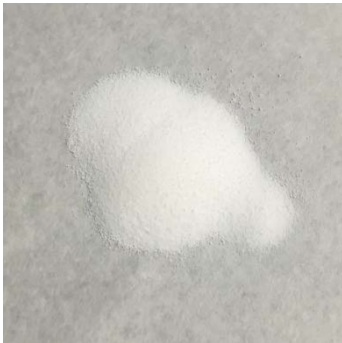
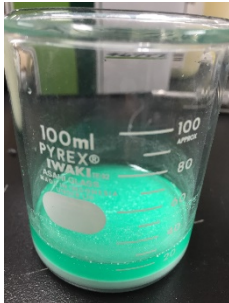

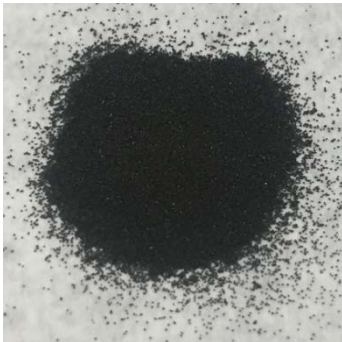
Details of the treatment conditions for the PF, the PS, and the CM are shown in Table 3-1. Table 3-1 illustrates that the distance between the microwave waveguide and the particle bed was changed for PF, while the treatment temperature was changed for the CM. Table 3-2 shows feedstock, aluminum hydroxide, and Ni-based alumina catalyst.

Table 3-1 Treatment conditions of the fixed bed with plasma irradiation (PF) and the plasma spouted bed (PS) for catalyst preparation.

Catalyst	Power (W)	Distance¹ (cm)	Ar Flow Rate (L/min)	H₂ Flow Rate (mL/min)	Treatment Time (min)	Mass (g)
PF-1	270	3.0	2.5	60	7	1.0
PF-2	270	5.0	2.5	60	15	1.0
PS	270	1.0	2.5	60	15	1.0

¹ The distance from the waveguide and the particle bed shown in chapter 2.

Table 3-2 Feedstock, aluminum hydroxide, and Ni-based alumina catalyst.

<p>Aluminum hydroxide</p>		<p>Nippon Light Metal Company, Ltd. SB93-809 Powder (<100 μm)</p>
<p>Aluminum hydroxide added nickel nitrate aqueous solution</p>		<p>Solution</p>
<p>Crushed particles used for PS, PF, and CM</p>		<p>Before reduction</p>
<p>Prepared catalyst</p>		<p>Ni/Al₂O₃ In-lab prepared</p>

3.2.2 Catalyst evaluation (Ethylene hydrogenation)

A stainless reactor of 6 mm id (internal diameter) with a temperature-programmed electric furnace was used for the acetylene hydrogenation reaction. The Schematic diagram of the reactor for catalytic activity is shown in Fig. 3-2.

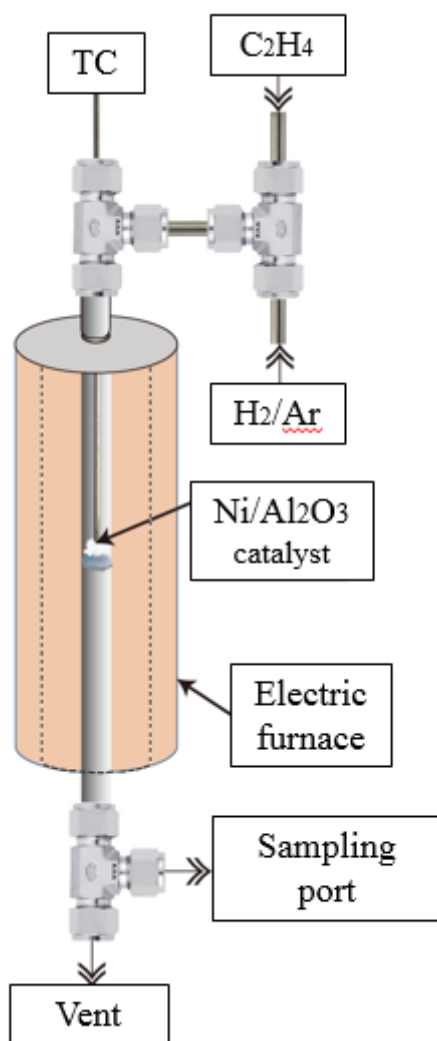


Fig. 3-2 Schematic diagram of the catalytic activity system.

For each test, the reaction temperature was set to 250°C, and 20 mg of the Ni/Al₂O₃ catalyst was added to the middle of the reactor. The gas was then fed into the

reactor at flow rates of 20 mL/min (C₂H₄), 80 mL/min (H₂), and 200 mL/min (Ar). The gas space velocity was 320,000 h⁻¹. The produced gas was extracted from the sampling port and quantitatively analyzed using a gas chromatograph (Shimadzu GC-8APF, Kyoto, Japan). Hydrogenation of ethylene is a simple reaction to produce ethane. However, on heating, dehydrogenation and hydrogen desorption usually occur, accompanied by the formation of several products such as ethylidyne, methylidyne groups, and vinyl species. [59, 60] Eventually, those products desorbed as CH₄. Those C-C cleavage reaction can happen over 540K and methane can be formed. [61, 62]. C-C bond breaking is kinetically hindered at low surface temperatures. At 250°C is chosen for methane formation.

The experimental results indicated that the produced gas consisted of ethylene, ethane, methane, and hydrogen. Thus, to evaluate catalyst activity, ethylene conversion and methane selectivity were calculated as follows:

$$\text{C}_2\text{H}_4 \text{ conversion (\%)} = \left(\frac{\text{C}_2\text{H}_4(\text{Feed}) - \text{C}_2\text{H}_4}{\text{C}_2\text{H}_4(\text{Feed})} \right) \times 100 \quad (7)$$

$$\text{CH}_4 \text{ selectivity (\%)} = \left(\frac{\text{CH}_4}{\text{C}_2\text{H}_4(\text{Feed}) - \text{C}_2\text{H}_4} \right) \times 100 \quad (8)$$

3.2.3 Catalyst characterization

The catalyst prepared using three different methods indicated above was examined using the following analyses. The surface morphology of the catalyst was analyzed using scanning electron microscopy (SEM, Keyence VE-9800, Osaka, Japan). Energy-dispersive X-ray spectroscopy (EDS, Genesis XM2, EDAX, NJ, USA) combined with SEM was performed to determine the distribution of Ni metal on the alumina support. To investigate the crystallite phase of the catalyst, X-ray power diffraction (XRD) was performed using Cu K α radiation (40 kV, 15 mA, Rigaku Mini Flex 600, Tokyo, Japan). The diffraction patterns were recorded for 2θ values between 20° and 80° in 0.010° steps. Field-emission transmission electron microscope (FE-TEM) measurements were carried out using JEOL JEM-2010F (Tokyo, Japan) The crystal planes of Ni on the catalyst were confirmed using FE-TEM. Ni metal dispersion and crystallite size were analyzed using H $_2$ chemisorption (Quantachrome ChemBET Pulsar, Boynton beach, FL, USA). H $_2$ can undergo dissociative absorption on a Ni surface at room temperature. The dispersion of Ni on the surface of the catalyst was estimated from the amount of H $_2$ adsorbed, assuming a Ni/H $_2$ stoichiometry of 2. H $_2$ chemisorption was conducted under the following conditions. The Ni/Al $_2$ O $_3$ catalyst was reduced at a temperature of 573 K for 1 h, and hydrogen was flushed out under a N $_2$ atmosphere for 30 min at the same temperature as a pretreatment [63]. The measurements were then performed at 300 K under a N $_2$ atmosphere with a pure H $_2$ pulse flow.

3.3 Result and discussion

3.3.1 Surface morphology by SEM

Compared to the surface of the alumina support only in chapter 2, nickel-based substances would be expected to be confirmed on the alumina surface for all of the Ni/Al₂O₃ catalyst samples. Fig. 3-3 and 3-4 show SEM images of the Ni/Al₂O₃ catalysts prepared by the microwave induced plasma (PF, PS), and heated by the typical thermal treatment using the electric furnace (CM), respectively.

From the surface morphology of the Ni/Al₂O₃ catalyst samples, the large number of agglomerated particles and structural inhomogeneities on the alumina support can be observed. Those are Ni derived particles with the size range from several hundreds of nanometer to several microns. Ni agglomerations covered a large part of the surface of the alumina support because of a high impregnation percent of 15% (Ni/Al₂O₃). The particles and the surface didn't show any effect from the charge up of the apparatus. Sphere shape grain with the size less than micron can be seen on the surface of the PF-1 (Fig. 3-3 PF-1 a-b). High temperature condition derived from a closer distance between the particle and the cavity with the fixed bed causes the Ni agglomerate structure change. For PF-1, the surface was cracked at several places in accordance with the results of the plasma treatment of aluminum hydroxide.

PF-2, further distance between the particle and the cavity showed relatively similar surface morphology as that of CM-700 and CM-900. The structure of Ni agglomerate in PF-1 showed different compared with those of other catalysts, which indicates the distance between the particle and the cavity is an important factor to decide the structure of Ni agglomerate. The effect on agglomerate was maximized on PF-1. For PS sample, the cracking of the surface can be observed for several places. It had more

cracking than any other sample. The closest distance could induce more cracking deriving the rapid heat transfer in the plasma spouted bed. However, the structure of Ni agglomerate was similar to CM-700, CM-900, and PF-2 samples. This indicates that even the closest distance between the particle and the cavity with 1cm, the circulation process in the spouted bed could prevent the agglomeration of Ni on the particles.

For CM-500 (Fig. 3-4 CM-500 a-b), the surface of the alumina support also had several cracks but relatively smoother than any other samples, which has a similar tendency of thermal treatment of aluminum hydroxide itself. Fragments like structure of Ni agglomerations in CM-500 was changed to a strongly crystallized structure at higher temperature condition on CM-700 (Fig. 3-4 CM-700 a-b). Further temperature rise made the shape of Ni agglomeration to a round shape structure (Fig. 3-4 CM-900 a-b). This is because migration at high temperature could occur. Particles' migration made it start the sintering, allowing larger crystallographic agglomerate.

Fig. 3-5 shows SEM image and SEM-EDS mapping of PF-1 and CM-500 at the same position. On SEM-EDS mapping, red light scattering indicates Ni derived particles. Due to high impregnation rate of Ni with 15%, the whole surface of the alumina was covered by nickel. This results show that not only nickel agglomeration but also nickel particles were homogeneously dispersed on the surface of whole alumina support.

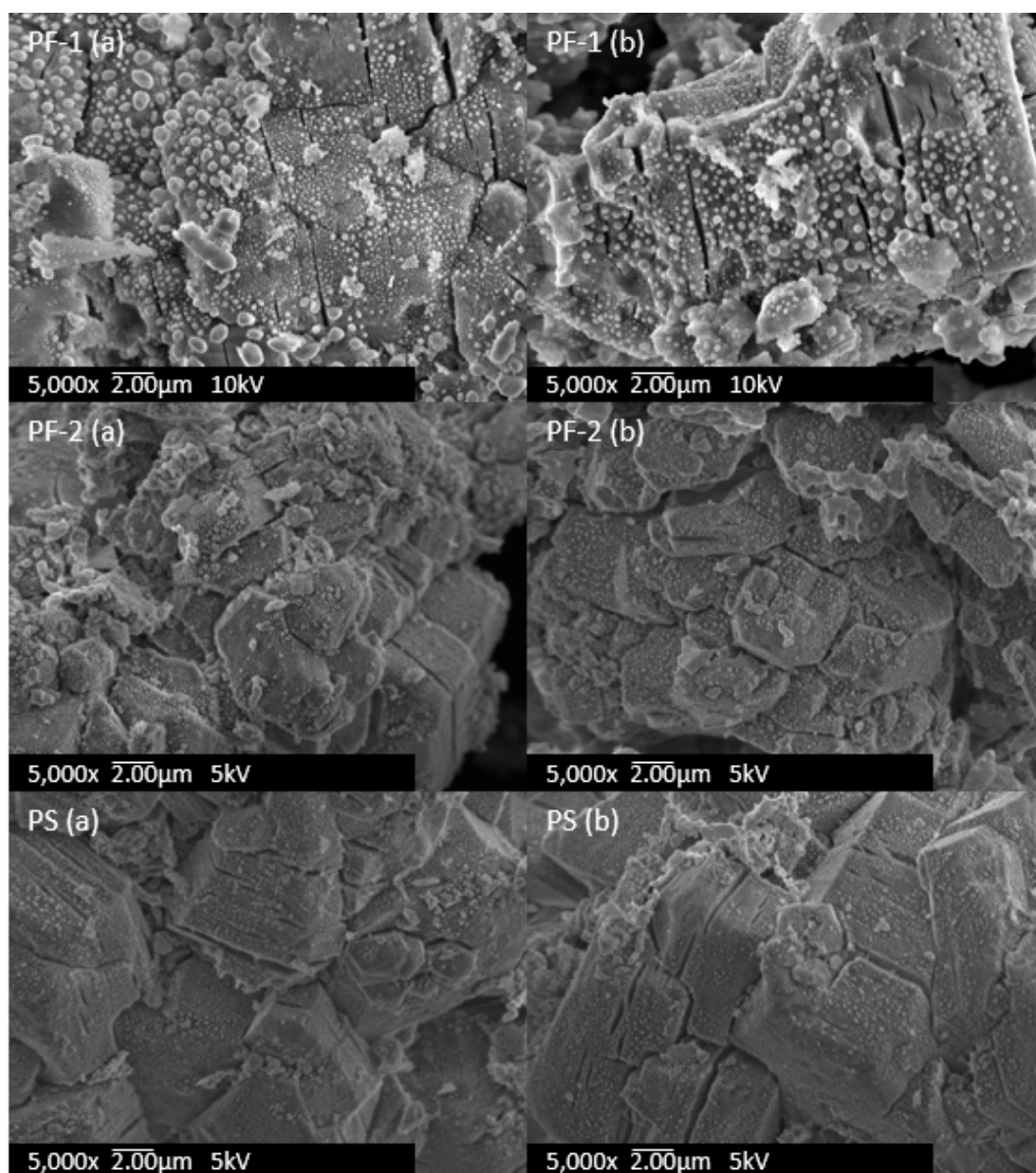


Fig. 3-3 SEM images of the Ni/Al₂O₃ catalysts prepared by the fixed bed with plasma irradiation and the plasma spouted bed.

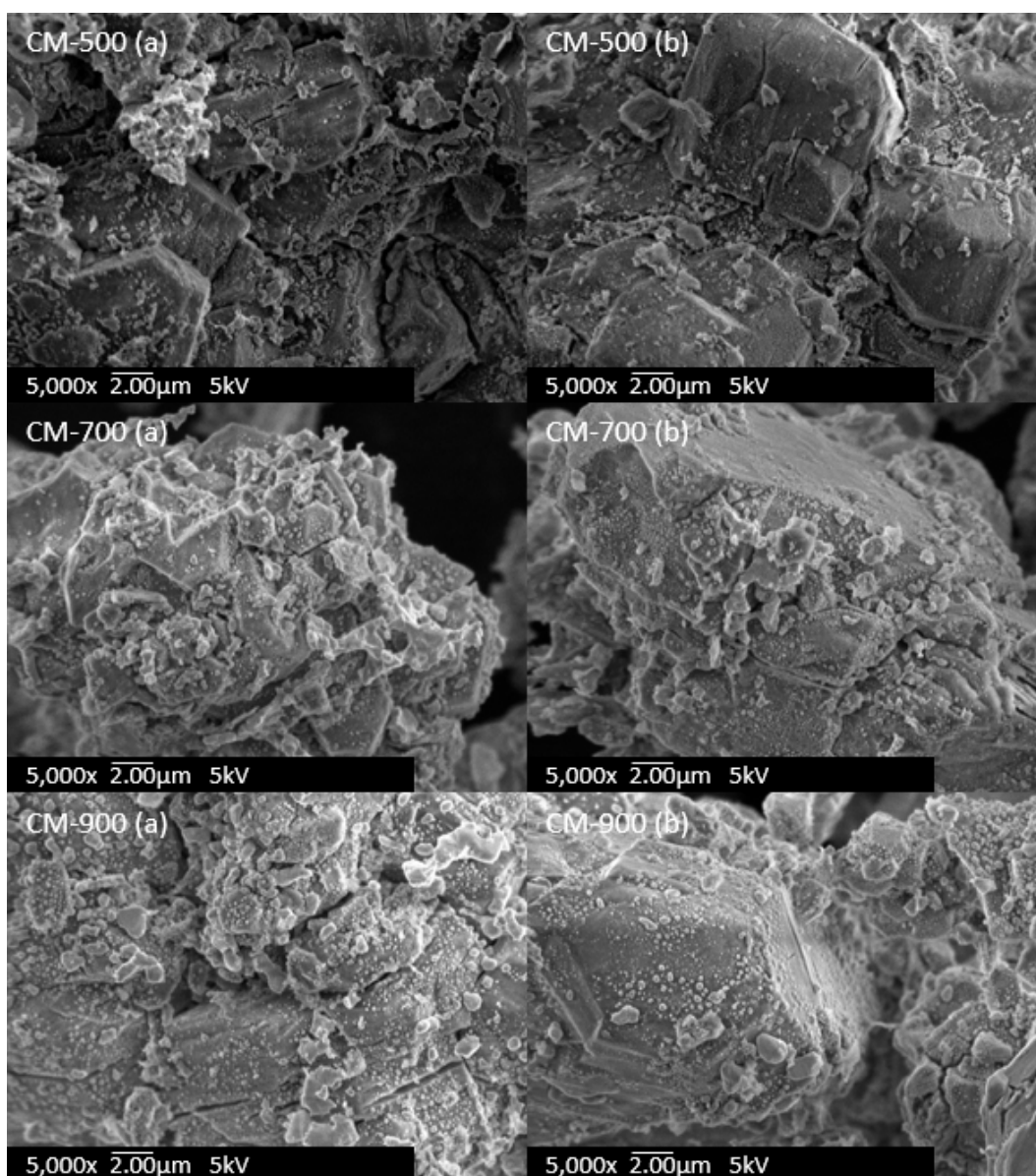


Fig. 3-4 SEM images of the Ni/Al₂O₃ catalysts prepared by the typical thermal treatment using the electric furnace.

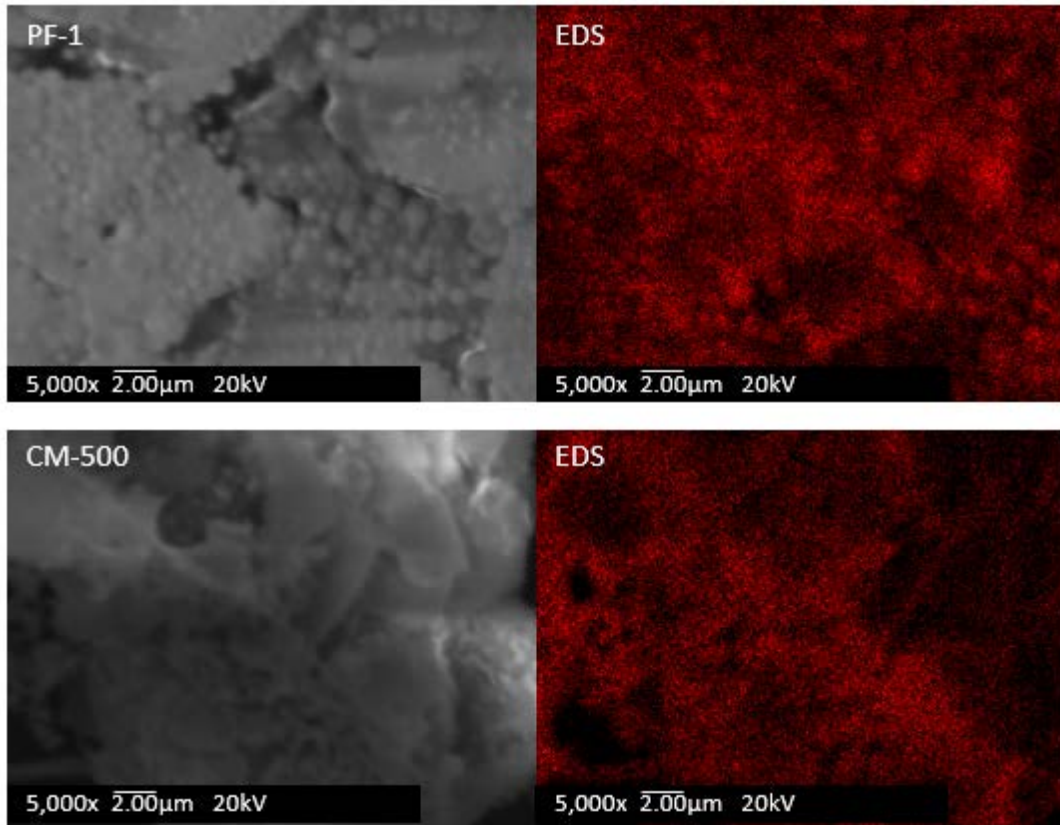


Fig. 3-5 SEM and EDS images of PF-1 and CM-500.

3.3.2 Crystal structure analysis by XRD

The peaks (2θ) of Ni are corresponding to 44.5° , 51.8° , and 76.4° , that can be assigned to the (111), (200), and (200), respectively (JCPDS card no. 04-0850), while the peaks (2θ) of NiO arrays are observed at 37.3° , 43.3° , and 62.9° , which can be assigned to the (110), (200), and (220) planes of cubic NiO, respectively (JCPDS card no. 47-1049). Fig. 3-6 shows Ni impregnated aluminum hydroxide before the reduction step. The peaks derived from Ni-based precursor are shown as compared with aluminum hydroxide, which assigned to the range of 20° to 35° , and no NiO or Ni peaks were detected.

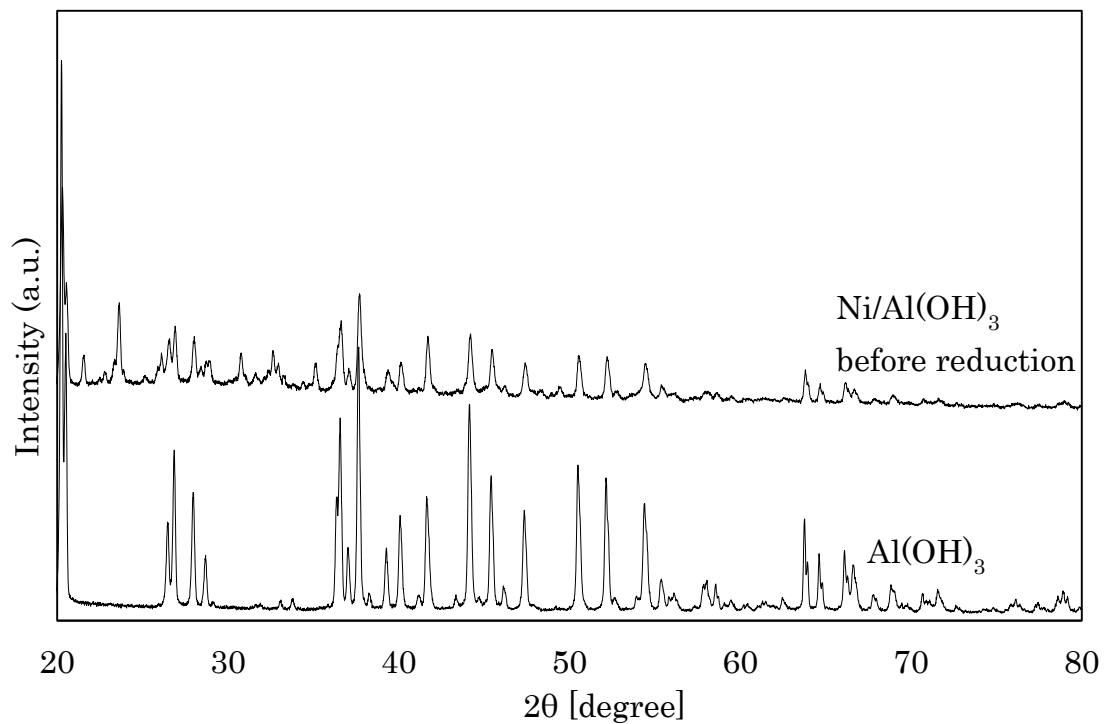
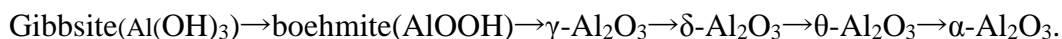


Fig. 3-6 XRD pattern of impregnated Ni/Al(OH)₃ before reduction and original aluminum hydroxide.

Fig. 3-7 shows the Ni/Al₂O₃ catalysts treated by the plasma with the fixed particle bed and the spouted bed (PF-1, PF-2, and PS) for the reduction. For all of the plasma treated samples, sharp intensities corresponding to Ni (111), Ni (200), and Ni (220) were observed at 44.5°, 51.8°, and 76.4°, respectively.

Fig. 3-8 shows the Ni/Al₂O₃ catalysts reduced by the typical heat treatment using electric furnace (CM-500, CM-700, and CM-900). The same as those of plasma treatment, peaks indicating Ni (111), Ni (200), and Ni (220) were detected, which correspond to 44.5°, 51.8°, and 76.4°, respectively. Fig. 3-9 shows the enlarged peaks range from 60.0° to 70.0° of CM-500 and CM-700 for detecting γ -alumina and those peaks corresponding to γ -alumina were detected.

For all of the catalysts, the crystalline phase of γ -alumina was detected at one value, 67.2° (JCPDS card, file No. 10-0425). The diffraction peaks (2 θ) at 25.6°, 35.1°, 37.8°, 43.4°, and 52.6° corresponded to the α -alumina peak (JCPDS card, file No. 46-1212). Only the PF-1 sample demonstrated an α -alumina phase. It is generally accepted that aluminum hydroxide cycles through various intermediate phases of alumina before it reaches its final state (α -alumina) with increasing temperature. As mentioned in chapter 2, aluminum hydroxide has numerous decomposition pathways after it has transitioned into α -alumina. These depend on several parameters including temperature, heating rate, and particle size. The following pathway is the most common for aluminum hydroxide decomposition and was also observed in our work when using the electric furnace:



The peaks of γ -alumina coexisted with those of α -alumina in the PF-1 sample. However, the peaks corresponding to θ -alumina were not detected. Significantly, θ -alumina is an essential intermediate in the transition pathway from γ -alumina to α -

alumina. A typical thermal treatment could not derive the direct phase transformation from γ -alumina to α -alumina without θ -alumina. The other samples did not reach the temperature at which θ -alumina formed. It is expected that those results could derive different catalytic performance between each sample.

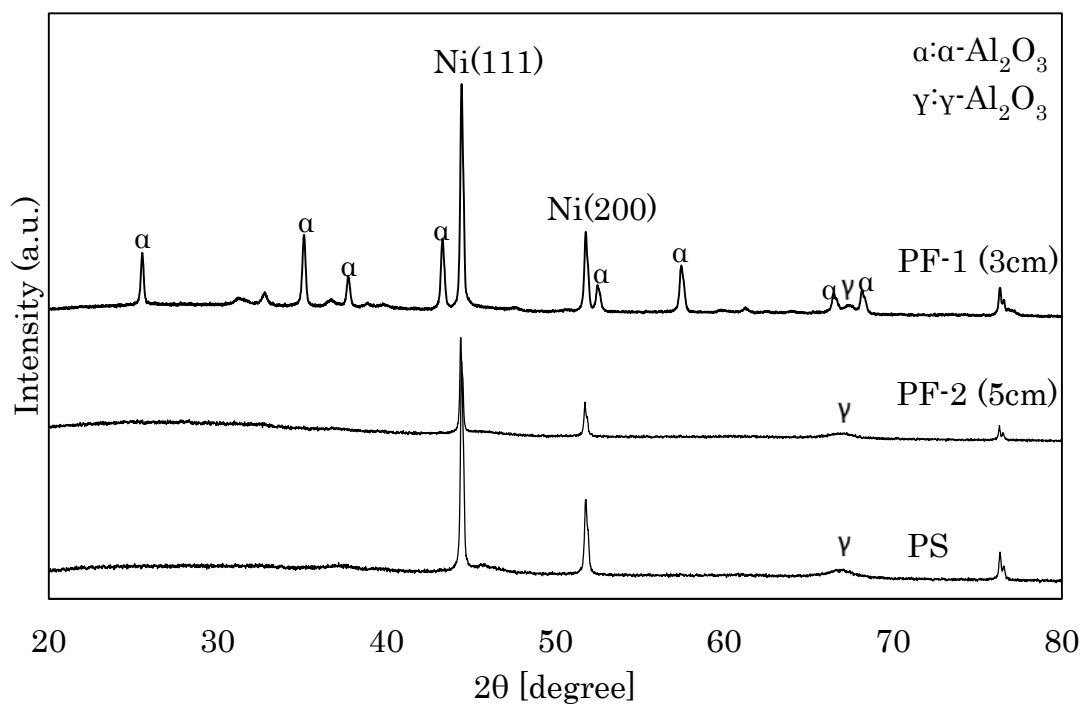


Fig. 3-7 XRD pattern of PF-1, PF-2, and PS.

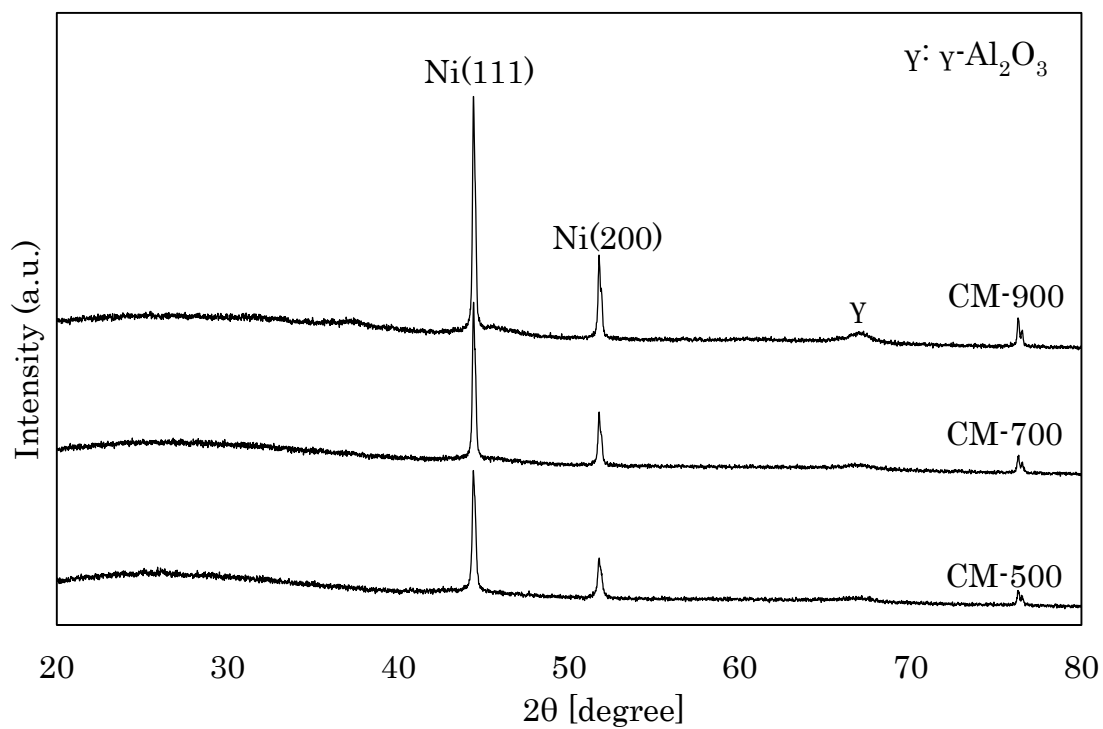


Fig. 3-8 XRD pattern of CM-500, CM-700, and CM-900.

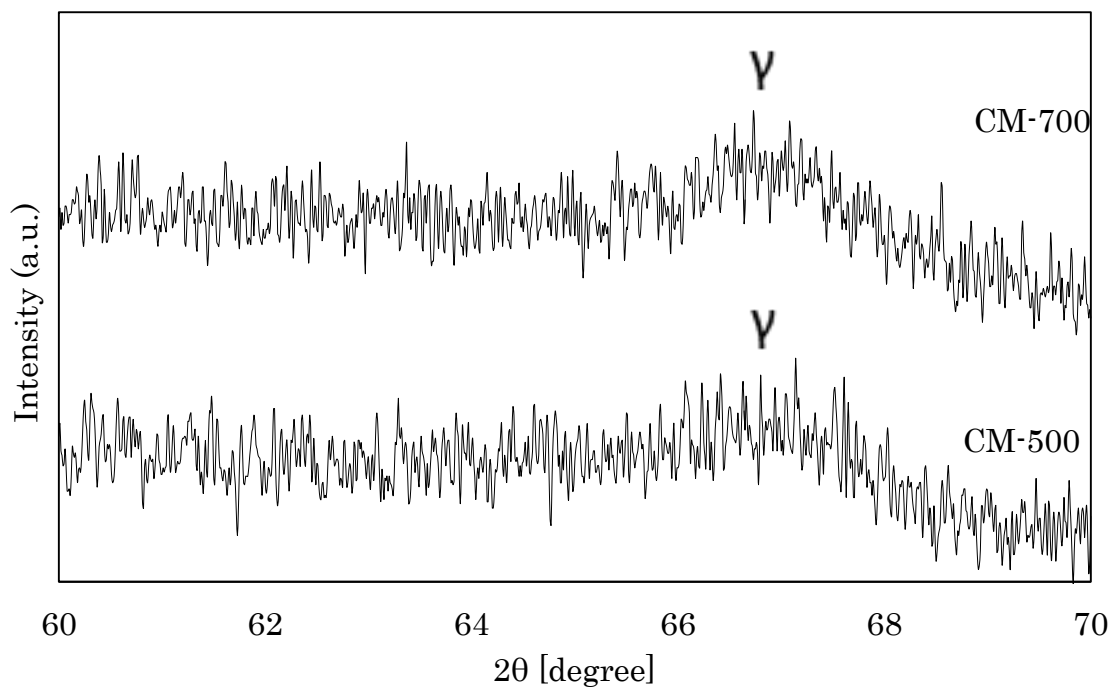


Fig. 3-9 XRD pattern for CM-500 and CM-700 peak range from of 60.0° to 70.0°.

3.3.3 TEM analysis

Fig. 3-10 and 3-11 show TEM images of the Ni/Al₂O₃ catalysts prepared by the microwave induced plasma (PF, PS), and heated by the typical thermal treatment using the electric furnace (CM), respectively. The each sample was crushed and analyzed for the TEM measurements. It is generally accepted that a diffraction pattern could be used to determine lattice plane spacing. For lattice fringe spacing measurements, the simplest way is to measure the spacing between lattice fringes in the TEM images. In this work, measurements were averaged over more than 10 fringes to further reduce errors for each sample. In the case of Ni, it can be calculated from lattice constants of 0.3499nm for Ni at 300 K, which assigned to Ni (111) for 0.202nm and Ni(200) for 0.175nm. The TEM images showed the results in accordance with the results from XRD. Lattice planes belonging to (111) and (200) were detected for all the samples except PF-2. It is generally accepted that peaks corresponding to the (100) plane could be offset by that of the (200) plane due to destructive interference with the FCC structure. A square symmetry for the spots represents Ni(100) plane. For PF-2, Ni(200) was not observed here. Since XRD showed Ni(200) corresponded peaks in the PF-2 sample, it could be assumed that Ni(200) was not detected probabilistically in the measurement of TEM for PF-2.

As described above, the difference in the crystallinity was observed. However since the analysis of the TEM was performed by crushing the sample, it could not represent the surface information, thus, TEM results do not seem to be suitable for using the discussion of catalytic activity observed in the experiments.

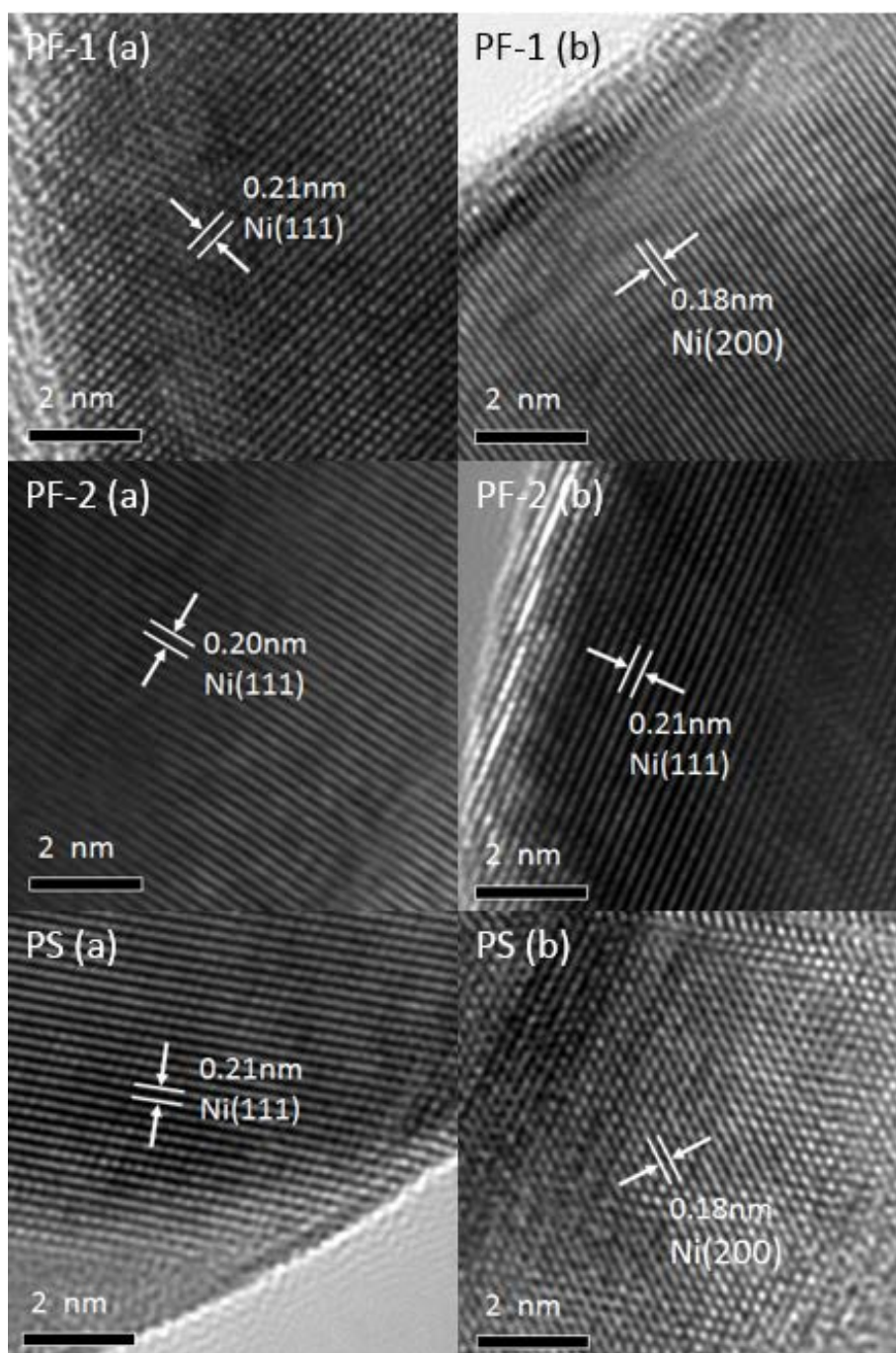


Fig. 3-10 TEM images of PF-1, PF-2, and PS.

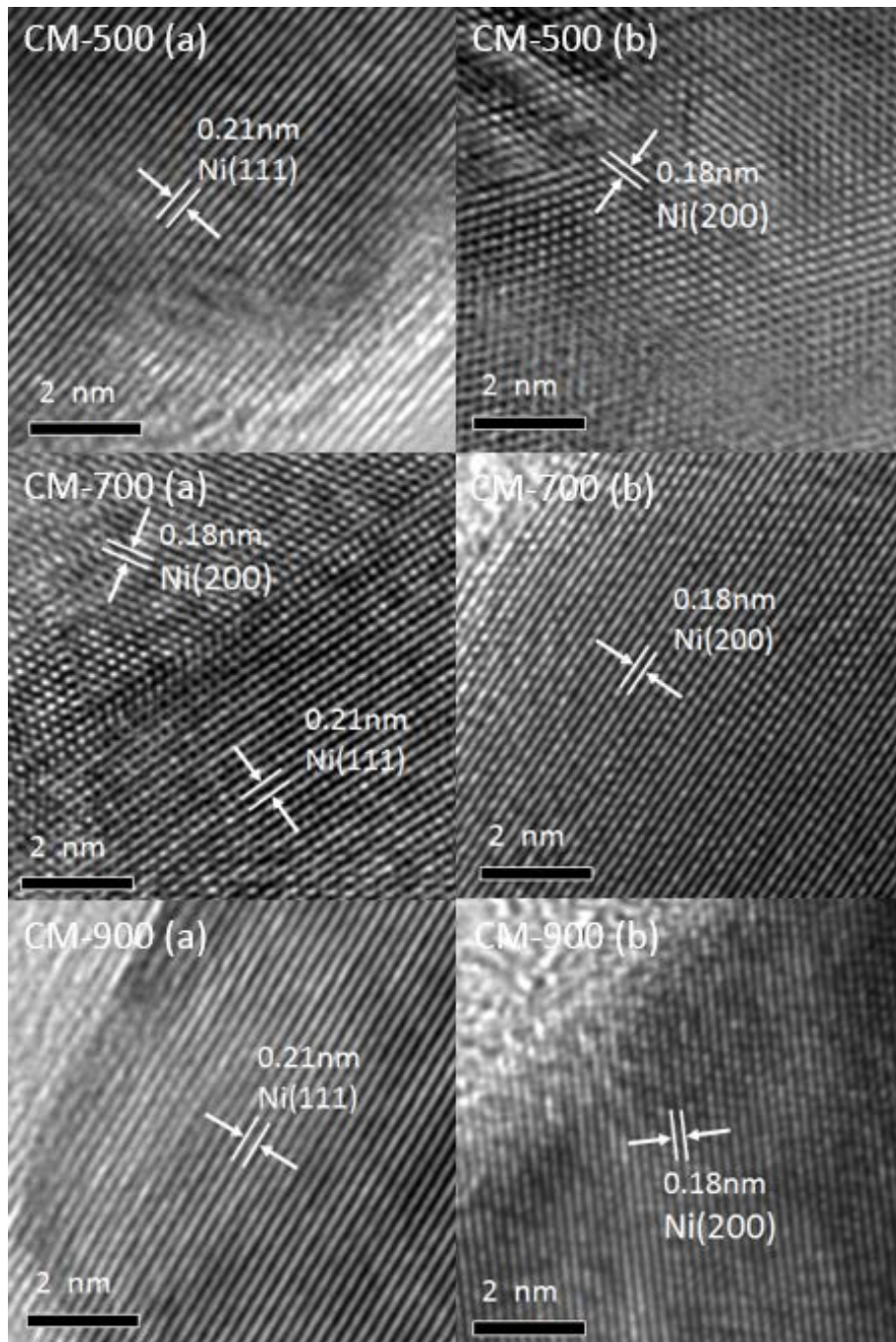


Fig. 3-11 TEM images of CM-500, CM-700, and CM-900.

3.3.4 Catalytic activity: Ethylene conversion

The conversion of ethylene is shown in Fig. 3-12. The highest ethylene conversion was obtained for PF-1 and PF-2 showed the lowest conversion. When comparing the catalyst prepared by the conventional method, CM-500, CM-700, and CM-900, C₂H₄ conversion slightly declined as reduction temperature increased. A decrease in ethylene conversion with temperature rise might be derived from sintering at high temperature conditions, which led to low dispersion. It is generally accepted that the sintering of metal can be promoted with temperature rise.

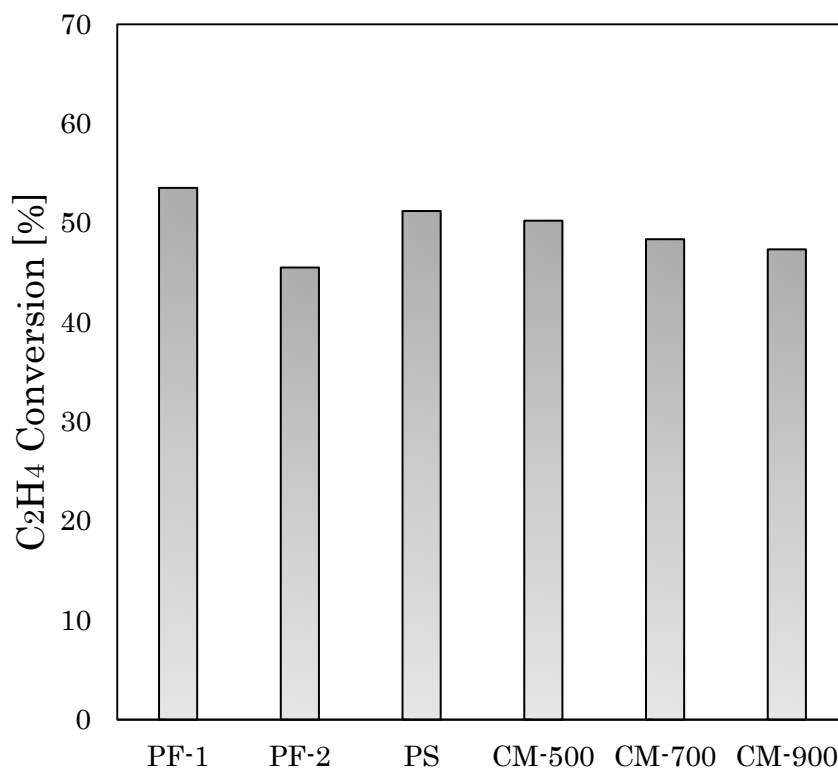


Fig. 3-12 Ethylene conversion for Ni/Al₂O₃ catalyst under all conditions.

In the plasma treated catalyst, shorter distance from the cavity and the particle bed for PF-1 and PS could induce the high gas temperature, which expected larger particle

formation with low dispersion leading to low activity of the catalyst for ethylene conversion. However, despite the high gas temperature condition for the plasma treatment, it showed higher ethylene conversion than those of others prepared by the conventional method. A shorter distance for PF-1 could provide more marked effects of the plasma and the gas temperature on the preparation. Although, the effects of the plasma on the catalyst have not yet been discussed in detail, the plasma treatment could enhance the metal dispersion on the support has also been reported in other researches [64-66]. From the facts of the plasma temperature in Chapter 2, recombination of plasma was suggested. This indicates that the further away from the plasma, the less the effect of the radicals could be expected. Thus, for PF-2, which far away from the plasma irradiation, the plasma was mostly used as heat source and a marginal effect of radicals on the catalyst could be expected. Considering these facts, it is reasonable to assume that the plasma treatment enhanced the distribution of Ni metal on the support by preventing the particles from migrating, leading to high catalytic activity. Different catalyst preparation mechanism was suggested for the plasma treatment compared with the electric furnace.

To investigate the dispersion of Ni metal on the support, H₂ chemisorption was conducted, and the crystallite size of Ni metal from the full width at half-height of the (111) reflections was also calculated from XRD pattern. The Ni (111) was calculated by using Scherrer's equation from the values based on XRD pattern:

$$\tau = K\lambda / \beta \cos \theta \quad (9)$$

where τ is the mean size of the ordered (crystalline) domains, K is a dimensionless shape factor, taken as 0.9, λ is the X-ray wavelength Cu $k\alpha = 1.54 \times 10^{-10}$ m, β is the full width of the diffraction line at half of the maximum intensity (Full width at Half Maximum FWHM), and θ is the Bragg angle (in degrees).

Table 3-3 shows the results of H₂ chemisorption and Crystallite size of Ni (111) calculated from XRD pattern for all Ni/Al₂O₃ catalyst. First of all, it has been reported that Scherrer's equation is not applicable to grains size larger than tens and hundreds of nanometers [89]. As confirmed in SEM images (Fig. 3-3 and Fig. 3-4), micro-sized Ni agglomerates were observed. This fact indicates that Scherrer's equation could be less accurate.

For H₂ chemisorption, the other study investigated on the dispersion of the Ni metal showed relatively low metal dispersion around or below 1% due to the high impregnation rate of the Ni metal on the support [67]. Thus, the chemisorption results obtained here, roughly 0.3% could be a reasonable value. It is not clear to decide the catalyst characteristic from dispersion; however, when focused on specific volume adsorbed for each sample, it can determine the amount of hydrogen adsorbed over Ni metal. The value of specific volume adsorbed was in accordance with the result of ethylene conversion. These results indicate that Ni dispersion on the support is directly related to their catalytic activity for ethylene conversion. These results indicate that Ni dispersion obtained from H₂ chemisorption is directly related to their catalytic activity for ethylene conversion. It was suggested that the plasma treatment could improve catalytic performance, such as the conversion of hydrocarbon.

Table 3-3 H₂ chemisorption results and crystallite size of Ni (111) from XRD pattern.

Catalyst	Dispersion¹ (%)	Specific volume adsorbed (μL)	Surface area/gr of metal	Crystallite size² (nm)	Crystallite size Ni(111)³ (nm)
PF-1	0.34	98.13	2.28	984	13.41
PF-2	0.28	80.28	1.87	1203	22.58
PS	0.33	93.70	2.18	1031	14.30
CM-500	0.30	93.19	2.17	1036	20.43
CM-700	0.32	90.88	2.11	1063	17.88
CM-900	0.33	87.32	2.03	1106	15.32

¹ The fraction of Ni atoms exposed to the surface of the catalyst.

² Crystallite size of Ni metal analyzed by H₂ chemisorption.

³ Crystallite size of Ni (111) calculated from XRD pattern.

3.3.5 Catalytic activity: Methane and ethane selectivity

Fig. 3-13 shows methane and ethane selectivity for all Ni/Al₂O₃. From the result, the main product from the hydrogenation of ethylene was ethane, which contains small amounts of methane. PS showed the highest amount of methane and other samples produced the similar amount of methane. Catalytic activity for PF-1 and PS showed a different tendency for the hydrogenation of ethylene. It has been reported that the methane production rate increased in proportion to the ethylene conversion [60]. Despite the highest ethylene conversion for PF-1 (Fig. 3-12), PS showed the highest methane selectivity.

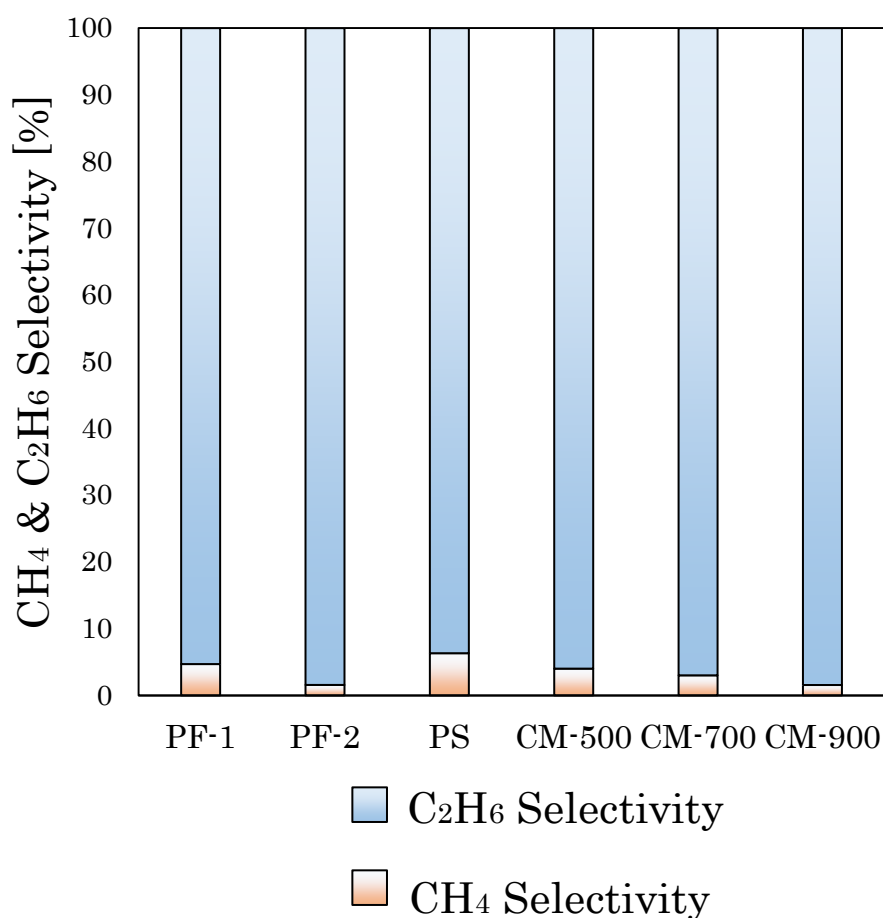


Fig. 3-13 Methane and ethane selectivity for Ni/Al₂O₃ catalyst under all conditions.

For the ethylene hydrogenation reaction, cleavage of a C-C bond occurs at a temperature higher than 500K and produces methane [68]. The reaction mechanism is as follows [68, 69]:

1. Hydrogen and ethane are adsorbed dissociatively over the metal.
2. Cleavage of a C-H bond occurs.
3. Further dehydrogenation of the adsorbed ethyl species ($C_2H_5^-$) occurs, accompanied by the creation of additional bonds between the $C_2H_x(ads)$ species and the metal surface.
4. The C-C bond breaks into $CH_y(ads)$ species.
5. Hydrogenation of the $CH_y(ads)$ species takes place, followed by the desorption of methane.

Moreover, ethylene chemisorption on Ni metal occurs via a di- σ -bond (Fig. 3-14) or a π -bond (Fig. 3-15). Di- σ -bonding between ethylene and Ni occurs with strong rehybridization (near sp_3) [70]. As shown in Fig. 3-14, when ethylene is chemisorbed via di- σ -bond, cleavage of a C-H bond occurs and methane is formed. Meanwhile in Fig. 3-15, π -bonding between ethylene and Ni is observed with no significant rehybridization. Weakly π -adsorbed ethylene reacts with hydrogen atoms strongly held in the interstices of the Ni metal and the formation of adatoms is rate limiting [61, 71, 72]. Thus, when ethylene is chemisorbed via π -bond, ethylene is easily desorbed as ethane suppressing methane production.

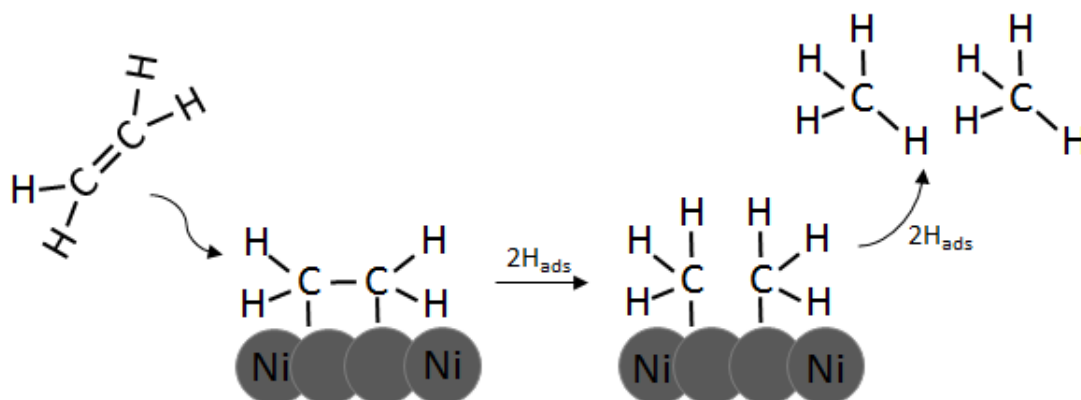


Fig. 3-14 Reaction mechanism of ethylene hydrogenation on Ni via di- σ -bond.

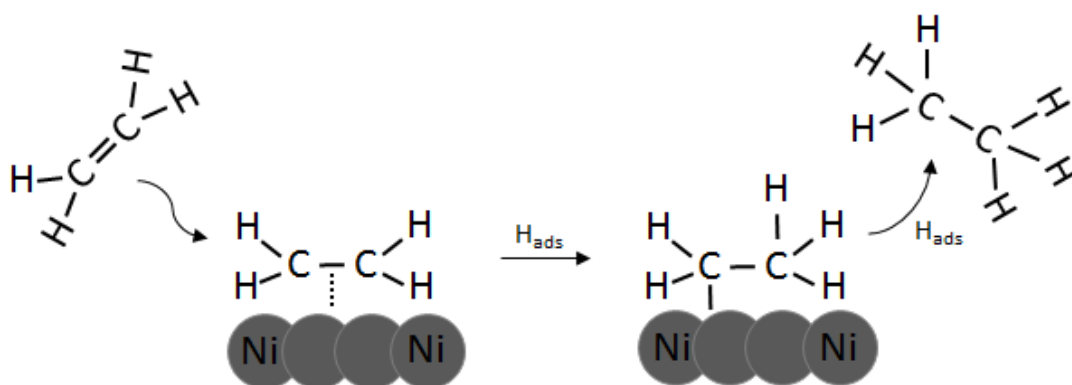


Fig. 3-15 Reaction mechanism of ethylene hydrogenation on Ni via π -bond.

As mentioned above, from the results of the catalytic activity, different catalyst properties for PF-1 and PS were suggested. For the causes of these differences, although the specific mechanism was not clarified in this study, the following possibilities could be considered:

1) Ni metal would have different properties for PF-1 and PS. In the plasma spouted bed, the particles could experience a temperature repetition, while the particles were maintained at the same temperature condition in the fixed bed. Different treatment conditions for PS and PF could affect the properties of Ni metal such as interaction between the metal and the support. Although the effect of the metal on the support may not be significant due to the large size of the metal particles, it could be considered as one of the possibilities for the reaction mechanism.

2) The presence of NiO would affect the catalytic reaction for producing methane. Although the peaks corresponding to NiO were not detected from XRD due to low amount or poor crystallinity of NiO, NiO species on the surface would affect the reaction. The effect of NiO on the catalytic reaction of the hydrogenolysis of glycerol has been reported [90]. For hydrogenolysis of glycerol, 1,2-propanediol and ethylene glycol are produced as the main products. The modelling of the formation of 1,2-propanediol with NiO is shown in Fig. 3-16. The adjacent two hydroxyls of glycerol adsorbed on the NiO surface react with atomic hydrogen on the Ni surface, and the C-O bond cleavage and hydrogen atom addition occur. Meanwhile, for the formation of ethylene glycol, NiO on the Ni-base catalysts reduces the active sites for dehydrogenation which is the first step in producing ethylene glycol. Thus, the presence of NiO on the Ni-base catalysts could increase the selectivity of 1,2-propanediol and decrease the selectivity of ethylene glycol. Considering these facts, as another possibility for different tendency for methane

formation of PF-1 and PS, different treatment conditions could affect the presence of the NiO on the surface.

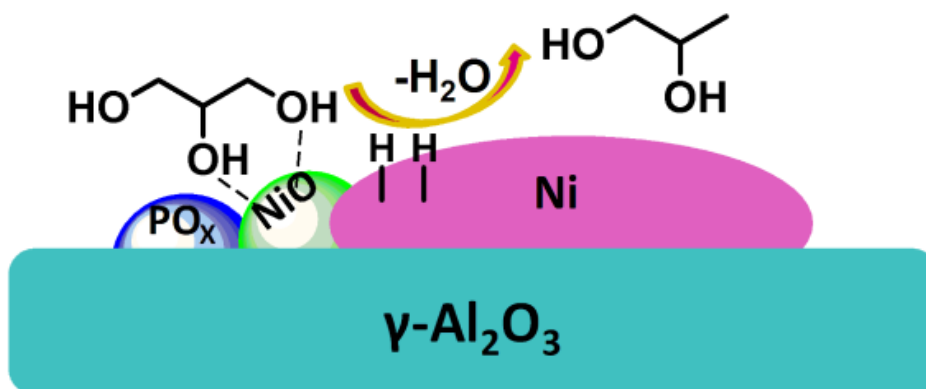


Fig. 3-16 Modelling of the hydrogenolysis of glycerol to 1,2-propanediol over Ni-P/ γ - Al_2O_3 [90].

Even the reaction mechanism of the methane formation was not clearly revealed here, considering the catalytic behavior for PF-1 and PS, it can be concluded that the plasma spouted bed and the plasma irradiation with the fixed bed could derive different catalytic hydrogenolysis behavior of ethane. In this regard, the spouting condition could be an important parameter for the catalyst preparation. As mentioned above, the particles repeatedly experience the high temperature region near the plasma and the low temperature region away from the plasma. This circulation process might affect the property of the catalyst. It is still uncertain; however, it was suggested that the repetition of heating and cooling process for the particles could induce different properties of the catalyst.

3.4 Conclusion

The plasma spouted bed was applied for the Ni/Al₂O₃ catalyst preparation in this chapter. For comparison, the plasma irradiation with the fixed bed and the typical thermal treatment using an electric furnace were also applied for the Ni/Al₂O₃ catalyst preparation. Despite short treatment time, the Ni/Al₂O₃ catalyst was successfully produced using the plasma spouted bed. The surface morphology of the Ni/Al₂O₃ catalyst under all conditions was investigated by SEM. A large number of agglomerated particles derived from Ni metal loading on the alumina support was observed. From the results of XRD pattern, the same results as in chapter 2 for aluminum hydroxide treatment and the peaks corresponding to Ni(111) and Ni(200) were detected under all conditions. According to the results of the catalytic activity for ethylene hydrogenation, the plasma treated Ni/Al₂O₃ catalyst (PF-1 and PS) showed great performance in the conversion of ethylene hydrogenation than those prepared by the electric furnace. From H₂ chemisorption, the dispersion was in accordance with the conversion of ethylene for all the Ni/Al₂O₃ catalysts. It was suggested that the plasma treatment enhanced the distribution of Ni metal on the support by preventing the particles from migrating, leading to high catalytic activity. Concerning methane selectivity, despite the highest ethylene conversion for PF-1, PS showed the highest methane selectivity.

In this chapter, it was suggested that the plasma spouted bed treatment had a potential for the Ni/Al₂O₃ catalyst preparation, especially for the improvement of dispersion of impregnated metal on the catalyst support. Moreover, the different catalytic behavior in the catalytic activity of methane selectivity was suggested for the plasma spouted bed and the fixed bed with the plasma irradiation.

CHAPTER 4

**Preparation of Pd/Al₂O₃ with
microwave induced plasma jet**

4.1 Preparation of Pd/Al₂O₃ with the microwave induced plasma jet combined with the spouted bed

4.1.1 Introduction

Ethylene hydrogenation used in Chapter 3 is often used as a model reaction in catalyst evaluation because the reaction itself is simple. However, from the industrial point of view, since ethylene is more valuable than ethane, the dehydrogenation of ethane or the selective reaction of acetylene has been widely investigated in practice [73, 74]. In the selective hydrogenation of acetylene, a high ethylene yield is important, and ethane is generated by a strong adsorption reaction in nickel metal [75]. In this chapter, palladium metal was used as a model catalyst for the selective hydrogenation of acetylene to investigate how its properties are affected by the plasma spouted bed.

4.1.2 Experimental set-up

The same experiment equipment of the plasma spouted bed was used as shown in Chapter 2. A mixture of Ar and H₂ was used as a plasma gas for the reduction of Pd catalyst precursor and was injected from the bottom of the spouted bed to spout the particles.

4.1.2.1 Catalyst preparation & treatment conditions

Pd/Al₂O₃ catalyst containing 1wt% of Pd was prepared by the plasma spouted bed as follows:

<Step 1> Al(OH)₃ powder was added into 5wt% of Pd(NO₃)₂ solution.

<Step 2> The solution was dried at 80°C until slurry-like.

<Step 3> The slurry was dried at 110°C for 12 hours and crushed.

<Step 4> The crushed particles in the size range 250-595 μm were treated in the plasma spouted bed with the following conditions: power of 150-270 W, Ar flow rate of 2.5-4 L/min, H₂ flow rate of 60 ml/min and treatment time of 20 min.

Detailed treatment conditions of the plasma spouted bed for PS-1, PS-2, PS-3 and PS-4 are shown in Table 4-1. From the initial condition of PS-1, only the microwave power was increased for PS-2, resulting in the particles spout at a higher point. For PS-3, the spouting height was set equal to that of PS-1 by reducing argon flow rate. Based on PS-3, the distance between the cavity and the spouted bed was reduced, which is PS-4. For comparison, Pd/Al₂O₃ catalyst was also prepared by the conventional method with an electric furnace at 300°C (CM-300) or 500°C (CM-500) because Pd catalyst was reduced and calcined at the temperature range of 300-500°C in the previous studies [77-79]. Preparation procedure is as follows:

<Step 4c> The crushed particles were heated at 300°C or 500°C with 16.7% of H₂ gas (60 ml/min) for reduction for 2 hours.

Table 4-1 Treatment conditions of the plasma spouted bed for catalyst preparation

Catalyst	Power (W)	Distance ¹ (cm)	Ar flow rate (L/min)	H ₂ flow rate (mL/min)	Treatment time (min)	Mass (g)	Height ² (cm)
PS-1	150	3.0	4.0	60	20	1.0	5
PS-2	270	3.0	4.0	60	20	1.0	9
PS-3	270	3.0	2.5	60	20	1.0	5
PS-4	270	1.0	2.5	60	20	1.0	5

¹ Distance from the cavity and the spouted bed.

² Maximum height of the particles spouting in the plasma spouted bed.

4.1.2.2 Catalyst evaluation (Acetylene hydrogenation)

As shown in Chapter 3 (Fig.3-2), a stainless reactor (i.d., 6mm) with a temperature programmed electric furnace was used for the acetylene hydrogenation reaction. For each test, reaction temperature was set at 160°C and 20 mg of Pd/Al₂O₃ catalyst was filled in the middle of the reactor followed by gas feed into the reactor at flow rates of C₂H₂:20 ml/min, H₂:80 ml/min and Ar:200 ml/min, and a gas space velocity was 320,000 h⁻¹. The gas extracted from the sampling port was analyzed with a gas chromatograph (Shimadzu GC-8APF). The hydrogenation of C₂H₂ is a sequential reaction to be converted into C₂H₄ and C₂H₆. For the evaluation of the catalyst activity, their concentration was quantified, and C₂H₂ conversion and C₂H₄ selectivity were calculated as follows:

$$\text{C}_2\text{H}_2 \text{ conversion (\%)} = \left(\frac{\text{C}_2\text{H}_2(\text{Feed}) - \text{C}_2\text{H}_2}{\text{C}_2\text{H}_2(\text{Feed})} \right) \times 100 \quad (10)$$

$$\text{C}_2\text{H}_4 \text{ selectivity (\%)} = \left(1 - \frac{\text{C}_2\text{H}_6}{\text{C}_2\text{H}_2(\text{Feed}) - \text{C}_2\text{H}_2} \right) \times 100 \quad (11)$$

4.1.2.3 Catalyst characterization

The surface morphology of the catalyst was analyzed with scanning electron microscopy (SEM, Keyence VE-7800). Energy-dispersive X-ray spectroscopy (EDS, Genesis XM2) combined with SEM was performed to determine Pd metal on the alumina support. For the investigation of the crystallite phase of the catalyst, XRD analysis was performed using Cu K α radiation (40kV-15mA, Rigaku Mini Flex 600). The diffraction patterns were recorded for 2θ values between 20° and 80° in 0.010° steps. Transmission electron microscope (TEM) measurements were carried out using JEOL JEM-1010BS. The average diameters of Pd nanoparticles were estimated from the TEM images by examining 50-100 of particles. Pd metal dispersion and its crystallite size were analyzed by H $_2$ chemisorption (Quantachrome ChemBET Pulsar). Pd/Al $_2$ O $_3$ catalyst was reduced at the temperature of 573K for 1 hour, and flushed out hydrogen under N $_2$ atmosphere for 30 min at the same temperature [63]. The measurements were performed at 300K under N $_2$ atmosphere with pure H $_2$ pulse flow. The dispersion of Pd on the surface of the catalyst was estimated assuming a stoichiometry of Pd/H $_2$ =2.

4.1.3 Result and discussion

4.1.3.1 Characterization of the Pd/Al₂O₃ catalysts

Fig. 4-1 shows SEM image for all Pd/Al₂O₃ catalysts under all conditions. For the plasma treated samples of PS-1, PS-2, and PS-4, the surface cracked at several places especially on PS-4. Whereas, on the surface of PS-2, rarely no crack was shown which is similar to that of CM-300 and CM-500. There were few effects on the surface change for PS-2. The cracks on the surface might derived from the rapid heat change in the plasma spouted bed. Fig. 4-2 shows XRD pattern for all Pd/Al₂O₃ catalysts under all conditions. For all catalyst, the crystalline phase of γ -alumina was detected at 2θ value at 47.4° and 67.2° (JCPDS card, file No. 10-0425). For CM-300 and CM-500, in addition to γ -alumina, boehmite peaks were detected. It was reported that boehmite are coexist with γ -alumina at the temperature range of 300°C to 500°C and further temperature increase above 500°C made boehmite phase entirely change into γ -alumina phase [39-44]. For PS-1 and PS-2, boehmite phase coexist with γ -alumina as like CM-300 and CM-500. However, for PS-3 and PS-4, the peaks of boehmite disappear and only γ phase alumina exist, indicating that the particles of PS-3 and PS-4 were treated in higher temperature condition than those of other samples. The diffraction peak (2θ) at 40.1° corresponds to Pd⁰ (111) peak (JCPDS card, file No. 46-1043). Weak diffraction peak of Pd was observed for all samples and no PdO peaks were detected. This indicates that PdO successfully reduced into Pd metal despite their short treatment time in the plasma spouted bed. The diffraction peak of CM-500 for Pd⁰ showed sharp intensity than those of PS-3 and PS-4. It is generally accepted that the Bragg width in XRD pattern is inversely proportional to the crystallite size [82]. Thus, the diffraction patterns of sharp intensity peaks have a bigger crystallite size than those of broad peaks. These facts indicated that PS-3 and PS-4 has smaller crystallite size

than those of CM-500. Fig. 4-3 shows TEM images and the size distribution of Pd nanoparticles distinguished from Al₂O₃ support for PS-4, CM-300, and CM-500. The average Pd nanoparticle sizes of PS-4, CM-300, and CM-500 are 4.29, 2.26, and 5.79 nm, respectively. The large average Pd particles size of CM-500 compared with that of CM-300 might be derived from its high gas temperature with a long period of treatment time because high temperature condition could make Pd metal grow to larger crystallite size by sintering [83]. From the TEM images, the average diameter of Pd nanoparticles of PS-4 was smaller than that of CM-500 despite high temperature condition in the plasma spouted bed in accordance with the results of XRD. From the results described above, it is suggested that the plasma spouted bed treatment could made Pd particles size small by preventing Pd metal from sintering.

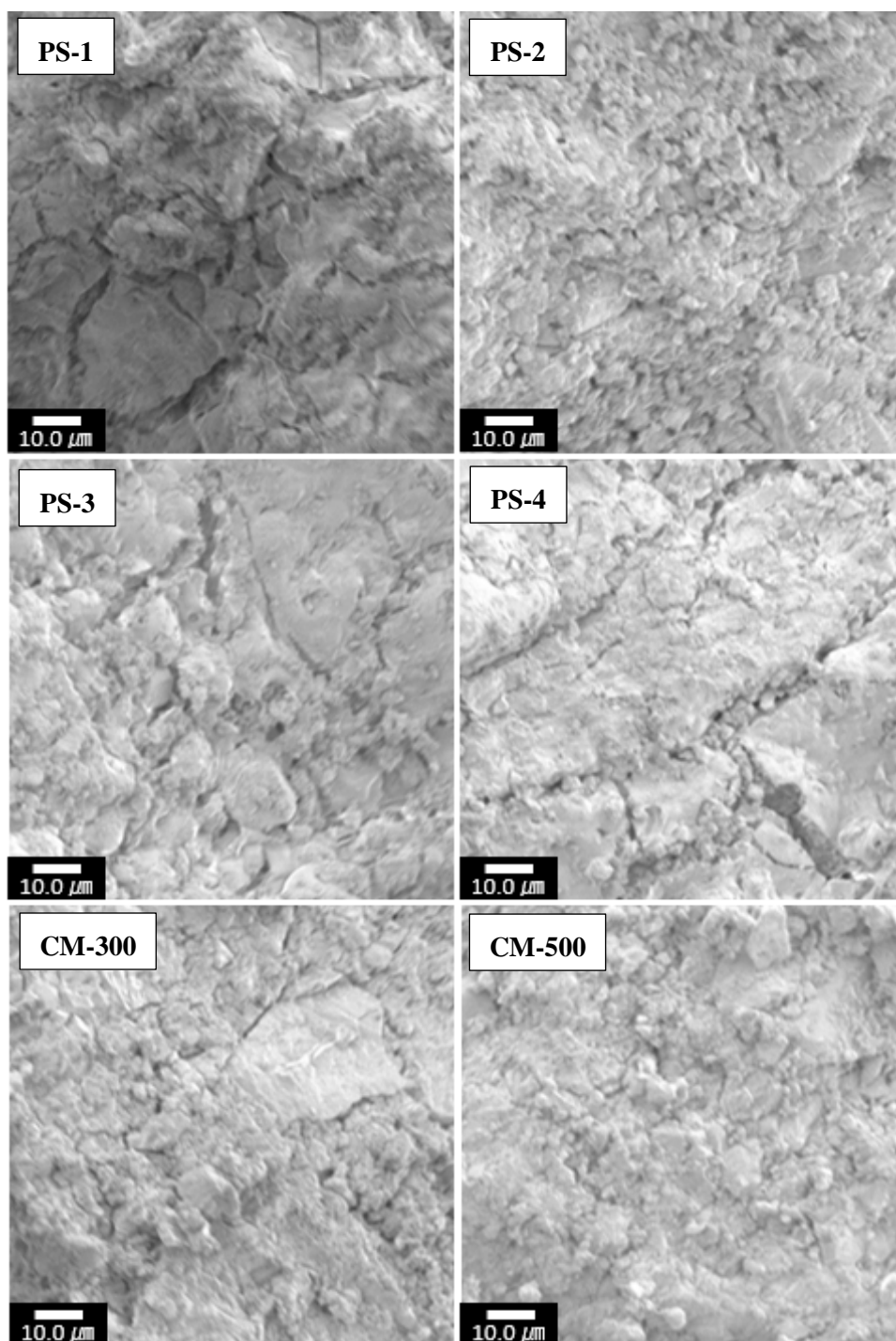


Fig. 4-1 SEM image of Pd/Al₂O₃ catalysts under all conditions.

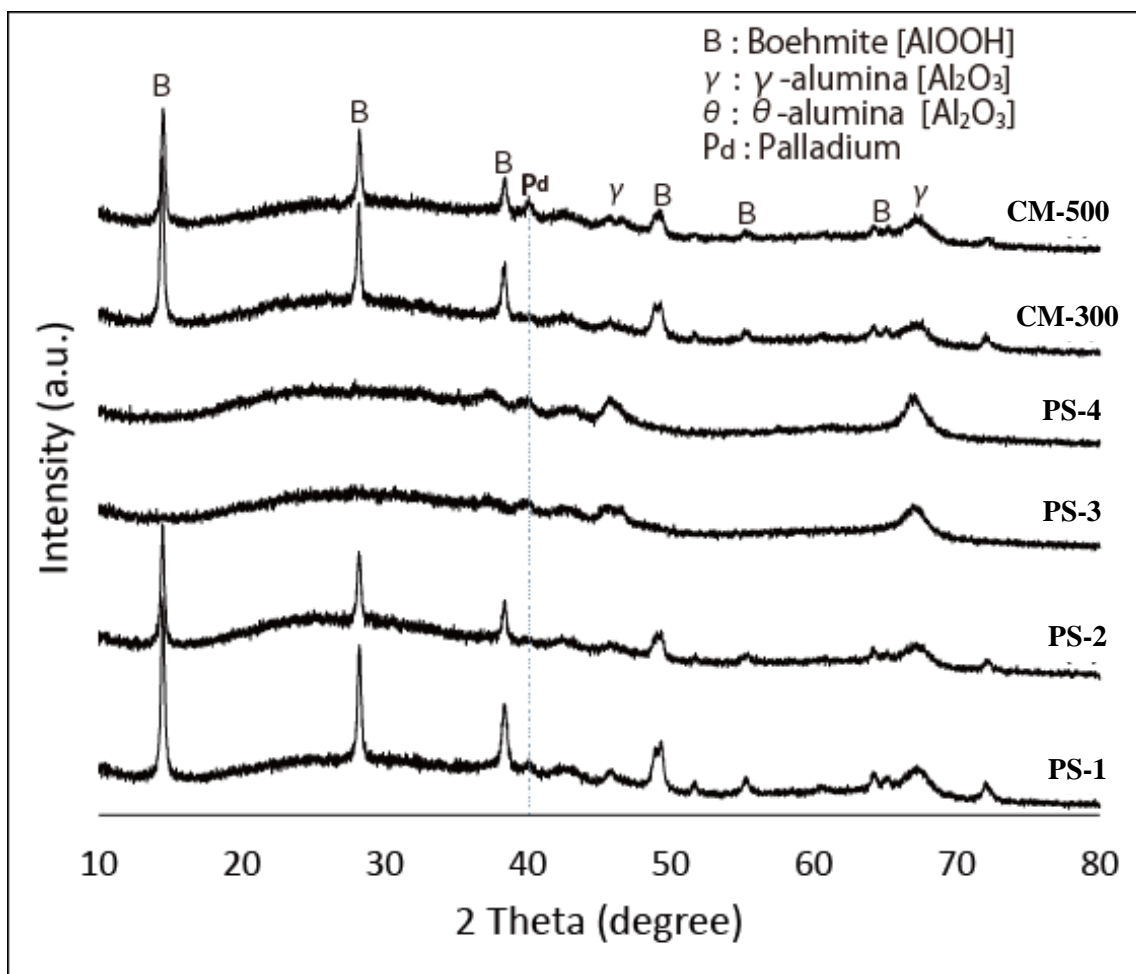


Fig. 4-2 XRD patterns of all Pd/ Al_2O_3 catalysts under all conditions

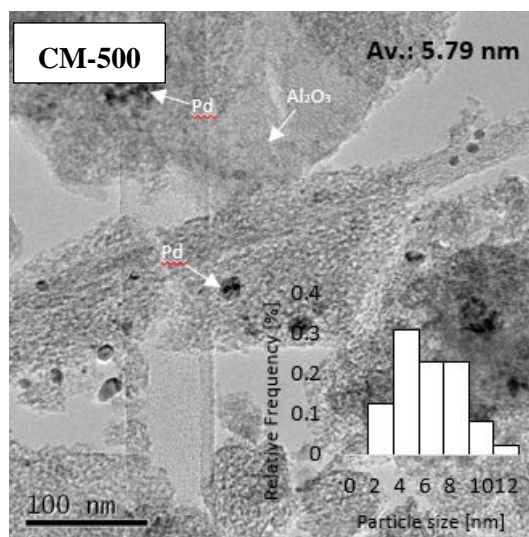
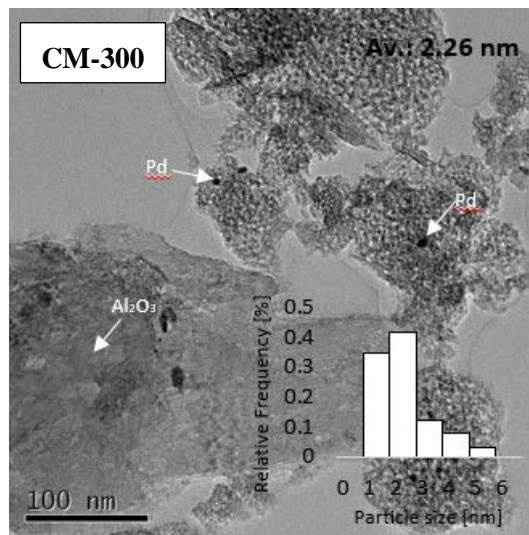
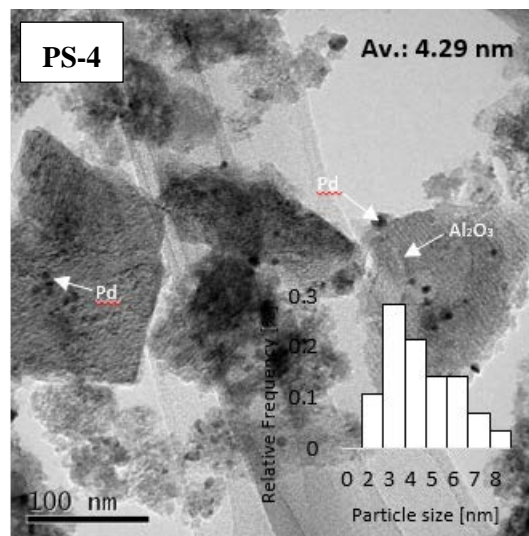


Fig. 4-3 TEM images and size distribution of PS-4, CM-300, and CM-500.

4.1.3.2 Catalytic activity: Acetylene conversion

Fig. 4-4 shows the C_2H_2 conversion for the plasma and conventional heat treated catalysts. When comparing CM-300 and CM-500, C_2H_2 conversion declined as reduction temperature increased. PS-1, PS-2, and PS-3 showed almost the same values for C_2H_2 conversion, while PS-4 showed higher C_2H_2 conversion than those of PS-1, PS-2 and PS-3. The temperature inside the plasma spouted bed could not be measured, however the temperature of the outer surface of the reactor for PS-2 was $380^\circ C$. Considering the microwave power, the gas flow rate and the distance from the cavity to the spouted bed, the gas temperatures could be assumed to be in the order $PS-1 < PS-2 < PS-3 < PS-4$. Pd metal dispersion and its crystallite size of PS-4, CM-300 and CM-500 are shown in Table 4-2. From the results, CM-300 has the highest value of Pd dispersion and CM-500 lowest. From Fig. 4-4, in accordance with the results of crystallite size, C_2H_2 conversion was in proportional to Pd metal dispersion. As mentioned earlier, rather low C_2H_2 conversion for CM-500 compared with CM-300 might be derived from sintering at high temperature condition which led to low dispersion. Meanwhile, for the plasma spouted bed treatment, it had contrary effect of the conventional method. In the plasma spouted bed, shorter distance from the cavity and spouted bed could induce the high gas temperature which expected larger particle formation with low dispersion leading to low activity of the catalyst for C_2H_2 conversion. However, even though high gas temperature condition for PS-4, it showed higher C_2H_2 conversion than those of others prepared by the plasma spouted bed. Considering these facts, it is suggested that the plasma spouted bed treatment prevented Pd metal from sintering and different catalyst preparation mechanisms were occurred for the plasma spouted bed compared with the electric furnace.

Table 4-2 H₂ chemisorption results.

Catalyst	Avg. crystallite size of Pd (Å)	Metal Surface area (m ² /g)	Dispersion ¹ (%)
PS-1	12.0	1.39	31.1
PS-2	10.9	1.52	34.2
PS-3	16.5	1.01	22.6
PS-4	16.3	1.02	22.9
CM-300	8.5	1.96	44.0
CM-500	19.0	0.88	19.7

¹ The fraction of Pd atoms exposed to the surface of the catalyst.

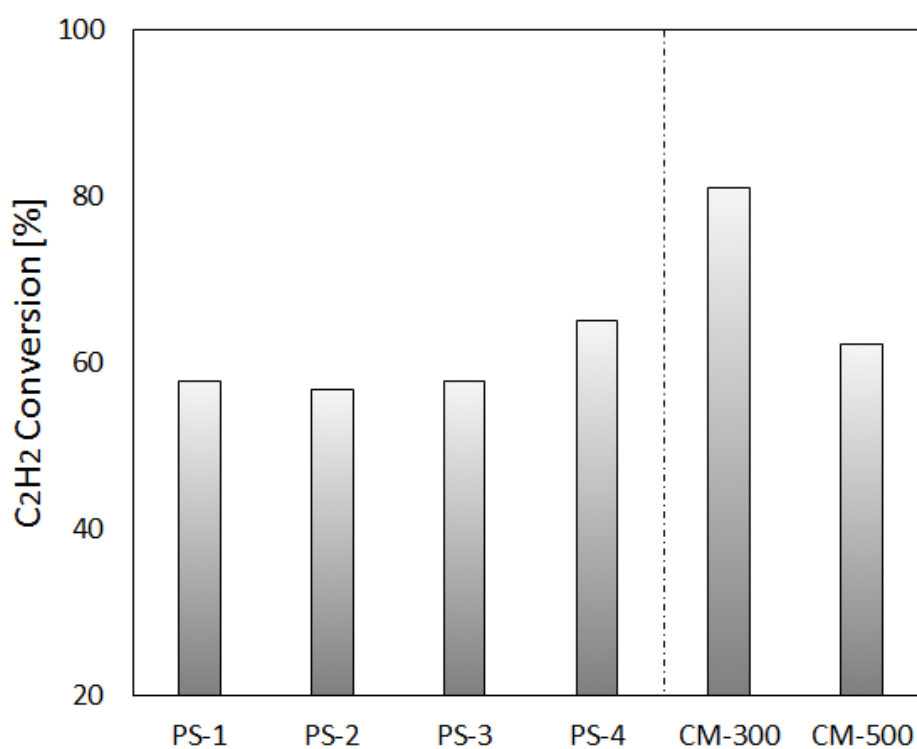


Fig. 4-4 Acetylene conversion for Pd/Al₂O₃ catalysts under all conditions.

4.1.3.3 Catalytic activity: Ethylene selectivity

Fig. 4-5 shows C_2H_4 selectivity for the catalyst prepared by the plasma spouted bed and the electric furnace. From Fig. 4-5, in the plasma treated samples, PS-1 and PS-3 had similar value of C_2H_4 selectivity and PS-2 showed the lowest C_2H_4 selectivity. All conditions were the same for PS-1 and PS-2 except for the microwave power as indicated in Table 4-1. The observation indicated that the particle spouting height from the bottom of the reactor to its maximum point was 5 cm and 9 cm for PS-1 and PS-2, respectively. Additional microwave power made the gas temperature high, thus the gas flow rate increased which leads to the particles spout at the higher point. Different particles spouting height would make spouting condition different such as a particle circulating rate. Hence, it is suggested that the spouting condition might affect the properties of the catalyst leading to different value of C_2H_4 selectivity. To clarify the effect of the spouting condition, the spouting height was set equal to that of the PS-1 (The particles spouting height:5 cm) by reducing argon flow rate shown as PS-3. By comparing with PS-1 and PS-3, C_2H_4 selectivity as well as C_2H_2 conversion was the same values even under the different microwave power conditions. This result suggests that the spouting condition is also an important factor for the properties of the catalyst in the plasma spouted bed. It has been reported that a high reduction temperature made low C_2H_2 conversion, but high C_2H_4 selectivity [80, 81]. In our work, similar behavior was observed for CM-300 and CM-500. In terms of C_2H_4 selectivity, the plasma treatment showed the same tendency as the conventional method. For PS-4, it showed the highest C_2H_4 selectivity above all else. Even though it contains many more active sites for PS-4, it could prevent further hydrogenation of C_2H_4 . These facts indicate that the treatment in the plasma spouted bed could enhance the properties of the catalyst for the specific catalytic activity.

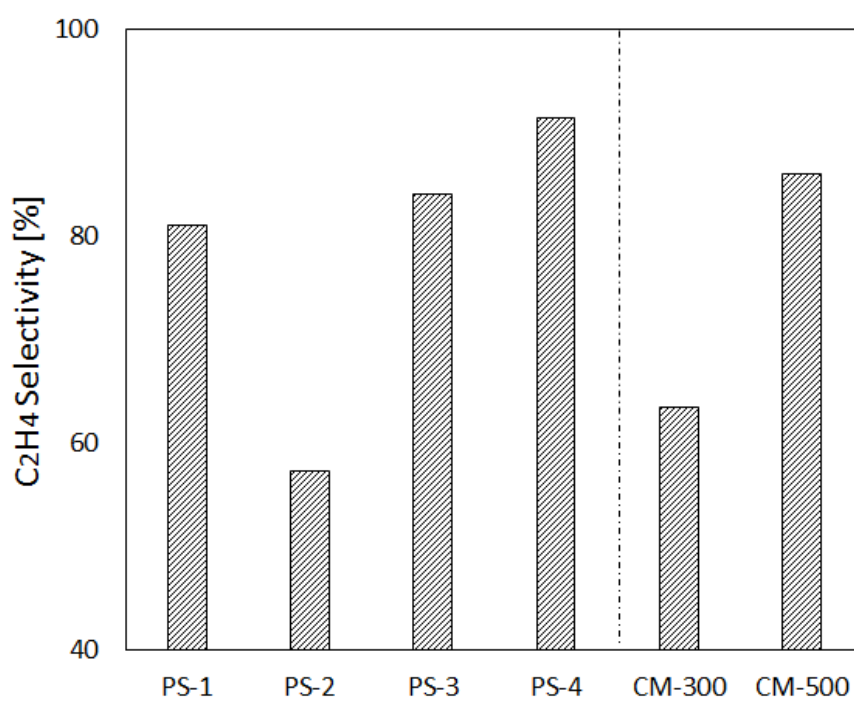


Fig. 4-5 Ethylene selectivity for Pd/Al₂O₃ catalysts under all conditions.

4.1.3.4 The effects of the plasma spouted bed

It is reported that performance of the plasma can enhance the catalyst activity such as conversion or selectivity by modifying the catalyst [84]. In addition to the effect of the plasma, considering the results described above, the spouting condition was also an important parameter for the catalyst preparation. For the plasma spouted bed, there are high temperature region in the vicinity of the plasma and low temperature region on the upper side of the spouted bed as shown in Fig. 4-6. Therefore, as one possibility of these facts, a rapid temperature change between high temperature near the plasma and relatively low temperature away from the plasma might affect the catalyst activity when the particles circulate. Repetition of heating and cooling of the particles would prohibit the particles from sintering which made higher C_2H_2 conversion despite high gas temperature condition. With regard to C_2H_4 selectivity, one possible reason for the different results of C_2H_4 selectivity for the catalyst prepared in our work might be derived from Pd-alumina interaction. A strong interaction between Pd and alumina support can easily desorb C_2H_4 than a weaker interaction [74]. The weaker interaction between Pd and support could induce di- σ -bonded C_2H_4 on Pd proceeding to further hydrogenation. As mentioned above, the high reduction temperature condition can increase C_2H_4 selectivity by inducing the strong interaction between Pd and alumina support which would produce π -bonded C_2H_4 on Pd. Thus, high C_2H_4 selectivity shown in PS-4 might be derived from their strong interaction between Pd metal and alumina support. However, from the Fig. 4-5, PS-2 showed the lowest C_2H_4 selectivity even though the temperature would be higher than that of PS-1. These result might be related to a contact frequency between the plasma and the particles which derived from the spouting condition. The particles of PS-2 spouting at higher place would have low contact frequency between plasma and the particles than

those of other samples leading to low effect on Pd-alumina interaction. Considering these facts, it is suggested that a specific treatment condition in the plasma spouted bed could make the strong interaction between Pd metal and alumina support, leading to high C₂H₄ selectivity. A possible structural changes which graphically explains the behavior of the present system is shown in Fig. 4-7. When the reduction process occurred, the sintering of the Pd metal was accompanied with a crystallite migration of Pd metal. In the high temperature condition, Pd metals are easy to migrate to form a large crystallite of Pd metal. However, considering the results obtained above, the plasma spouted bed could prevent Pd metal from the sintering leading to relatively high dispersion. Moreover, high C₂H₄ selectivity of PS-4 suggested that it would have the strong interaction between Pd and support.

In this work, the plasma spouted bed had beneficial effects on the size of the Pd nanoparticles and the interaction between Pd metal and alumina support. It was suggested that the rapid temperature change could affect the properties of the catalyst. However, the effects of the plasma spouted bed are still unclear at this stage. To further understand how the effect of the temperature history (a repetition of rapid temperature change) on the Pd-support interaction, binding energy between Pd-support and C₂H₄ bonding energy with Pd will be analyzed.

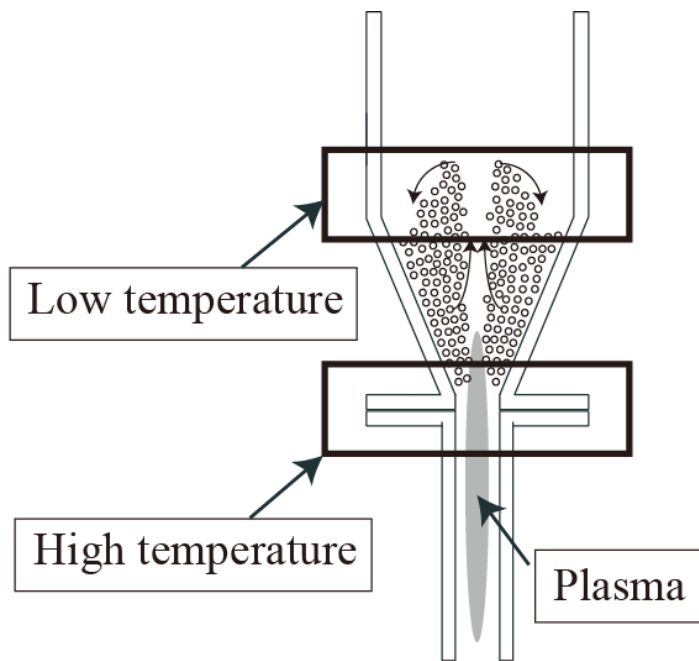


Fig. 4-6 Temperature difference with respect to the region in the plasma spouted bed.

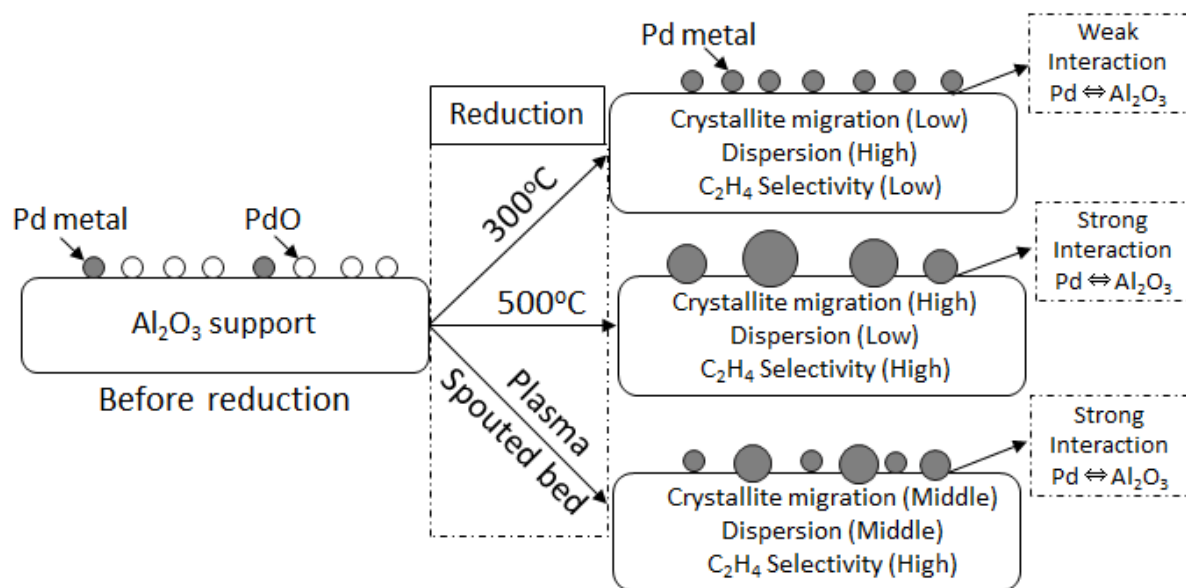


Fig. 4-7 Modeling of the structure change in Pd/Al₂O₃ catalyst prepared by the plasma spouted bed and the conventional method.

4.2 Preparation of Pd/Al₂O₃ by the fixed bed with the microwave induced plasma irradiation

4.2.1 Introduction

The microwave-induced plasma jet combined with the spouted bed demonstrated excellent performance of Pd/Al₂O₃ in the selective hydrogenation of acetylene to ethylene as shown in previous section. A synergetic effect of the plasma and the spouted bed was suggested. However, it is still unclear exactly how the plasma spouted bed could affect the properties of catalysts due to its multiple effects on catalyst preparation. Therefore, we focused on the effects of microwave-induced plasma irradiation alone on the catalyst. The Pd/Al₂O₃ catalyst was prepared using the fixed-bed with microwave-induced plasma jet irradiation, and the activity of the catalyst was compared with that of catalysts made using the plasma spouted bed and the conventional furnace.

4.2.2 Experimental set-up

The experimental equipment of the fixed bed with the plasma irradiation is the same as that in Chapter 2.

4.2.2.1 Catalyst preparation & treatment conditions

As mentioned above, three preparation methods were conducted for the Pd/Al₂O₃ catalyst: fixed particle bed with plasma irradiation (PF), plasma spouted bed reactor (PS-4 in the previous), and the conventional method (CM). PS-4, showed the best performance in 4.1, chosen for the comparative analysis. Here, it is simply named PS. Details of treatment conditions for the PF and the PS are shown in Table 4-3. Table 4-3

illustrates that the distance between the microwave waveguide and the particle bed was changed for PF. For the conventional method (CM), the particles were heated to 900°C as well as 500°C using the electric furnace with 16.7% H₂ gas (60 ml/min) and reduced for 2 h. Since the plasma contains radicals with high gas temperature, the temperature of 900°C was chosen to investigate the effect of high temperature condition on the catalyst properties.

Table 4-3. Treatment conditions of the fixed bed with plasma irradiation and the plasma spouted bed for catalyst preparation.

Catalyst	Power (W)	Distance ¹ (cm)	Ar flow rate (L/min)	H ₂ flow rate (mL/min)	Treatment time (min)	Mass (g)
PF-1	270	3.0	2.5	60	7	1.0
PF-2	270	5.0	2.5	60	15	1.0
PF-3	270	7.0	2.5	60	15	1.0
PS	270	1.0	2.5	60	15	1.0

¹ The distance from the waveguide and the particle bed.

4.2.2.2 Catalyst evaluation (Acetylene hydrogenation)

For the catalyst evaluation of PF, the same procedure as in 4.1.2.2 was conducted and methane selectivity was also considered as follow:

$$\text{C}_2\text{H}_6 \text{ selectivity (\%)} = \left(\frac{\text{C}_2\text{H}_6}{\text{C}_2\text{H}_2(\text{Feed}) - \text{C}_2\text{H}_2} \right) \times 100 \quad (12)$$

4.2.2.3 Catalyst characterization

The catalysts prepared by three different methods (PF, PS, and CM) were examined as the same analysis in 4.1.2.3. Here, the crystal planes of Pd on the catalyst were confirmed using FE-TEM.

4.2.3 Result and discussion

4.2.3.1 Surface morphology by SEM

Fig. 4-8 shows the SEM image of the catalysts prepared under all conditions. The surfaces were cracked at several places in all of the samples. However, PF-3 was relatively smooth, and few cracks existed. No significant differences were observed on the surface for CM-500 and CM-900, suggesting that higher temperatures had little effect on the surface morphology of the catalyst. Meanwhile, an obvious difference was observed in PF-1 when compared with other samples. Sphere-shaped objects on the surface that corresponded to Pd nanoparticles were formed. This phenomenon might be resulted from extreme high temperatures by the plasma due to the short distance between the waveguide and the particle bed.

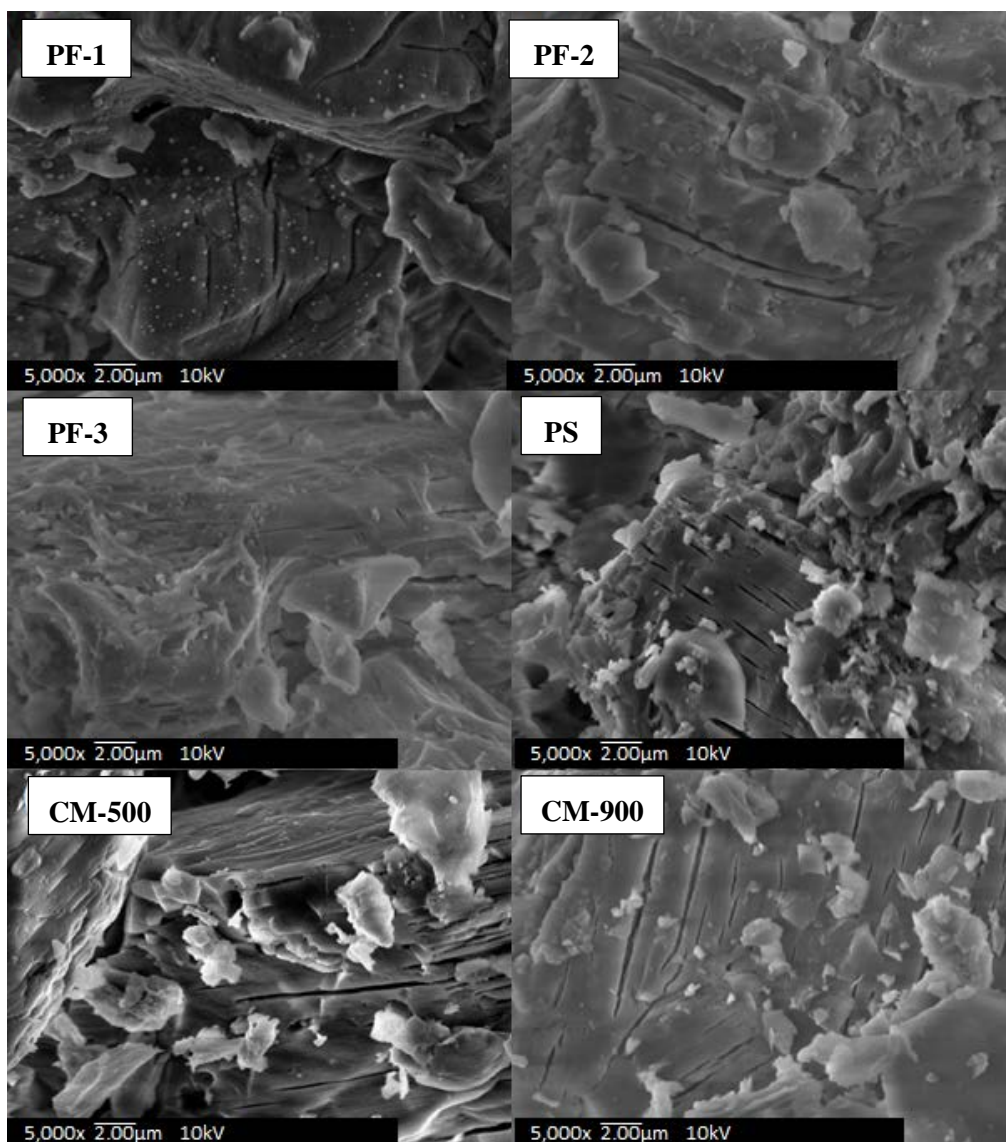
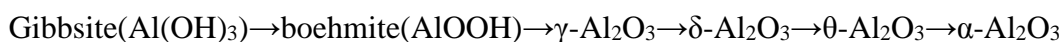


Fig. 4-8 SEM images for Pd/Al₂O₃ catalysts under all conditions.

4.2.3.2 Crystal structure analysis by XRD

Fig. 4-9 shows the XRD pattern of the catalysts. The diffraction peaks (2θ) of XRD at 33.9° , 42.0° , 54.8° , and 60.8° corresponding to PdO (JCPDS card, file No. 47-1107) were not detected for all the plasma-treated samples, indicating that the plasma treatment successfully reduced PdO to Pd in a short period of time. The diffraction peaks at 40.1° and 46.7° corresponded to the Pd(111) and Pd(200) planes of the face-centered cubic (FCC) metal crystal of Pd (JCPDS card, file No. 46-1043), respectively.

PF-1 indicated a diffraction peak at 46.7° , while the other samples did not. For all of the catalysts, the crystalline phase of γ -alumina was detected at two values, specifically 47.4° and 67.2° (JCPDS card, file No. 10-0425). The diffraction peaks (2θ) at 25.6° , 35.1° , 37.8° , 43.4° , and 52.6° corresponded to the α -alumina peak (JCPDS card, file No. 46-1212). Only the PF-1 sample demonstrated an α -alumina phase. As mentioned in chapter 2, the following pathway is most common for aluminum hydroxide decomposition and was also observed in our work when using the electric furnace:



The peaks of γ -alumina coexisted with those of α -alumina in the PF-1 sample. However, the peaks corresponding to θ -alumina were not detected. Significantly, θ -alumina is an essential intermediate in the transition pathway from γ -alumina to α -alumina. Typical thermal treatment could not derive the direct phase transformation from γ -alumina to α -alumina without θ -alumina. These results are in accordance with the results obtained in Chapter 2 and 3. It was surmised that the plasma treatment and the conventional heating process using the electric furnace would have different pathways of pyrolysis for aluminum hydroxide.

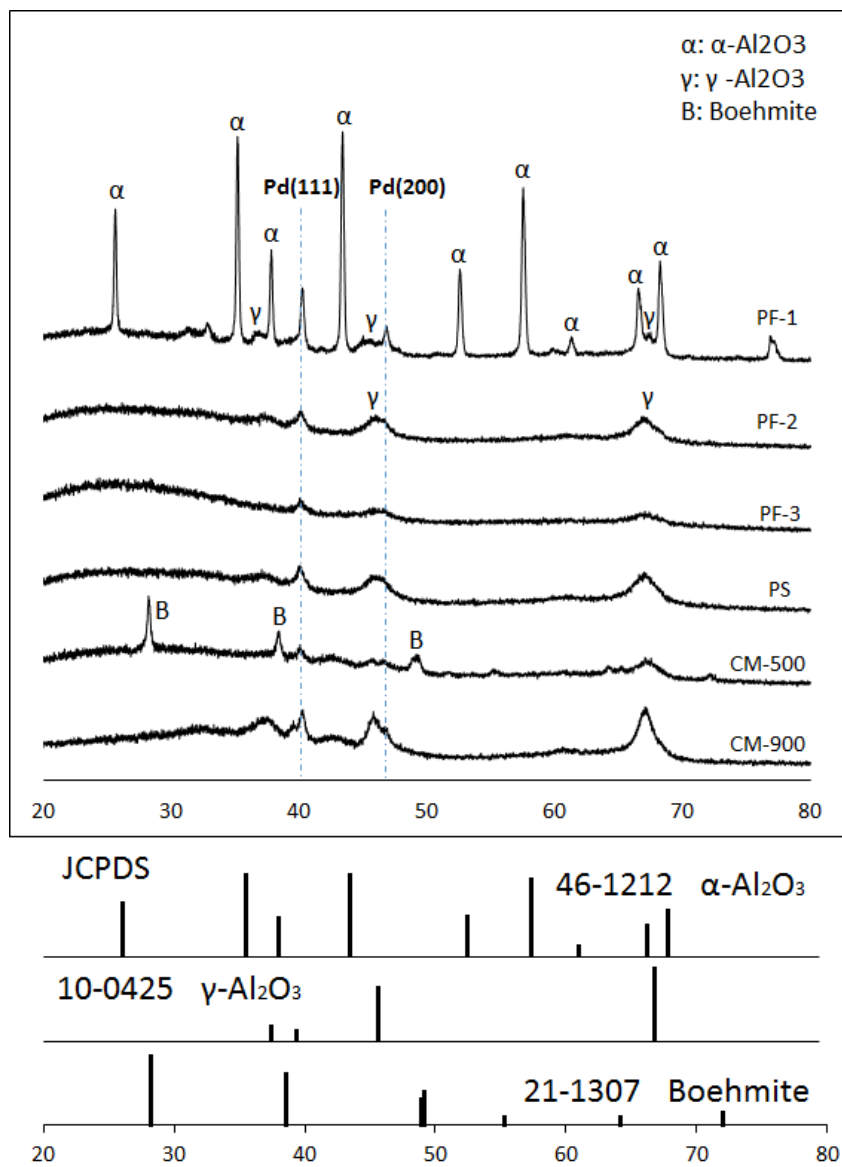


Fig. 4-9 XRD patterns for Pd/Al₂O₃ catalysts under all conditions.

4.2.3.3 TEM analysis

High-resolution TEM images of the catalysts are shown in Fig. 4-10. From the images, the lattice plane spacing of 0.20 nm and 0.22–0.23 nm corresponded to the (200) plane and the (111) plane of Pd, respectively. All samples except PF-1 showed only the Pd(111) plane. Considered together with the XRD results above, the Pd(200) crystal structure and the Pd(111) plane were obtained for PF-1. It is generally accepted that the peaks corresponding to the (100) plane could be offset by that of the (200) plane due to destructive interference for the FCC structure. A square symmetry for the spots represents Pd(100) facets [29]. In this respect, the Pd(200) plane was regarded as the Pd(100) plane observed in PF-1. That is, PF-1 had both Pd(100) and Pd(111) simultaneously. It is reported that precursors such as Na_2PdCl_4 are typically required to obtain selective formations of Pd(111) or Pd(100) [28, 87]. Thus, the plasma treatment was suggested that it could form Pd plane independently of its precursors.

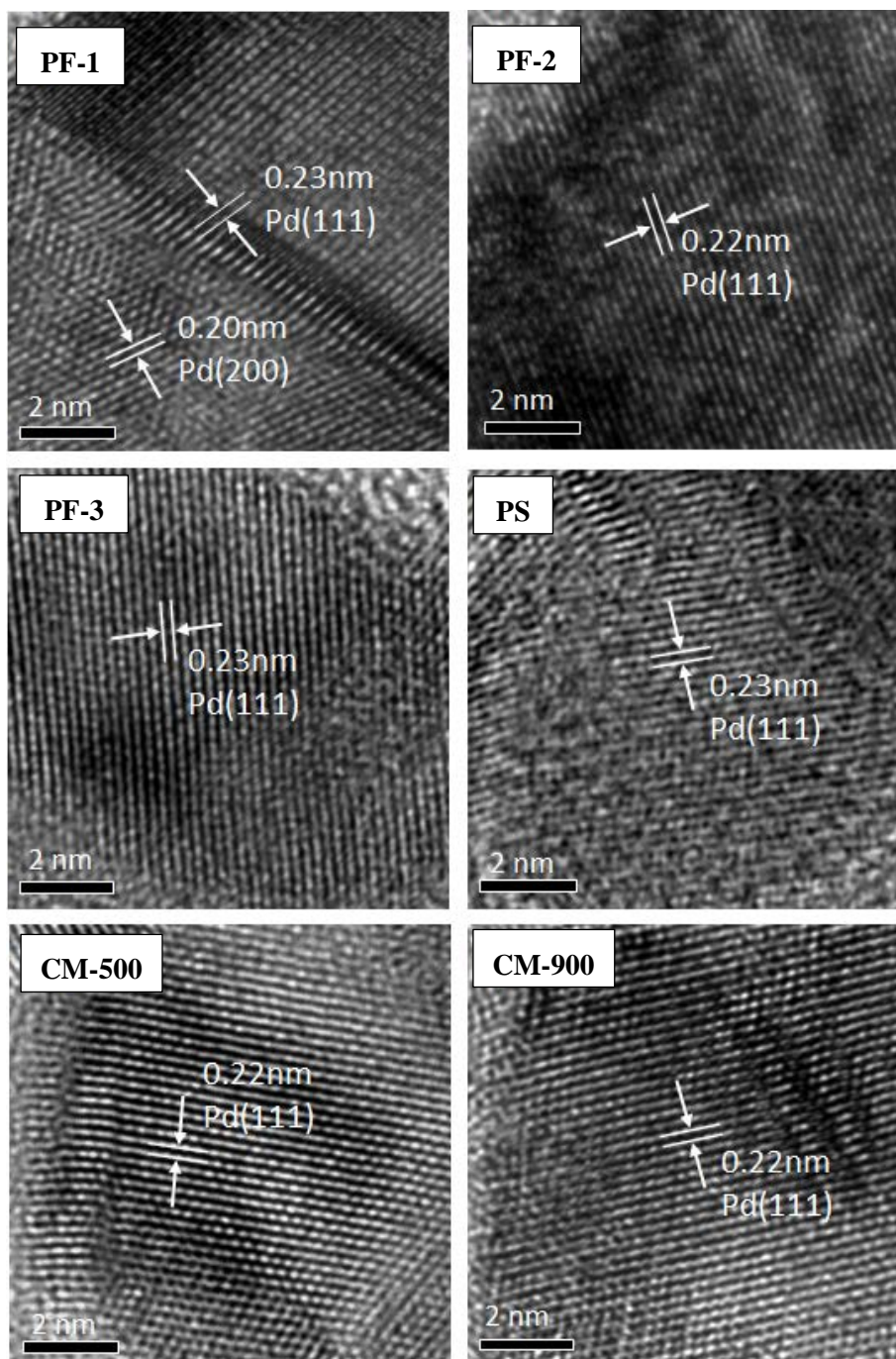


Fig. 4-10 TEM images for Pd/Al₂O₃ catalysts under all conditions.

4.2.3.4 Catalytic activity: Acetylene conversion

C_2H_2 conversion of the catalysts prepared at all conditions is shown in Fig. 4-11. Table 4-4 indicates the Pd metal dispersion, the crystallite size of Pd, and metal surface area. From the H_2 chemisorption results, PF-1 showed the greatest Pd dispersion, and PF-3 showed the lowest. Generally, high metal dispersion on the catalyst equates to high-performance reactions. The results of the C_2H_2 conversion are consistent with the results of H_2 chemisorption. The crystallite size corresponding to Pd(111) for each sample was also calculated by Scherrer's equation (Equation 9) from XRD, and shown in Table 4-4. Compared with the results from H_2 chemisorption, the Pd crystallite size from XRD is one digit different. In H_2 chemisorption, the stoichiometry of Pd/ H_2 was assumed as 2. Since Pd metal has the ability to adsorb more hydrogen than its own volume, the crystallite size would be smaller than the value from XRD. Similar to the H_2 chemisorption results, the results of crystallite size from XRD tended to be inversely proportional to the C_2H_2 conversion except for PF-1. In the case of PF-1, not only the Pd(111) plane but also Pd(100) plane was detected from the XRD analysis, thus, the highest C_2H_2 conversion might be affected by both Pd(111) and Pd(100) plane.

For the thermal treatment, high temperature caused metal sintering, leading to low dispersion as mentioned above. Therefore, the lower C_2H_2 conversion of CM-900 compared with that of CM-500 might be derived from the sintering under high-temperature conditions. Considering the results obtained here, the catalyst prepared using the plasma fixed bed opposed typical results. The conversion of C_2H_2 increased as the distance of the waveguide and particle bed decreased (i.e., the order of C_2H_2 conversion was PF-1>PF-2>PF-3). As shown in the XRD data, the detection of α -alumina within the PF-1 sample indicated that the treated temperature was greater than 1050 °C. A shorter

distance could provide more marked effects of the plasma and the gas temperature on the preparation. In general, C_2H_2 conversion decreases as temperature increases as a result of sintering. However, even at extremely high plasma temperatures, the plasma treatment had a positive effect on Pd dispersion. In accordance with the result of Chapter 3, the distance from the plasma irradiation (PF-3) had a lower effect on the catalyst. Therefore, it is reasonable to indicate that the plasma treatment enhanced the distribution of Pd nanoparticles on the support by preventing the particles from migrating, leading to sintering.

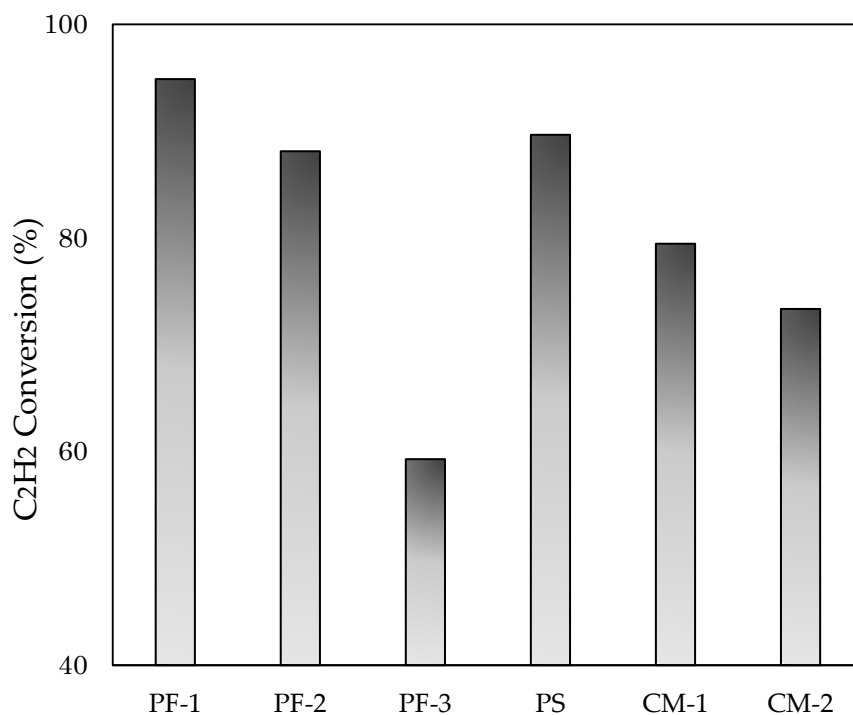


Fig. 4-11 Acetylene conversion for Pd/Al₂O₃ catalysts.

Table 4-4 H₂ chemisorption results and the crystallite size of Pd (111) from XRD.

Catalyst	Avg. crystallite size of Pd (Å)	Metal Surface area (m ² /g)	Dispersion ¹ (%)	Crystallite size Pd(111) ² (nm)
PF-1	14.8	1.13	25.3	22.9
PF-2	16.2	1.02	22.9	12.3
PF-3	25.5	0.65	14.8	29.2
PS	16.2	1.03	23.2	11.4
CM-500	19.2	0.86	19.6	16.0
CM-900	22.1	0.75	17.0	23.5

¹ The fraction of Pd atoms exposed to the surface of the catalyst.

² Crystallite size of Pd (111) calculated from XRD pattern.

4.2.3.5 Catalytic activity: Ethylene and ethane selectivity

C_2H_4 and C_2H_6 selectivity for all samples are shown in Fig. 4-12. For C_2H_4 selectivity, the catalysts prepared using the fixed bed with plasma irradiation (PF-2, PF-3, PS) showed greater catalytic performance in the C_2H_4 selectivity than those prepared using conventional thermal treatment. The plasma spouted bed-treated catalyst showed the highest ethylene selectivity. For C_2H_6 selectivity, the difference in C_2H_6 selectivity between PF-1 and all other samples was significant. The longer the distance between the waveguide and the particles, the lower the C_2H_6 selectivity (PF-3 < PF-2 < PF-1). For PF-1, a remarkably high hydrogenation of C_2H_4 was observed when compared with other samples. This catalytic performance might be derived from the formation of the Pd(100) plane. This has been widely studied for various catalytic reactions (e.g., alkene hydrogenation, formic acid oxidation, and oxygen reduction reactions) for Pd(111) and Pd(100) [27-29]. In particular, Pd(100) has an effect on the consecutive hydrogenation of acetylene to ethane as compared with that of the Pd(111) plane [25-26]. Since the surface energy of Pd(100) is greater than that of Pd(111) [87, 88], ethylene could be strongly attached to the Pd metal, promoting further hydrogenation of ethylene to ethane. From the XRD pattern and the TEM images, the Pd(100) plane was clearly verified for PF-1. A greater selectivity of C_2H_6 could be elucidated by the formation of the Pd(100) plane. As a consequence, the plasma treatment had the potential to induce specific modification of the catalyst for certain catalytic reactions as compared with conventional preparation methods.

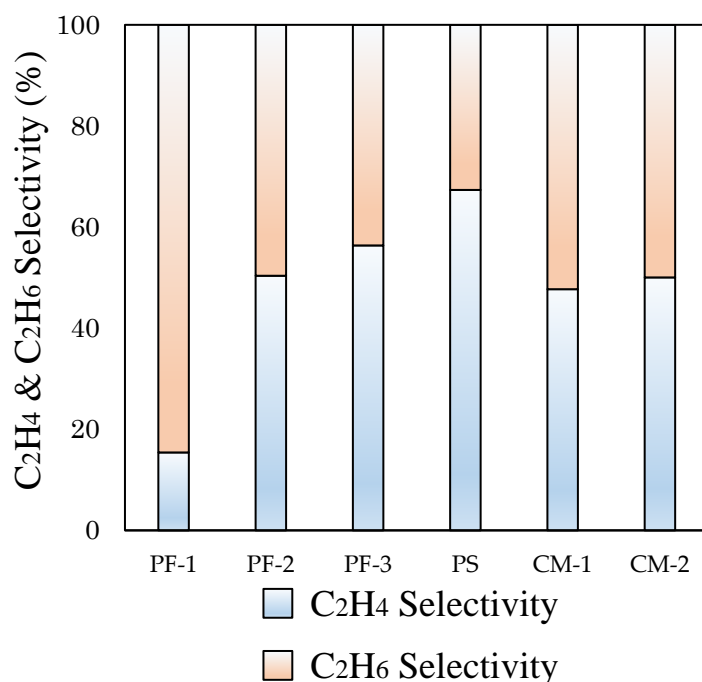


Fig. 4-12 Ethylene selectivity and ethane selectivity for Pd/Al₂O₃ catalysts.

4.2.3.6 Comparison of the fixed bed with the plasma irradiation and the plasma spouted bed

As mentioned above, the catalyst prepared by the fixed bed with plasma irradiation showed lower catalytic performance in the C₂H₄ selectivity than that prepared by the plasma spouted bed. This is illustrated by the significant difference in the formation of Pd(100) that was observed in PF-1. The plane of Pd(100) was not detected for PS, even when in close proximity to the waveguide. Moreover, for the samples without the Pd(100) plane (PF-2 and PF-3), C₂H₄ selectivity was also inferior to those of the plasma spouted bed. In 4.1.3.4, high C₂H₄ selectivity for PS was explained by a strong interaction between the Pd metal and the alumina support. Regarding the surface energy, the strong interaction could encourage the Pd metal to easily desorb ethylene [84]. When considering the

treatment conditions of PS and PF, the most remarkable difference was in the temperature fluctuation of the particles. The fixed bed with plasma irradiation could make the particle temperature constant, that is, the temperature was held constant from the beginning to the end during treatment. On the other hand, the particle temperature was fluctuated due to the circulation in the bed. It is still unclear how the particles are affected by these processes. However, we may conclude that these effects are involved in the modification of phase components and induce the strong metal-support interaction (SMSI). In conclusion, an intensive effect of the plasma in the proximity of the irradiation could develop the formation of different crystal phases, and the spouted bed could control those effects by modulating temperature fluctuations.

4.3 Conclusion

In this chapter, the microwave plasma jet combined with the spouted bed was applied for Pd/Al₂O₃ catalyst preparation. Pd/Al₂O₃ catalyst prepared by the plasma spouted bed showed different catalytic reaction behavior in acetylene hydrogenation compared with those prepared by the conventional method. It was suggested that the plasma spouted bed treatment could prevent Pd metal from sintering even at high temperature condition in the plasma spouted bed and could induce strong interaction between Pd metal and alumina support. Further investigation of the plasma spouted bed, the Pd/Al₂O₃ catalyst was also prepared by the fixed-bed with microwave-induced plasma irradiation. A high dispersion of Pd metal on the support was also fabricated in PF. From the XRD pattern and the TEM images, the Pd(100) plane coexisted with the Pd(111) plane, and a direct decomposition pathway of alumina ($\gamma \rightarrow \alpha$) without the essential intermediate, θ -alumina, was observed in PF-1. Concerning the catalytic performance of the acetylene hydrogenation, the plasma-treated catalysts (PF-1, PF-2, and PS) with a shorter distance between the waveguide and the particles exhibited greater activity when compared with the furnace-treated catalysts. This was due to the smaller size of the Pd metal because the plasma treatment had a positive effect on preventing Pd nanoparticles from sintering. However, the highest selectivity of ethane for PF-1 could be explained by the creation of a higher surface energy in the Pd(100) plane obtained only for this condition. In conclusion, the effectiveness of plasma irradiation on the phase transition of Pd and alumina, as well as preparing the catalyst, was put into perspective by comparing it to conventional thermal treatment.

CHAPTER 5

Conclusion

5.1 Concluding remarks

The microwave induced plasma was applied to the catalyst preparation using two types of reactors including a fixed bed and a spouted bed. The plasma jet was directly irradiated to the particle bed in the former reactor, while the latter used the plasma jet for spouting particles. For comparison, typical heat treatment using an electric furnace was also applied. In this research work, the effects of the microwave induced plasma were investigated with three kinds of catalysts and catalyst support, which summarized in chapter 2 (alumina), chapter 3 (Ni/alumina), and chapter 4 (Pd/alumina).

First, in Chapter 2, the treatment of aluminum hydroxide with microwave induced plasma jet was carried out. The crystal structure analysis by XRD proved new discovery of the decomposition pathway of aluminum hydroxide. Typically, θ -alumina is an essential intermediate in the transition pathway from γ -alumina to α -alumina, however, a direct decomposition pathway of alumina ($\gamma \rightarrow \alpha$) without θ -alumina was observed in the plasma treated samples (PS, PF). Analysis of the surface morphology by SEM indicated that rapid dehydration would occurred for the plasma treated samples (PS, PF), compared with the typical thermal heating (CM). Considering these facts, the prospect was suggested that the plasma treatment for impregnated metal on alumina could affect the catalyst properties.

Next in chapter 3, to investigate the effects as above mentioned, Ni metal was impregnated onto alumina support and treated by the microwave induced plasma. The Ni/Al₂O₃ catalyst was prepared by three different preparation method (PS, PF, and CM). The plasma treated Ni/Al₂O₃ catalysts (PF-1 and PS) showed better performance in the conversion of ethylene hydrogenation than those prepared by the electric furnace. It was suggested that the plasma treatment enhanced the distribution of Ni metal on the support

by preventing the particles from migrating, leading to high catalytic activity. The methane selectivity was in proportion to the ethylene conversion for the catalyst prepared by the conventional method. However, methane selectivity for PF-1 and PS resulted in different tendencies. From these results, it was suggested that the plasma spouted bed and the fixed bed had different reduction mechanism on the Ni/Al₂O₃ catalyst even with the same plasma jet irradiation.

Lastly in chapter 4, instead of Ni metal, Pd metal was impregnated onto alumina, which has better industrial value. Three different preparation method (PS, PF, and CM) were also applied for Pd/Al₂O₃ catalyst preparation. Their catalytic performance were evaluated for the acetylene hydrogenation. The spouting condition and the distance between the waveguide and the particle was changed for PS, and PF, respectively. From the results, the spouting condition might affect the properties of the catalyst leading to different value of ethylene selectivity. It was proposed that a repetition of rapid temperature change in spouted bed could affect the interaction between Pd metal and alumina support. Meanwhile, a remarkably high hydrogenation of ethylene was observed in PF-1. From the XRD pattern and the TEM images, the Pd(100) plane was clearly verified only for PF-1. Thus, this catalytic performance might be derived from the formation of the Pd(100) plane. The effectiveness of plasma irradiation on the phase transition of Pd and alumina, as well as preparing the catalyst, was put into perspective by comparing it to the conventional thermal treatment.

In this thesis, a novel methodology for catalyst preparation using the microwave induced plasma was introduced. It was clearly confirmed that the treatment of the microwave induced plasma had an effect on the decomposition pathway of catalyst support and enhancements of catalyst properties as compared with those of the typical

thermal treatment. It can be an alternative to conventional processes as it resolves issues with the enhancement of the catalyst properties.

5.2 Prospects and future studies

The present work is an early step of revealing the effect of the microwave induced plasma when combined with the spouted bed and with the fixed bed. A new discovery of the decomposition pathway and the catalytic enhancements were confirmed by the experimental investigation. However, it is still unknown how it affects the transformation and the properties of the catalysts. As mentioned in the content, many other researchers are dedicated to figuring out the exact effects of the plasma. The following is recommended for future works.

- The difference in the reduction mechanism between the plasma spouted bed and the fixed bed with the plasma irradiation should be clarified. As a first step, details of the spouted bed such as accurate temperature in the high temperature region and the low temperature region and particle residence time of the particles have to be investigated, followed by simulating the temperature change of the catalyst.
- The same thermal environment as the plasma needs to be developed to further understanding of the effects of the radicals on the preparation of the catalyst. To achieve this, the measurement of accurate temperature of the plasma has to be done. Next, prepared a gas at the temperature as same as the plasma followed by spouting the particles with high temperature gas for reduction process. This also could be an attempt to promote a better understanding of the plasma spouted bed.
- Compare other types of plasma such as DC plasma or RF plasma with the microwave induced plasma. Since the microwave induced plasma has a higher temperature than that of others, and it contains different density of radicals, it could show different behavior in catalytic activity. This can provide information for possible future applications.

REFERENCES

- [1] Goldston, R. J., & Rutherford, P. H. (1995). *Introduction to plasma physics*. CRC Press.
- [2] Fridman, A. (2008). *Plasma chemistry*. Cambridge university press.
- [3] Conrads, H., & Schmidt, M. (2000). Plasma generation and plasma sources. *Plasma Sources Science and Technology*, 9(4), 441.
- [4] M. Pahl, Neure Ergebnisse über Sekundärprozesse langsamer Ionen in Gasen, *Ergebn. Exakt. Naturw.* **34**, 182–235 (1962).
- [5] Moreau, M., Orange, N., & Feuilloley, M. G. J. (2008). Non-thermal plasma technologies: new tools for bio-decontamination. *Biotechnology advances*, 26(6), 610-617.
- [6] Everaert, E. M., Belt-Gritter, B. V. D., Van der Mei, H. C., Busscher, H. J., Verkerke, G. J., Dijk, F., ... & Reitsma, A. (1998). In vitro and in vivo microbial adhesion and growth on argon plasma-treated silicone rubber voice prostheses. *Journal of Materials Science: Materials in Medicine*, 9(3), 147-157.
- [7] Yousefi Rad, A., Ayhan, H., Kisa, Ü., & Pişkin, E. (1998). Adhesion of different bacterial strains to low-temperature plasma treated biomedical PVC catheter surfaces. *Journal of Biomaterials Science, Polymer Edition*, 9(9), 915-929.
- [8] Terajima, T., & Koinuma, H. (2004). Development of a combinatorial atmospheric pressure cold plasma processor. *Applied surface science*, 223(1-3), 259-263.
- [9] Shirai, H., Nguyen, M. T., Čempel, D., Tsukamoto, H., Tokunaga, T., Liao, Y. C., &

- Yonezawa, T. (2016). Preparation of Au/Pd bimetallic nanoparticles by a microwave-induced plasma in liquid process. *Bulletin of the Chemical Society of Japan*, 90(3), 279-285.
- [10] Jasiński, M., Mizeraczyk, J., Zakrzewski, Z., Ohkubo, T., & Chang, J. S. (2002). CFC-11 destruction by microwave torch generated atmospheric-pressure nitrogen discharge. *Journal of Physics D: Applied Physics*, 35(18), 2274.
- [11] Asmussen, J. (1989). Electron cyclotron resonance microwave discharges for etching and thin - film deposition. *Journal of Vacuum Science & Technology A: Vacuum, Surfaces, and Films*, 7(3), 883-893.
- [12] Ferreira, C. M., & Moisan, M. (Eds.). (2013). *Microwave discharges: fundamentals and applications* (Vol. 302). Springer Science & Business Media.
- [13] Hayashi, M., Takahashi, M., & Sakurai, Y. (2007). Preparation of positive LiCoO₂ films by electron cyclotron resonance (ECR) plasma sputtering method and its application to all-solid-state thin-film lithium batteries. *Journal of Power Sources*, 174(2), 990-995.
- [14] Tang, J., Staller, K. D., & Beenakker, C. I. M. (2015). Decapsulation of Multi-Chip BOAC Devices with Exposed Copper Metallization Using Atmospheric Pressure Microwave Induced Plasma. In *Proceedings of 41th International Symposium for Testing and Failure Analysis* (pp. 485-495).
- [15] García, M. C., Mora, M., Esquivel, D., Foster, J. E., Rodero, A., Jiménez-Sanchidrián, C., & Romero-Salguero, F. J. (2017). Microwave atmospheric pressure plasma jets for wastewater treatment: Degradation of methylene blue as a model dye. *Chemosphere*, 180, 239-246.
- [16] Liu, L., Wang, T., Huang, J., He, Z., Yi, Y., & Du, K. (2016). Diamond-like carbon

- thin films with high density and low internal stress deposited by coupling DC/RF magnetron sputtering. *Diamond and Related Materials*, 70, 151-158.
- [17] Dey, R. M., Patil, D., & Kulkarni, S. (2017). Integrated characterization study of diamond like carbon (DLC) synthesized by 2.45 GHz microwave electron cyclotron resonance (ECR) plasma CVD. *Surface and Coatings Technology*, 328, 30-43.
- [18] Economou, D. J. (2014). Pulsed plasma etching for semiconductor manufacturing. *Journal of Physics D: Applied Physics*, 47(30), 303001.
- [19] Abe, H., Yoneda, M., & Fujiwara, N. (2008). Developments of plasma etching technology for fabricating semiconductor devices. *Japanese Journal of Applied Physics*, 47(3R), 1435.
- [20] Zhi, C. Y., Bai, X. D., & Wang, E. G. (2002). Enhanced field emission from carbon nanotubes by hydrogen plasma treatment. *Applied Physics Letters*, 81(9), 1690-1692.
- [21] Yang, J., Wang, X., Wang, X., Jia, R., & Huang, J. (2010). Preparation of highly conductive CNTs/polyaniline composites through plasma pretreating and in-situ polymerization. *Journal of Physics and Chemistry of Solids*, 71(4), 448-452.
- [22] Zhang, Y., Ouyang, B., Xu, J., Chen, S., Rawat, R. S., & Fan, H. J. (2016). 3D Porous Hierarchical Nickel–Molybdenum Nitrides Synthesized by RF Plasma as Highly Active and Stable Hydrogen - Evolution - Reaction Electrocatalysts. *Advanced Energy Materials*, 6(11), 1600221.
- [23] Hinokuma, S., Fujii, H., Katsuhara, Y., Ikeue, K., & Machida, M. (2014). Effect of thermal ageing on the structure and catalytic activity of Pd/CeO₂ prepared using arc-plasma process. *Catalysis Science & Technology*, 4(9), 2990-2996.
- [24] Yan, X., Zhao, B., Liu, Y., & Li, Y. (2015). Dielectric barrier discharge plasma for preparation of Ni-based catalysts with enhanced coke resistance: Current status and

- perspective. *Catalysis Today*, 256, 29-40.
- [25] Kang, J. H., Shin, E. W., Kim, W. J., Park, J. D., & Moon, S. H. (2002). Selective hydrogenation of acetylene on TiO₂-added Pd catalysts. *Journal of catalysis*, 208(2), 310-320.
- [26] Sárkány, A., Weiss, A. H., & Guzzi, L. (1986). Structure sensitivity of acetylene-ethylene hydrogenation over Pd catalysts. *J. Catal.:(United States)*, 98(2).
- [27] Doyle, A. M., Shaikhutdinov, S. K., & Freund, H. J. (2005). Surface - Bonded Precursor Determines Particle Size Effects for Alkene Hydrogenation on Palladium. *Angewandte Chemie International Edition*, 44(4), 629-631.
- [28] Jin, M., Zhang, H., Xie, Z., & Xia, Y. (2012). Palladium nanocrystals enclosed by {100} and {111} facets in controlled proportions and their catalytic activities for formic acid oxidation. *Energy & Environmental Science*, 5(4), 6352-6357.
- [29] Shao, M., Yu, T., Odell, J. H., Jin, M., & Xia, Y. (2011). Structural dependence of oxygen reduction reaction on palladium nanocrystals. *Chemical Communications*, 47(23), 6566-6568.
- [30] Foix, M.; Guyon, C.; Tatoulian, M.; Da Costa, P. Microwave plasma treatment for catalyst preparation: Application to alumina supported silver catalysts for SCR NO_x by ethanol. *Mod. Res. Catal.* **2013**, 2, 68–82.
- [31] Stark, Robert H., and Karl H. Schoenbach. "Direct current glow discharges in atmospheric air." *Applied Physics Letters* 74.25 (1999): 3770-3772.
- [32] Staack, David, et al. "Characterization of a dc atmospheric pressure normal glow discharge." *Plasma Sources Science and Technology* 14.4 (2005): 700.
- [33] Duan, Yixiang, Chun Huang, and Qingsong Yu. "Low-temperature direct current glow discharges at atmospheric pressure." *IEEE Transactions on Plasma Science*

- 33.2 (2005): 328-329.
- [34] Chung, J. Y., Kodama, S., & Sekiguchi, H. (2019). Preparation of Catalyst with Microwave Induced Plasma Jet Combined with Spouted Bed. *Journal of nanoscience and nanotechnology*, 19(10), 6849-6855.
- [35] Du, S., Sun, Y., Gamliel, D. P., Valla, J. A., & Bollas, G. M. (2014). Catalytic pyrolysis of miscanthus× giganteus in a spouted bed reactor. *Bioresource technology*, 169, 188-197.
- [36] Amutio, M., Lopez, G., Artetxe, M., Elordi, G., Olazar, M., & Bilbao, J. (2012). Influence of temperature on biomass pyrolysis in a conical spouted bed reactor. *Resources, Conservation and Recycling*, 59, 23-31.
- [37] Mathur, K. B., & Gishler, P. E. (1955). A technique for contacting gases with coarse solid particles. *AIChE Journal*, 1(2), 157-164.
- [38] Góral, D., Kluza, F., & Kozłowicz, K. (2017). Spouted Bed and Jet Impingement Fluidization in Food Industry. In *Heat Transfer-Models, Methods and Applications*. IntechOpen.
- [39] Wefers, Karl, and Chanakya Misra. "Oxides and hydroxides of aluminum." (1987).
- [40] Perander, Linus. Evolution of nano-and microstructure during the calcination of Bayer gibbsite to produce alumina. Diss. ResearchSpace@ Auckland, 2010.
- [41] Ingram-Jones, Victoria J., et al. "Dehydroxylation sequences of gibbsite and boehmite: study of differences between soak and flash calcination and of particle-size effects." *Journal of Materials Chemistry* 6.1 (1996): 73-79.
- [42] Whittington, B., and D. Ilievski. "Determination of the gibbsite dehydration reaction pathway at conditions relevant to Bayer refineries." *Chemical Engineering Journal* 98.1-2 (2004): 89-97.

- [43] Yamada, K., et al. "Dehydration products of gibbsite by rotary kiln and stationary calciner." *Essential Readings in Light Metals*. Springer, Cham, 2016. 719-726.
- [44] Contreras, César A., et al. "A new production method of submicron alumina powders." *Advances in Technology of Materials and Materials Processing Journal* 5.2 (2003): 36-39.
- [45] Anabtawi, M. Z. (1998). Minimum spouting velocity for binary mixture of particles in rectangular spouted beds.
- [46] Ohji, T., & Eagar, T. W. (1992). Infrared radiation from an arc plasma and its application to plasma diagnostics. *Plasma chemistry and plasma processing*, 12(4), 403-419.
- [47] Yefimov, N. A., & Naboychenko, S. (2009). *Handbook of non-ferrous metal powders: technologies and applications*. Elsevier.
- [48]. Chauruka, S.R.; Hassanpour, A.; Brydson, R.; Roberts, K.J.; Ghadiri, M.; Stitt, H. Effect of mill type on the size reduction and phase transformation of gamma alumina. *Chem. Eng. Sci.* 2015, 134, 774–783.
- [49]. Kostić, E.; Kiss, S.J.; Zec, S.; Bošković, S. Transition of γ -Al₂O₃ into α -Al₂O₃ during vibro milling. *Powder Technol.* 2000, 107, 48–53.
- [50]. Zielinski, P.A.; Schulz, R.; Kaliaguine, S.; Van Neste, A. Structural transformations of alumina by high energy ball milling. *J. Mater. Res.* 1993, 8, 2985–2992.
- [51] Kwan, C. C., Mio, H., Chen, Y. Q., Ding, Y. L., Saito, F., Papadopoulos, D. G., & Ghadiri, M. (2005). Analysis of the milling rate of pharmaceutical powders using the Distinct Element Method (DEM). *Chemical Engineering Science*, 60(5), 1441-1448.

- [52] Chauruka, S. R., Hassanpour, A., Brydson, R., Roberts, K. J., Ghadiri, M., & Stitt, H. (2015). Effect of mill type on the size reduction and phase transformation of γ -alumina. *Chemical Engineering Science*, 134, 774-783.
- [53] Bodaghi, M., Mirhabibi, A. R., Zolfonun, H., Tahriri, M., & Karimi, M. (2008). Investigation of phase transition of γ -alumina to α -alumina via mechanical milling method. *Phase Transitions*, 81(6), 571-580.
- [54] Bian, Z., Das, S., Wai, M. H., Hongmanorom, P., & Kawi, S. (2017). A review on bimetallic nickel - based catalysts for CO₂ reforming of methane. *ChemPhysChem*, 18(22), 3117-3134.
- [55] Ali, S., Zagho, M. M., Al-Marri, M. J., Arafat, Y. I., & Khader, M. M. (2015, January). Development of Nickel-based Catalysts for Methane Steam Reforming. In *Proceedings of the 4th International Gas Processing Symposium* (pp. 111-116). Elsevier.
- [56] Xia, J., He, G., Zhang, L., Sun, X., & Wang, X. (2016). Hydrogenation of nitrophenols catalyzed by carbon black-supported nickel nanoparticles under mild conditions. *Applied Catalysis B: Environmental*, 180, 408-415.
- [57] Shaw, M. H., Shurtleff, V. W., Terrett, J. A., Cuthbertson, J. D., & MacMillan, D. W. (2016). Native functionality in triple catalytic cross-coupling: sp³ C–H bonds as latent nucleophiles. *Science*, 352(6291), 1304-1308.
- [58] Perego, C., & Villa, P. (1997). Catalyst preparation methods. *Catalysis Today*, 34(3-4), 281-305.
- [59] Nishijima, M., Yoshinobu, J., Sekitani, T., & Onchi, M. (1989). Chemisorption and thermal decomposition of ethylene on Pd (110): Electron energy loss spectroscopy, low - energy electron diffraction, and thermal desorption spectroscopy studies. *The*

Journal of Chemical Physics, 90(9), 5114-5127.

- [60] Williams, K. J., Levin, M. E., Salmeron, M., Bell, A. T., & Somorjai, G. A. (1988). Ethylene hydrogenation and ethane hydrogenolysis on a Rh foil with titania overlayers. *Catalysis letters*, 1(10), 331-338.
- [61] Richardson, J. T., & Friedrich, H. (1975). Pulsed thermo kinetic (PTK) measurements: Ethylene hydrogenation. *Journal of Catalysis*, 37(1), 8-21.
- [62] Chen, Y., & Vlachos, D. G. (2010). Hydrogenation of ethylene and dehydrogenation and hydrogenolysis of ethane on Pt (111) and Pt (211): a density functional theory study.
- [63] Duan, Y., Huang, C., & Yu, Q. (2005). Low-temperature direct current glow discharges at atmospheric pressure. *IEEE Transactions on Plasma Science*, 33(2), 328-329.
- [64] Liu, C. J., Yu, K., Zhang, Y. P., Zhu, X., He, F., & Eliasson, B. (2004). Characterization of plasma treated Pd/HZSM-5 catalyst for methane combustion. *Applied Catalysis B: Environmental*, 47(2), 95-100.
- [65] Rahmani, F., Haghghi, M., & Estifaei, P. (2014). Synthesis and characterization of Pt/Al₂O₃-CeO₂ nanocatalyst used for toluene abatement from waste gas streams at low temperature: Conventional vs. plasma-ultrasound hybrid synthesis methods. *Microporous and Mesoporous Materials*, 185, 213-223.
- [66] Zhu, X., Huo, P., Zhang, Y. P., Cheng, D. G., & Liu, C. J. (2008). Structure and reactivity of plasma treated Ni/Al₂O₃ catalyst for CO₂ reforming of methane. *Applied Catalysis B: Environmental*, 81(1-2), 132-140.
- [67] Dieuzeide, M. L., Laborde, M., Amadeo, N., Cannilla, C., Bonura, G., & Frusteri, F. (2016). Hydrogen production by glycerol steam reforming: How Mg doping affects

- the catalytic behaviour of Ni/Al₂O₃ catalysts. *International Journal of Hydrogen Energy*, 41(1), 157-166.
- [68] Martin, G. A. (1979). The kinetics of the catalytic hydrogenolysis of ethane over Ni/SiO₂. *Journal of Catalysis*, 60(3), 345-355.
- [69] Cortright, R. D., Watwe, R. M., Spiewak, B. E., & Dumesic, J. A. (1999). Kinetics of ethane hydrogenolysis over supported platinum catalysts. *Catalysis today*, 53(3), 395-406.
- [70] Lehwald, S., & Ibach, H. (1979). Decomposition of hydrocarbons on flat and stepped Ni (111) surfaces. *Surface Science*, 89(1-3), 425-445.
- [71] Zaera, F., & Hall, R. B. (1987). Low temperature decomposition of ethylene over Ni (100): Evidence for vinyl formation. *Surface science*, 180(1), 1-18.
- [72] Vattuone, L., Yeo, Y. Y., Kose, R., & King, D. A. (2000). Energetics and kinetics of the interaction of acetylene and ethylene with Pd {100} and Ni {100}. *Surface Science*, 447(1-3), 1-14.
- [73] Wang, L., Murata, K., & Inaba, M. (2003). Production of pure hydrogen and more valuable hydrocarbons from ethane on a novel highly active catalyst system with a Pd-based membrane reactor. *Catalysis today*, 82(1-4), 99-104.
- [74] Li, Y., & Jang, B. W. L. (2017). Selective hydrogenation of acetylene over Pd/Al₂O₃ catalysts: Effect of non-thermal RF plasma preparation methodologies. *Topics in Catalysis*, 60(12-14), 997-1008.
- [75] Cassar, L. (1975). Synthesis of aryl- and vinyl-substituted acetylene derivatives by the use of nickel and palladium complexes. *Journal of Organometallic Chemistry*, 93(2), 253-257.
- [76] Puskas, I., & Cerefice, S. A. (1984). *U.S. Patent No. 4,476,242*. Washington, DC:

U.S. Patent and Trademark Office.

- [77] Cider, L., & Schöön, N. H. (1991). Competition between ethyne, ethene and carbon monoxide for the active sites during hydrogenation at transient conditions over supported metal catalysts. *Applied catalysis*, 68(1), 191-205.
- [78] Asplund, S. (1996). Coke formation and its effect on internal mass transfer and selectivity in Pd-catalysed acetylene hydrogenation. *Journal of Catalysis*, 158(1), 267-278.
- [79] Didillon, B., Cameron, C., & Gautreau, C. (1999). *U.S. Patent No. 5,955,397*. Washington, DC: U.S. Patent and Trademark Office.
- [80] Pei, G. X., Liu, X. Y., Wang, A., Lee, A. F., Isaacs, M. A., Li, L., ... & Wilson, K. (2015). Ag alloyed Pd single-atom catalysts for efficient selective hydrogenation of acetylene to ethylene in excess ethylene. *Acs Catalysis*, 5(6), 3717-3725.
- [81] Haruta, M., Yamada, N., Kobayashi, T., & Iijima, S. (1989). Gold catalysts prepared by coprecipitation for low-temperature oxidation of hydrogen and of carbon monoxide. *Journal of catalysis*, 115(2), 301-309.
- [82] Pecharsky, V., & Zavalij, P. (2008). *Fundamentals of powder diffraction and structural characterization of materials*. Springer Science & Business Media.
- [83] Akita, T., Lu, P., Ichikawa, S., Tanaka, K., & Haruta, M. (2001). Analytical TEM study on the dispersion of Au nanoparticles in Au/TiO₂ catalyst prepared under various temperatures. *Surface and Interface Analysis: An International Journal devoted to the development and application of techniques for the analysis of surfaces, interfaces and thin films*, 31(2), 73-78.
- [84] Liu, C. J., Vissokov, G. P., & Jang, B. W. L. (2002). Catalyst preparation using plasma technologies. *Catalysis Today*, 72(3-4), 173-184.

- [85] Flamant, G. (1990). Hydrodynamics and heat transfer in a plasma spouted bed reactor. *Plasma Chemistry and Plasma Processing*, 10(1), 71-85.
- [86] Uglov, A. A., & Gnedovets, A. G. (1991). Effect of particle charging on momentum and heat transfer from rarefied plasma flow. *Plasma chemistry and plasma processing*, 11(2), 251-267.
- [87] Xiong, Y., & Xia, Y. (2007). Shape - controlled synthesis of metal nanostructures: the case of palladium. *Advanced Materials*, 19(20), 3385-3391.
- [88] Ge, C., Fang, G., Shen, X., Chong, Y., Wamer, W. G., Gao, X. & Yin, J. J. (2016). Facet energy versus enzyme-like activities: the unexpected protection of palladium nanocrystals against oxidative damage. *ACS nano*, 10(11), 10436-10445.
- [89] Jacob, R., Nair, H. G., & Isac, J. (2015). Structural and morphological studies of nano-crystalline ceramic BaSr_{0.9}Fe_{0.1}TiO₄. *international Letters of chemistry, physics and Astronomy*, 41, 100-117.
- [90] Li, X., Cheng, H., Liang, G., He, L., Lin, W., Yu, Y., & Zhao, F. (2015). Effect of phosphine doping and the surface metal state of Ni on the catalytic performance of Ni/Al₂O₃ catalyst. *Catalysts*, 5(2), 759-773.

ACKNOWLEDGEMENTS

I would like to express my sincerest and deepest gratitude to my supervisor, Professor Hidetoshi Sekiguchi, for his guidance, support, encouragement, and patience in the past six years from undergraduate studies. I appreciate his supervising technique, which made me more confident and independent in my research. In every progress report meeting, he gave me the stimulation of a new idea. About every draft that I wrote for the publication, he kindly checked the paper with highly technical skills even in his busy time. Since I was an undergrad student, he had trained me that it is important to consider the principle and understand why we get those results and not just get the results.

I am also deeply grateful to Assistant Professor Satoshi Kodama for his kind advice and help throughout the entire study process right next to me. It would have been impossible to carry out and complete my research study without his support.

I would like to thank all the members of the Sekiguchi Laboratory for their help, discussions, friendship and moral support during the period of my study. Especially, I want to deliver my thanks to Nada that helped me by proofreading the thesis in terms of English grammar and finding mistakes.

I would like to acknowledge the 「Rotary Yoneyama Memorial Foundation」 for financially supporting my graduate studies.